ASSESSMENT OF SENSITIVITY OF DEPTH INTEGRATED SOLUTIONS TO LONGITUDINAL DISCONTINUITIES ON THE CHANNEL BED

A THESIS SUBMITTED TO
THE GRADUATE SCHOOL OF NATURAL AND APPLIED SCIENCES
OF
MIDDLE EAST TECHNICAL UNIVERSITY

BY

RAMEZ MOHAMMADI

IN PARTIAL FULFILLMENT OF THE REQUIREMENTS
FOR
THE DEGREE OF MASTER OF SCIENCE
IN
CIVIL ENGINEERING

SEPTEMBER 2019

Approval of the thesis:

ASSESSMENT OF SENSITIVITY OF DEPTH INTEGRATED SOLUTIONS TO LONGITUDINAL DISCONTINUITIES ON THE CHANNEL BED

submitted by **RAMEZ MOHAMMADI** in partial fulfillment of the requirements for the degree of **Master of Science in Civil Engineering Department, Middle East Technical University** by,

Prof. Dr. Halil Kalıpçılar
Dean, Graduate School of **Natural and Applied Sciences** _____

Prof. Dr. Ahmet Türer
Head of Department, **Civil Engineering** _____

Prof. Dr. İsmail Aydın
Supervisor, **Civil Engineering, METU** _____

Examining Committee Members:

Prof. Dr. Ahmet Cevdet Yalçıner
Civil Engineering, METU _____

Prof. Dr. İsmail Aydın
Civil Engineering, METU _____

Prof. Dr. Mete Köken
Civil Engineering, METU _____

Assoc. Prof. Dr. Utku Kanoğlu
Aerospace Engineering, METU _____

Assoc. Prof. Dr. Ender Demirel
Civil Engineering., ESOGÜ _____

Date: 09.09.2019

I hereby declare that all information in this document has been obtained and presented in accordance with academic rules and ethical conduct. I also declare that, as required by these rules and conduct, I have fully cited and referenced all material and results that are not original to this work.

Name, Surname: Ramez Mohammadi

Signature:

ABSTRACT

ASSESSMENT OF SENSITIVITY OF DEPTH INTEGRATED SOLUTIONS TO LONGITUDINAL DISCONTINUITIES ON THE CHANNEL BED

Mohammadi, Ramez
Master of Science, Civil Engineering
Supervisor: Prof. Dr. İsmail Aydın

September 2019, 103 pages

Depth integrated equations can be easily solved over large domains to provide flood inundation maps. In urban and rural areas however, there may be numerous natural or artificial bottom boundary discontinuities in the form of rapid variations in bed elevation. Such discontinuities cause abrupt changes in the source terms of the governing equations and can significantly affect stability and accuracy of the numerical solution. This study concentrates on the assessment of sensitivity of the governing equations to longitudinal discontinuities and proposes solutions to alleviate associated numerical complications. The presence of dry regions in the domain is also considered which requires additional modifications in the code to deal with the wet/dry fronts.

In this thesis, Godunov's type Finite Volume Method (FVM) is used for the numerical solution of the shallow water equations. Weighted Averaged Flux (WAF) method, that is 2nd order extension of the first order Godunov's scheme, based on HLL Riemann solver, is used to compute the fluxes. The source term treatment is based on the "hydrostatic reconstruction" and first and second order well-balanced schemes are obtained. Creation of probable negative water depths during linear piecewise reconstruction of the water surface near dry areas has been prevented in the 2nd order well-balanced scheme.

Eight test cases with their available analytical solutions that are widely used in the literature are selected to validate the developed codes. The results of the developed codes are also compared with sets of experimental data if available. Test cases are solved by pure WAF method without well-balancing property, WAF method with first order well-balanced scheme, and WAF method with second order well-balanced scheme. Two test cases are specifically selected to show the capability of the developed codes in solving flows in regions with wet and dry areas. In the end, a new test case is introduced to observe behavior of the numerical solutions in a bed consisting of a series of sharp corners due to positive and negative steps. It is observed that well-balanced schemes can produce water surface profiles without spurious oscillations and steady-state horizontal hydrostatic water surface is recovered without noisy fluctuations.

Keywords: Shallow Water Equations, Well-balanced schemes, Weighted Average Flux, Hyperbolic partial differential equations, Finite volume method

ÖZ

DERİNLİK İNTEGRALLİ ÇÖZÜMLERİN KANAL TABANININDA BOYUNA SÜREKSİZLİKLERE DUYARLILIĞININ BELİRLENMESİ

Mohammadi, Ramez
Yüksek Lisans, İnşaat Mühendisliği
Tez Danışmanı: Prof. Dr. İsmail Aydın

Eylül 2019, 103 sayfa

Derinlik integralli denklemler taşkın haritaları hazırlamak amacıyla büyük alanlar üzerinde kolaylıkla çözülebilir. Bununla beraber, kırsal ve kentsel alanlarda yatak yüksekliğinde hızlı değişimlere neden olan sayısız doğal veya yapay süreksizlikler olabilir. Bu tür süreksizlikler akım denklemlerinin kaynak terimlerinde ani değişimlere neden olacağından sayısal çözümün stabilitesini ve hassasiyetini belirgin şekilde etkileyebilir. Bu çalışma, akım denklemlerinin boyuna süreksizliklere duyarlılığının değerlendirilmesine ve ortaya çıkan sayısal sorunların giderilmesine yönelik olacaktır.

Bu tezde sığ akım denklemlerinin sayısal çözümü için Godunov tipi Sonlu Hacim Metodu (FVM) kullanılmıştır. Akıların hesabında Godunov metodunun ikinci dereceden uzantısı olan, HLL Riemann çözücüsüne dayandırılmış Ağırlıklı Ortalama Akı (WAF) metodu kullanılmıştır. Kaynak teriminin değerlendirilmesinde 'hidrostatik yeniden kurma' yaklaşımıyla birinci ve ikinci dereceden iyi-dengeli şemalar elde edilmiştir. Kuru alanlar yakınında su yüzeyinin lineer parçalı olarak yeniden tanımlanması aşamasında negatif su derinliklerinin oluşması olasılığı ikinci dereceden iyi-dengeli şema ile önlenmiştir.

Geliştirilen yazılımları doğrulamak için literatürde yaygın olarak kullanılan sekiz adet test vakası analitik çözümlerinden yararlanılmıştır. Sayısal çözüm sonuçları literatürde mevcut deneysel veri setleri ile de karşılaştırılmıştır. Test vakaları iyi-dengeli özelliği olmadan yalın WAF metodu, birinci dereceden iyi-dengeli WAF metodu ve ikinci dereceden iyi-dengeli WAF metodu ile çözülmüştür. Yazılımların ıslak-kuru geçişli alanlardaki akımların çözümündeki yeteneklerini sergilemek için özel iki vaka seçilmiştir. Ve son olarak sayısal çözümlerin davranışını değerlendirmek için pozitif ve negatif basamakların oluşturduğu bir dizi keskin köşeler içeren yeni bir test vakası tanımlanmıştır. İyi-dengeli şemaların su yüzü profillerini yapay salınımlara neden olmadan üretebildiği ve zamandan bağımsız yatay hidrostatik su yüzünün sayısal çalkantılar olmadan elde edilebildiği gözlemlenmiştir.

Anahtar Kelimeler: Sığ Akım Denklemleri, Dengeli şemalar, Ağırlıklı Ortalama Akı, Hiperbolik kısmi diferansiyel denklemler, Sonlu hacim metodudu

To My Love, Naeimeh

ACKNOWLEDGEMENTS

First and foremost, I would like to express my sincere gratitude to my supervisor, Prof. Dr. İsmail Aydın for his support, guidance, and encouragement he has provided me throughout my M.Sc. study. His insightful comments helped me a lot in all the time of researching and writing of this thesis.

I am beyond thankful to Prof. Dr. Ahmet Cevdet Yalçıner for all his continued advice, support, and kindness. His guidance and recommendations helped me to overcome difficulties and brightened my way moving forward.

My special thanks goes to my beautiful wife, Naeimeh, for all her caring and love. This would not have been possible without you. Thank you for always being so patience and kind in my stressful times and pushing me to think positive in every moment.

Last but not least, I would like to thank my family for all their support. This accomplishment would not have been possible without them. I also would like to thanks all my friends who supported and encouraged me during this step of my life.

TABLE OF CONTENTS

LIST OF FIGURES

FIGURES

CHAPTER 1

INTRODUCTION

Free surface flows are of particular interest to the many scientists and engineers in the fields of hydraulic and ocean engineering. These flows consist of a wide range of physical phenomena such as tsunamis, tides, and wind waves in the sea and oceans, and river floods, dam-break flows, and open channel flows on the land. Since the exact governing equations of these problems are usually too complex and may not be easily applicable in engineering problems, these phenomena can be modeled and studied by proper mathematical models with proper assumptions and modifications.

The behavior of the flow in a wide variety of the above mentioned problems can be studied using the depth integrated equations, called Shallow Water Equations (SWE). Shallow Water Equations are a set of partial differential equations which are derived from the Navier-Stokes equations by assuming that the depth of water is small compared with characteristic length in the horizontal direction, such as wave length. This assumption leads to the hydrostatic pressure distribution in the flow.

One of the difficulties in numerical solving of the shallow water equations may arise when the equations are solved in domains containing discontinuities in the channel beds. These natural or artificial bottom boundary discontinuities can be in the form of rapid variations in bed elevation. These discontinuities abruptly change the source term of the governing equations and may adversely affect the stability and accuracy of the numerical solutions. Another difficulty in the solution of the shallow water equations appears in the presence of dry regions in the domain, which requires additional modification in the numerical solution to deal with the wet/dry fronts.

In this thesis, Godunov's type Finite Volume Method (FVM) will be used for the numerical solution of the shallow water equations. Godunov's type methods come up

with the solution of the Riemann problem- an initial value problem with two constant states (left and right)- in each cell interface to calculate the fluxes. The solution of the Riemann problem can be exact or approximate. An efficient exact Riemann solver has been presented by (Toro, 1992) in which an iterative procedure is used to solve a single algebraic equation. Since the exact solution of the Riemann problem may be computationally expensive, approximate Riemann solvers are usually preferred due to their simplicity and lower computational cost. Primitive Variable Riemann Solver, Riemann Solver Based on Exact Depth Positivity, Two-Rarefaction Riemann Solver, Two-Shock Riemann Solver, HLL (Harten Lax and van Leer) and HLLC Riemann solver are examples of approximate Riemann solvers that are presented in (Toro, 2001). Primitive Variable Riemann Solver may give negative depth in very shallow waters that are formed due to strong rarefactions. This problem is solved by considering depth positivity condition in Riemann Solver Based on Exact Depth Positivity and leads to a robust Riemann solver. Two Rarefaction Approximate Riemann solver assumes that both left and right waves in the solution of the Riemann problem are rarefaction waves and uses the exact Riemann solution for the case of two rarefaction wave. Although this assumption is not always correct, it results in quite accurate solutions (Toro, 1992). Two-Shock Riemann Solver is similar to the previous one, but it assumes that both left and right waves are shock waves.

HLL Riemann solver is another well-known Riemann solver, which directly gives an estimation for the numerical flux instead of depth and velocity in the star region. This Riemann solver is appropriate to solve one-dimensional cases, where the intermediate waves (i.e., contact discontinuities and shear waves) are ignored. HLLC Riemann solver, on the other hand, is a modification of the HLL Riemann solver to include the intermediate wave effects, and therefore, it is suitable for two-dimensional problems.

HLL and HLLC Riemann solvers are first order accurate methods to calculate the fluxes. Higher order accuracy in calculation of the interface fluxes can be achieved by extension of the first order Godunov upwind method to the higher order. Examples of such schemes are MUSCL-Hancock scheme (van Leer, 1985) and Weighted Average

Flux (WAF) method. The second order accuracy in time and space in MUSCL-Hancock scheme achieved by data reconstruction in cell interfaces using a piecewise linear function, evolving the reconstructed data in time by half time step, and solving the Riemann problem, based on the evaluated data from last step (Toro, 2001). WAF method, on the other hand, reaches the higher order accuracy by integrating and averaging the fluxes in time and space in cell interfaces, without necessarily need for piece-wise reconstruction step.

In real life application of the shallow water equations, it is likely to have a flow with irregular bed topography. Therefore, special attention should be paid to the numerical treatment of the bed slope source term to get more accurate solutions. This is especially important in stationary (constant water surface level and zero velocity) or near stationary situation, where the numerical equilibrium between flux gradient and the source term should be provided. To hold this equilibrium, Bermudez & Vazquez, 1994 suggested the upwind discretization of the source term in one dimensional cases with constant breadth. In 1998, Bermúdez, et al., 1998 applied the same idea to the two dimensional problems with the constant breadth and unstructured meshes. Later, M. Elena Vázquez-Cendón, 1999 used the idea to solve more general flow problems in channels with irregular geometry, but locally rectangular cross section. Zhou, et al., 2001 developed a simple and accurate method based on surface gradient method (SGM) and centered discretization of the source term. Later, Zhou, et al., 2002 extended the SGM into the channel containing vertical step. Audusse, et al., 2004 obtained a fast and stable first order and second order well-balanced schemes, based on the hydrostatic reconstruction and discontinuous discretization of the bed topography, which guarantee the positivity of depth in the domain. Later, well-balanced scheme of arbitrary order accuracy based on hydrostatic reconstruction is proposed by Noelle, et al., 2006.

Finally, Bollermann, et al., 2013 proposed a second order well-balanced central-upwind scheme that is positively preserving of the water depth. They suggested new construction of the water surface near dry areas to prevent the creation of negative

water depths at the cell interfaces during the reconstruction step (i.e., reconstruction of the water surface in each cell using slope limiters).

This study aims to investigate the solution of the depth averaged shallow water equations in channels with irregular bed and step-like discontinuity on it. Various test cases including smooth and sudden changes in the bed slope will be studied. The numerical test cases will be generally solved with the pure WAF method without well-balancing property, first order well-balanced scheme, and second order well-balanced scheme. Two test cases will be studied specifically, to show the capability of the developed codes in solving flows in regions with wet and dry areas. A special test case will be introduced in a prismatic channel that contains a champion-stage like steps in the middle of the channel, and one dimensional dam break flow and overtopping the flow over the steps will be studied. The goal is to produce the water surface profile without spurious oscillations and recover the steady-state flat hydrostatic water surface at the end of the solution.

In this chapter, general information, the objective of the study, and a brief literature review of the study are given. In chapter two, derivation of the governing equations and numerical methods that are used to solve the equations are explained. Chapter three introduces numerical test cases and corresponding analytical solutions. Numerical solutions of each test case are given in chapter four, where they are compared with the exact solution of them and with each other. Finally, the conclusions of the study and recommendations to the future works are presented in chapter five.

CHAPTER 2

SHALLOW WATER EQUATIONS AND THEIR NUMERICAL SOLUTION

2.1. Governing Equations in a Free Surface Water Flow

In general, the conservation laws of mass and momentum, called Navier-Stokes equations, are used to describe a Newtonian fluid flow. For an incompressible fluid these equations may be written as

$$\frac{\partial u}{\partial x}+\frac{\partial v}{\partial y}+\frac{\partial w}{\partial z}=0 \tag{2.1}$$

$$\frac{\partial u}{\partial t}+u\frac{\partial u}{\partial x}+v\frac{\partial u}{\partial y}+w\frac{\partial u}{\partial z}=-\frac{1}{\rho}\frac{\partial p}{\partial x}+\frac{1}{\rho}\left(\frac{\partial \tau_{xx}}{\partial x}+\frac{\partial \tau_{yx}}{\partial y}+\frac{\partial \tau_{zx}}{\partial z}\right) \tag{2.2}$$

$$\frac{\partial v}{\partial t}+u\frac{\partial v}{\partial x}+v\frac{\partial v}{\partial y}+w\frac{\partial v}{\partial z}=-\frac{1}{\rho}\frac{\partial p}{\partial y}+\frac{1}{\rho}\left(\frac{\partial \tau_{xy}}{\partial x}+\frac{\partial \tau_{yy}}{\partial y}+\frac{\partial \tau_{zy}}{\partial z}\right) \tag{2.3}$$

$$\frac{\partial w}{\partial t}+u\frac{\partial w}{\partial x}+v\frac{\partial w}{\partial y}+w\frac{\partial w}{\partial z}=-\frac{1}{\rho}\frac{\partial p}{\partial z}+\frac{1}{\rho}\left(\frac{\partial \tau_{xz}}{\partial x}+\frac{\partial \tau_{yz}}{\partial y}+\frac{\partial \tau_{zz}}{\partial z}\right)-g \tag{2.4}$$

where u, v and w are the velocity components in x, y and z directions respectively, p is pressure and τ_{ij} represents the viscous terms acting in $j-direction$ on the plane with outward normal in $i-direction$.

However, these equations cannot be used directly for a free surface water flow and they need to be modified. The reason for the modification is that the free surface is a boundary, however, the location of the boundary itself is unknown and it may vary with time. One assumption to deal with this difficulty is to assume that the depth of water is small compared with horizontal length scale such as wave length or free

surface curvature. This assumption leads to non-linear initial value problem which is called non-linear shallow water equations (Toro, 2001).

2.2. Derivation of Shallow Water Equations

2.2.1. Boundary Conditions

In derivation of SWE two kinds of boundary conditions are imposed, namely, *kinematic condition* and *dynamic condition*. Kinematic boundary condition simply says that there is no normal flow through the free surface. Therefore, the *relative* normal velocity should vanish at the free surface; see equation (2.8). At the bottom boundary, normal velocity itself should vanish, not the relative normal velocity; see equation (2.9). Dynamic boundary condition is imposed on the free surface which implies that the pressure is atmospheric at the free surface.

A schematic sketch of a free surface shallow water flow is depicted in Figure 2.1.

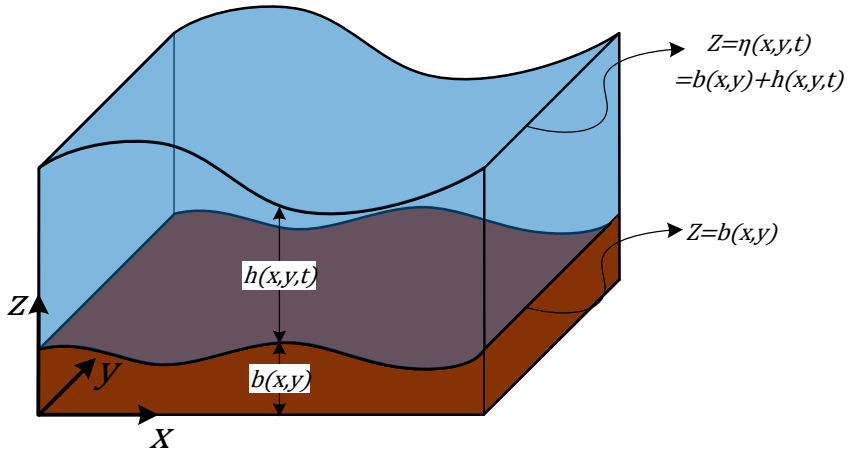

Figure 2.1. Free Surface Water Flow. The x-y plane is taken parallel to undisturbed water surface and z axis is in positive upward direction.

Mathematically, the kinematic boundary condition on the surface can be obtained by computing the total accelerations of the water particles at the surface boundary which is defined by the equation

$$z - \eta(x, y, t) = 0 \tag{2.5}$$

where $\eta(x, y, t)$ shows surface boundary location. Total derivatives of equation (2.5) can be written as

$$\frac{D}{Dt}(z - \eta) = 0 \tag{2.6}$$

Expanding equation (2.6) yields

$$\frac{\partial z}{\partial t} + u\frac{\partial z}{\partial x} + v\frac{\partial z}{\partial y} + w\frac{\partial z}{\partial z} = \frac{\partial \eta}{\partial t} + u\frac{\partial \eta}{\partial x} + v\frac{\partial \eta}{\partial y} + w\frac{\partial \eta}{\partial z} \tag{2.7}$$

Since z is independent variable, $\partial z/\partial t$, $\partial z/\partial t$ and $\partial z/\partial t$ derivatives are equal zero, and since η is independent of z, $\partial \eta/\partial z$ is vanished. Thus, equation (2.7) is simplified to

$$\left(\frac{\partial \eta}{\partial t} + u\frac{\partial \eta}{\partial x} + v\frac{\partial \eta}{\partial y} - w\right)\Big|_{z=\eta} = 0 \tag{2.8}$$

Similarly, boundary condition for the bottom is obtained as

$$\left(u\frac{\partial b}{\partial x} + v\frac{\partial b}{\partial y} - w\right)\Big|_{z=b} = 0 \tag{2.9}$$

Dynamic boundary condition is applied at the free surface as

$$p|_{z=\eta} = p_{atm} = 0 \tag{2.10}$$

where, for simplicity, the atmospheric pressure is taken as zero.

2.2.2. Continuity Equation

First step in derivation of the shallow water equations is integrating the continuity equation (2.1) with respect to z from bed to free surface as follows

$$\int_b^\eta \left(\frac{\partial u}{\partial x}+\frac{\partial v}{\partial y}+\frac{\partial w}{\partial z}\right)dz = 0 \tag{2.11}$$

$$w|_{z=\eta} - w|_{z=b} + \int_b^\eta \frac{\partial u}{\partial x}dz + \int_b^\eta \frac{\partial v}{\partial y}dz = 0 \tag{2.12}$$

Substituting boundary conditions (2.8) and (2.9), into equation (2.12) gives

$$\left(\frac{\partial \eta}{\partial t}+u\frac{\partial \eta}{\partial x}+v\frac{\partial \eta}{\partial y}\right)\Big|_{z=\eta} - \left(u\frac{\partial b}{\partial x}+v\frac{\partial b}{\partial y}\right)\Big|_{z=b} + \int_b^\eta \frac{\partial u}{\partial x}dz + \int_b^\eta \frac{\partial v}{\partial y}dz = 0 \tag{2.13}$$

Both integral terms in equation (2.13) can be simplified using Leibniz Rule. Leibniz integral rule is about how to bring the partial derivative of a multivariable integral inside the integral when the integral limits are functions of the differentiation variable.

Leibniz rule may be written as

$$\begin{aligned} &\frac{\partial}{\partial x}\int_{a(x)}^{b(x)} f(x,t)dt \\ &= \int_{a(x)}^{b(x)} \frac{\partial f(x,t)}{\partial x}dt + f\big(x,b(x)\big)\frac{db(x)}{dx} - f\big(x,a(x)\big)\frac{da(x)}{dx} \end{aligned} \tag{2.14}$$

Integral terms of equation (2.13) using Leibniz rule become

$$\begin{aligned} \int_b^\eta \frac{\partial u}{\partial x}dz &= \frac{\partial}{\partial x}\int_b^\eta u dz - u|_{z=\eta}\frac{\partial \eta}{\partial x} + u|_{z=b}\frac{\partial b}{\partial x} \\ &= \frac{\partial}{\partial x}(\bar{u}h) - u|_{z=\eta}\frac{\partial \eta}{\partial x} + u|_{z=b}\frac{\partial b}{\partial x} \end{aligned} \tag{2.15}$$

$$\int_b^\eta \frac{\partial v}{\partial y} dz = \frac{\partial}{\partial y}\int_b^\eta v dz - v|_{z=\eta}\frac{\partial \eta}{\partial y} + v|_{z=b}\frac{\partial b}{\partial y}$$
$$= \frac{\partial}{\partial y}(\bar{v}h) - v|_{z=\eta}\frac{\partial \eta}{\partial y} + v|_{z=b}\frac{\partial b}{\partial y} \tag{2.16}$$

Substituting the results back into equation (2.13) and simplifying yields

$$\frac{\partial h}{\partial t} + \frac{\partial}{\partial x}(\bar{u}h) + \frac{\partial}{\partial y}(\bar{v}h) = 0 \tag{2.17}$$

Equation (2.17) is the continuity equation written in differential conservation law form for shallow water equations. Note that overbars show the depth averaged values of u and v, and

$$\frac{\partial \eta}{\partial t} = \frac{\partial b}{\underbrace{\partial t}_{=0}} + \frac{\partial h}{\partial t} = \frac{\partial h}{\partial t} \tag{2.18}$$

2.2.3. Momentum Equations

One important assumption in derivation of the shallow water equations is that the vertical acceleration of the flow particles can be assumed to be negligible, which leads to a hydrostatic pressure distribution in $z - direction$. To prove, we can write the total acceleration in $z - direction$ and make it equal to zero as

$$\frac{Dw}{Dt} = \frac{\partial w}{\partial t} + u\frac{\partial w}{\partial x} + v\frac{\partial w}{\partial y} + w\frac{\partial w}{\partial z} = 0 \tag{2.19}$$

Substituting equation (2.19) into momentum equation in $z - direction$ (2.4) with neglected viscous terms, integrating from the bed to the surface, and applying dynamic boundary condition (2.10) yield

$$p = \rho g(\eta - z) \tag{2.20}$$

which is nothing but the hydrostatic pressure distribution in $z - direction$.

According to equation (2.20), pressure gradients in x and $y-directions$ become

$$\frac{\partial p}{\partial x} = \rho g \frac{\partial \eta}{\partial x} \tag{2.21}$$

$$\frac{\partial p}{\partial y} = \rho g \frac{\partial \eta}{\partial y} \tag{2.22}$$

Equations (2.21) and (2.22) show that the u and v velocities are independent of variable z, since pressure gradients in x and $y-directions$ are independent of z, which means

$$\frac{\partial u}{\partial z} = \frac{\partial v}{\partial z} = 0 \tag{2.23}$$

Therefore, x and $y-$ momentum equations, (2.2) and (2.3) become

$$\frac{\partial u}{\partial t} + u\frac{\partial u}{\partial x} + v\frac{\partial u}{\partial y} = -g\frac{\partial \eta}{\partial x} + \frac{1}{\rho}\left(\frac{\partial \tau_{xx}}{\partial x} + \frac{\partial \tau_{yx}}{\partial y} + \frac{\partial \tau_{zx}}{\partial z}\right) \tag{2.24}$$

$$\frac{\partial v}{\partial t} + u\frac{\partial v}{\partial x} + v\frac{\partial v}{\partial y} = -g\frac{\partial \eta}{\partial y} + \frac{1}{\rho}\left(\frac{\partial \tau_{xy}}{\partial x} + \frac{\partial \tau_{yy}}{\partial y} + \frac{\partial \tau_{zy}}{\partial z}\right) \tag{2.25}$$

Now, the equations (2.24) and (2.25) should be integrated from bottom to free surface as follows. Integrating equation (2.24) yields

$$\begin{aligned} &\int_b^\eta \frac{\partial u}{\partial t}\, dz + \int_b^\eta u\frac{\partial u}{\partial x}\, dz + \int_b^\eta v\frac{\partial u}{\partial y}\, dz \\ &= \int_b^\eta -g\frac{\partial \eta}{\partial x} dz + \int_b^\eta \frac{1}{\rho}\left(\frac{\partial \tau_{xx}}{\partial x} + \frac{\partial \tau_{yx}}{\partial y} + \frac{\partial \tau_{zx}}{\partial z}\right) dz \end{aligned} \tag{2.26}$$

$$\begin{aligned} &h\frac{\partial \bar{u}}{\partial t} + \bar{u}h\frac{\partial \bar{u}}{\partial x} + \bar{v}h\frac{\partial \bar{u}}{\partial y} \\ &= -gh\frac{\partial b}{\partial x} - gh\frac{\partial h}{\partial x} + \int_b^\eta \frac{1}{\rho}\left(\frac{\partial \tau_{xx}}{\partial x} + \frac{\partial \tau_{yx}}{\partial y} + \frac{\partial \tau_{zx}}{\partial z}\right) dz \end{aligned} \tag{2.27}$$

Note that

$$\frac{\partial \eta}{\partial x} = \frac{\partial b}{\partial x} + \frac{\partial h}{\partial x} \tag{2.28}$$

By multiplying the continuity equation (2.17) with $\bar{u}$ and adding it up with equation (2.27), the conservative form of the momentum equation in $x - direction$ can be obtained. With some simplification, the conservative form of the momentum equation in $x - direction$ becomes

$$\begin{aligned} &\frac{\partial(\bar{u}h)}{\partial t} + \frac{\partial\left(h\bar{u}^2 + \frac{1}{2}gh^2\right)}{\partial x} + \frac{\partial(h\overline{uv})}{\partial y} \\ &= -ghS_{0,x} + \int_b^\eta \frac{1}{\rho}\left(\frac{\partial \tau_{xx}}{\partial x} + \frac{\partial \tau_{yx}}{\partial y} + \frac{\partial \tau_{zx}}{\partial z}\right) dz \end{aligned} \tag{2.29}$$

Now, the viscous stresses integral term can be simplified further by integrating it over depth as

$$\begin{aligned} &\int_b^\eta \frac{1}{\rho}\left(\frac{\partial \tau_{xx}}{\partial x} + \frac{\partial \tau_{yx}}{\partial y} + \frac{\partial \tau_{zx}}{\partial z}\right) dz \\ &= \frac{1}{\rho}\left(\frac{\partial}{\partial x}\int_b^\eta \tau_{xx}\, dz - \tau_{xx,\eta}\frac{\partial \eta}{\partial x} + \tau_{xx,b}\frac{\partial b}{\partial x}\right) \\ &+ \frac{1}{\rho}\left(\frac{\partial}{\partial y}\int_b^\eta \tau_{yx}\, dz - \tau_{yx,\eta}\frac{\partial \eta}{\partial y} + \tau_{yx,b}\frac{\partial b}{\partial y}\right) \\ &+ \left(\tau_{zx,\eta} - \tau_{zx,b}\right) \\ &= \frac{1}{\rho}\frac{\partial}{\partial x}\int_b^\eta \tau_{xx}\, dz + \frac{1}{\rho}\int_b^\eta \tau_{yx}\, dz - \frac{1}{\rho}\left(\tau_{xx,\eta}\frac{\partial \eta}{\partial x} + \tau_{yx,\eta}\frac{\partial \eta}{\partial y} - \tau_{zx,\eta}\right) \\ &+ \frac{1}{\rho}\left(\tau_{xx,b}\frac{\partial b}{\partial x} + \tau_{yx,b}\frac{\partial b}{\partial y} - \tau_{zx,b}\right) \\ &= \frac{1}{\rho}\frac{\partial \overline{\tau_{xx}}}{\partial x} + \frac{1}{\rho}\frac{\partial \overline{\tau_{yx}}}{\partial y} + \frac{1}{\rho}\left(\tau_{x,\eta} + \tau_{x,b}\right) \end{aligned} \tag{2.30}$$

where $\tau_{x,\eta}$ and $\tau_{x,b}$ are the shear stresses tangent to the free surface and bottom respectively,

$$\tau_{x,s} = \tau_{xx,\eta}\frac{\partial \eta}{\partial x} + \tau_{yx,\eta}\frac{\partial \eta}{\partial y} - \tau_{zx,\eta}$$
$$\tau_{x,b} = \tau_{xx,b}\frac{\partial b}{\partial x} + \tau_{yx,b}\frac{\partial b}{\partial y} - \tau_{zx,b} \tag{2.31}$$

Bottom shear stress in equation (2.31) can be estimated from

$$\tau_{x,b} = \rho C_f \bar{u}\sqrt{\bar{u}^2 + \bar{v}^2} \tag{2.32}$$

where C_f is the bed roughness coefficient and can be evaluated as

$$C_f = \frac{gn^2}{h^{1/3}} \tag{2.33}$$

where *n* is the Manning's roughness coefficient at the bottom surface.

Repeating the same procedure in y-direction, 2D conservative shallow water equations can be written as

$$\frac{\partial h}{\partial t} + \frac{\partial}{\partial x}(\bar{u}h) + \frac{\partial}{\partial y}(\bar{v}h) = 0 \tag{2.34}$$

$$\frac{\partial(\bar{u}h)}{\partial t} + \frac{\partial\left(h\bar{u}^2 + \frac{1}{2}gh^2\right)}{\partial x} + \frac{\partial(h\overline{uv})}{\partial y} = -ghS_{0,x} + \frac{1}{\rho}\left(\frac{\partial \overline{\tau_{xx}}}{\partial x} + \frac{\partial \overline{\tau_{yx}}}{\partial y} + \left(\tau_{x,s} + \tau_{x,b}\right)\right) \tag{2.35}$$

$$\frac{\partial(\bar{v}h)}{\partial t} + \frac{\partial(h\overline{uv})}{\partial x} + \frac{\partial\left(h\bar{v}^2 + \frac{1}{2}gh^2\right)}{\partial y} = -ghS_{0,y} + \frac{1}{\rho}\left(\frac{\partial \overline{\tau_{xy}}}{\partial x} + \frac{\partial \overline{\tau_{yy}}}{\partial y} + \left(\tau_{y,s} + \tau_{y,b}\right)\right) \tag{2.36}$$

These equations can be written in vector form as

$$\frac{\partial U}{\partial t}+\frac{\partial F(U)}{\partial x}+\frac{\partial G(U)}{\partial y}=S(U) \tag{2.37}$$

where

$$U=\begin{bmatrix} h \\ hu \\ hv \end{bmatrix} \tag{2.38}$$

$$F(U)=\begin{bmatrix} hu \\ hu^2+\frac{1}{2}gh^2 \\ huv \end{bmatrix} \tag{2.39}$$

$$G(U)=\begin{bmatrix} hv \\ hvu \\ hv^2+\frac{1}{2}gh^2 \end{bmatrix} \tag{2.40}$$

$$S(U)=\begin{bmatrix} 0 \\ -ghS_{0,x}-C_f u\sqrt{u^2+v^2} \\ -ghS_{0,y}-C_f v\sqrt{u^2+v^2} \end{bmatrix}-\begin{bmatrix} 0 \\ \frac{\partial \tau_{xx}}{\partial x}+\frac{\partial \tau_{yx}}{\partial y}+\tau_{x,\eta} \\ \frac{\partial \tau_{xy}}{\partial x}+\frac{\partial \tau_{yy}}{\partial y}+\tau_{y,\eta} \end{bmatrix} \tag{2.41}$$

In these equations, the overbars are eliminated for simplicity, assuming that all the variables are depth-averaged. In above equations, U is the vector of conserved variables, F(U) and G(U) are the fluxes vectors, and S(U) is the source term vector.

For homogeneous, incompressible and inviscid flow, source term vector (2.41) can reduce to

$$S(U)=\begin{bmatrix} 0 \\ -ghS_{0,x}-C_f u\sqrt{u^2+v^2} \\ -ghS_{0,y}-C_f v\sqrt{u^2+v^2} \end{bmatrix} \tag{2.42}$$

2.3. Numerical Solution of Shallow Water Equations

2.3.1. Finite Volume Method

In Finite Volume Method (FVM) the domain is divided into the finite number of non-overlapping cells, called control volumes (CV), at the centroid of which, computational nodes are located. In 2D these cells are polygons, e.g., triangles, quadrilaterals, etc. In FVM, the conservation laws are applied to each CV and the equations are integrated over each cell and over each time step.

System of one-dimensional conservation laws, neglecting the source term, can be written as

$$\frac{\partial}{\partial t}u + \frac{\partial}{\partial x}f(u) = 0 \tag{2.43}$$

Integrating equation (2.43) over cell *i*, which is $\Delta x_i = [x_{i-\frac{1}{2}}, x_{i+\frac{1}{2}}]$ yields

$$\frac{\partial}{\partial t}U_i \Delta x = -\left[f(u(t, x_{i+\frac{1}{2}})) - f(u(t, x_{i-\frac{1}{2}}))\right] \tag{2.44}$$

And, integrating equation (2.44) over time step Δt, from $[t^n, t^{n+1}]$, gives

$$U_i^{n+1} = U_i^n - \frac{\Delta t}{\Delta x}\left[F_{i+\frac{1}{2}} - F_{i-\frac{1}{2}}\right] \tag{2.45}$$

In above equations, U_i^n and U_i^{n+1} are the cell averaged of conserved variable u_i over Δx_i,

$$U_i = \frac{1}{\Delta x_i}\int_{x_{i-\frac{1}{2}}}^{x_{i+\frac{1}{2}}} u_i \, dx \tag{2.46}$$

at time levels n and $n+1$, respectively, and $F_{i\pm\frac{1}{2}}$ are the time average of the fluxes $f_{i\pm\frac{1}{2}}$ over time interval Δt,

$$F_{i\pm\frac{1}{2}} = \frac{1}{\Delta t}\int_{t^n}^{t^{n+1}} f_{i\pm\frac{1}{2}} \tag{2.47}$$

One challenging step in schemes based on Finite Volume Method is the computation of the interface fluxes $F_{i\pm\frac{1}{2}}$. Among several methods, the Weighted Averaged Flux (WAF) method is used in this study to calculate the fluxes, which will be discussed in detail in section 2.3.4.

2.3.2. Godunov's Method and Riemann Problem

The Godunov's method is a first order upwind method which uses the piecewise cell-averaged data (2.46) in each cell, to compute the interface fluxes by solving the Riemann Problem, exactly or approximately, in that interface. First order Godunov's scheme can be extended to higher order of accuracy in time and space. Examples of second order Godunov's type schemes in time and space are Weighted Average Flux (WAF) and MUSCL-Hancock schemes.

Considering discretized form of the equations (2.45), and assuming that the U_i^n are piecewise constant data in each cell, that is integral averaged of the data over cell $\Delta x_i = [x_{i-\frac{1}{2}}, x_{i+\frac{1}{2}}]$ at time $t = t^n$ as in equation (2.46), the flux value in each cell interface is computed by solving the initial value problem (2.48), where U_L (is equal U_i^n) and U_R (is equal U_{i+1}^n) are the constant cell-averaged data at the left and right of the cell interface, respectively. Initial value problem of the form (2.48) is called Riemann problem. In general, Godunov-type Methods are the methods which solve the Riemann Problem

$$\begin{aligned} &U_t + F_x(U) = 0 \\ &U(x,0) = \begin{cases} U_L & if\ x < 0 \\ U_R & if\ x > 0 \end{cases} \end{aligned} \tag{2.48}$$

locally at each cell interfaces to calculate fluxes.

The schematic stencil of the first order Godunov's scheme is depicted in Figure 2.2. Solution of the Riemann problem is depended on the wave speeds x/t. First order Godunov's scheme uses the solution of the Riemann problem at $x/t = 0$, which is $U_{i+\frac{1}{2}}(x/t) = U(x/t = 0)$, (see Figure 2.2) and flux function $F(U)$ to evaluate the flux value at each interface, i.e., $F\left(U_{i+\frac{1}{2}}(x/t = 0)\right)$.

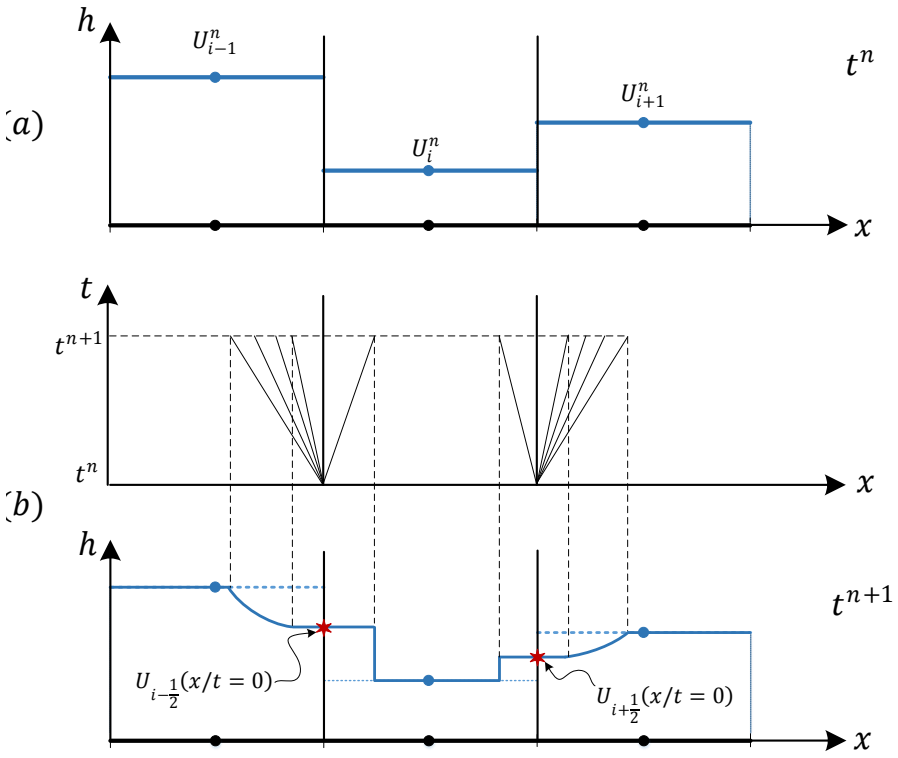

Figure 2.2. Stencil of first order Godunov's method: a) cell average data at t = t^n and, b) solution of Riemann problem at t = t^{n+1}

2.3.3. Approximate Riemann Solvers

The solution of Riemann Problem (2.48) consists of the left and right waves, which are either shock waves or rarefaction waves. The middle wave is a share wave, which appears in the presence of y-momentum equation, i.e., two-dimensional cases. There are four possible wave patterns in x-t domain that are shown in Figure 2.3.

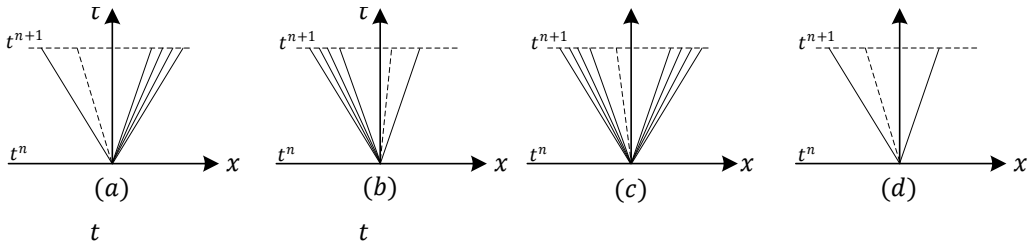

Figure 2.3. Four possible wave pattern in the solution of Riemann Problem for two dimensional shallow water equations in x-direction. a) left wave is shock wave and right wave is rarefaction wave b) left wave is rarefaction wave and right wave is shock wave c) left and right waves are rarefaction waves and, d) left and right waves are shock waves

These waves divide the x-t domain into three regions: (i) The left region where $U=U_L$, (ii) the right region where $U=U_R$ and (iii) the middle region where $U=U^*$ which is called star region.

U^* data can be calculated using an exact or approximate Riemann solver. As an example of exact Riemann solver, (Toro, 1992) proposed an efficient exact Riemann solver which uses an iterative procedure to determine the wave patterns and the star region data U^*.

No matter how the exact solvers are efficient, there are still approximate Riemann solvers, which are sufficiently accurate and can reduce the computation cost compared with the exact solvers. These solvers are preferred due to their simplicity and acceptable accuracy, alongside with their time and cost efficiency.

2.3.3.1. The HLL Approximate Riemann Solver

Harten, Lax, and van Leer (HLL) (Harten, et al., 1983) suggested an approximation to calculate the numerical flux at the star region directly, instead of estimation for data (i.e., depth and unit discharge (or speed)) in the star region. In HLL Riemann solver, which is used in this study, intermediate waves are ignored, therefore, it is not appropriate solver for two dimensional cases where there are contact shear waves due to the presence of y-momentum equation. HLLC is the modified version of HLL

Riemann solver that takes account of the presence of shear waves and thus, it is appropriate Riemann solver for two-dimensional problems (details can be found in (Toro, 2001)).

HLL Riemann solver uses data $U_L = U_i,\ U_R = U_{i+1}$, and corresponding fluxes $F_L = F(U_L)$ and $F_R = F(U_R)$, and assumes S_L and S_R to be the left and right wave speeds in the solution of the Riemann problem, and gives the numerical flux at cell interface as

$$F_{i+\frac{1}{2}} = \begin{cases} F_L & if \quad S_L > 0 \\ F^{HLL} = \dfrac{S_R F_L - S_L F_R + S_R S_L (U_R - U_L)}{S_R - S_L} & if \quad S_L \le 0 \le S_R \\ F_R & if \quad S_R < 0 \end{cases} \tag{2.49}$$

The solution structure of the Riemann problem with HLL Riemann solver with two waves (one dimensional case) is depicted in Figure 2.4.

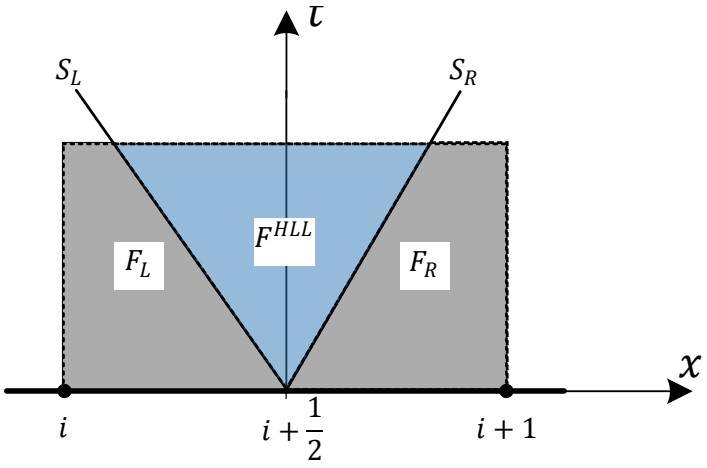

Figure 2.4. Illustration of the left and right waves in the solution of Riemann Problem and locations corresponded to the left, right, and star region fluxes in the structure of HLL Riemann solver for one-dimensional SWE.

In the calculation of HLL fluxes, left and right wave speeds (S_L and S_R) are needed. Toro, 2001 suggests formula (2.52) ~ (2.55) for the wave speeds that lead to accurate and robust scheme. In the corresponded approximations, the value of the depth at star region (h^*) is also needed, which can be obtained approximately from other Riemann solvers. Toro, 2001 recommends the following formula for the h^*:

$$h^* = \frac{1}{g}\left[\frac{1}{2}(c_L + c_R) + \frac{1}{4}(u_L - u_R)\right]^2 \tag{2.50}$$

where, u_L and u_R are the speeds at the left and right of the interface and, c_L and c_R are celerity according to the depths in the left and right of the cell interface, respectively,

$$\begin{aligned} c_L &= \sqrt{g h_L} \\ c_R &= \sqrt{g h_R} \end{aligned} \tag{2.51}$$

Wave speeds can be calculated as follows:

a) **Left Wave Speed (Wet Bed):** in the case of wet bed at both left and right sides of the interface, if $h^* \leq h_L$, then the left wave is a rarefaction wave; otherwise, the left wave is a shock wave. The speed is calculated from

$$\begin{cases} S_L = u_L - c_L & if\ h^* \leq h_L \\ S_L = u_L - c_L\sqrt{\frac{1}{2}\left[\frac{(h^* + h_L)h^*}{h_L^2}\right]} & if\ h^* > h_L \end{cases} \tag{2.52}$$

b) **Right Wave Speed (Wet Bed):** similarly, if $h^* \leq h_R$ then the right wave is a rarefaction wave; otherwise the wave is a shock wave. Right wave speed is calculated from

$$\begin{cases} S_R = u_R + c_R & if\ h^* \leq h_R \\ S_R = u_R + c_R\sqrt{\frac{1}{2}\left[\frac{(h^* + h_R)h^*}{h_R^2}\right]} & if\ h^* > h_R \end{cases} \tag{2.53}$$

In the presence of the dry region in the solution, the speeds are given as follow,

c) Dry Bed on the Right:

If the area at the right of the cell interface is dry, then the left and right waves are estimated as

$$\begin{cases} S_L = u_L - c_L \\ S_R = u_L + 2\,c_L \end{cases} \tag{2.54}$$

d) Dry Bed on the Right:

And, if the left region of the cell interface is dry then the speeds are

$$\begin{cases} S_L = u_R - 2\,c_R \\ S_R = u_R + c_R \end{cases} \tag{2.55}$$

2.3.4. Weighted Average Flux (WAF) Scheme

By integrating the set of one dimensional conservation laws, equations (2.43), over time and space, the discretized version of the equations were obtained as (2.45), where each particular scheme uses a particular method to calculate the interface fluxes $F_{i\pm\frac{1}{2}}$.

Among the several choices, Weighted Averaged Flux (WAF) is proposed by Toro, 1989, which is a second order extension of the first order Godunov's upwind method. Original WAF method is oscillatory; therefore, TVD version of the method which is oscillation-free must be used.

General structure of the Riemann problem and WAF method is depicted in Figure 2.5.

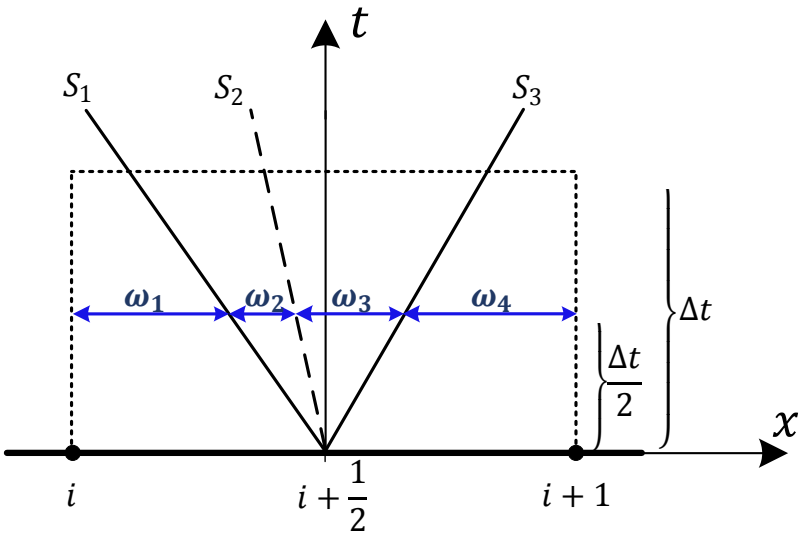

Figure 2.5. Structure of the Riemann problem solution and illustration of the weights in WAF method.

The numerical interface flux using Weighted Average Flux, can be written in integral average form as (Toro, 2001)

$$F_{i+\frac{1}{2}}^{waf} = \frac{1}{t_2 - t_1}\frac{1}{x_2 - x_1}\int_{t}^{t+\Delta t}\int_{-\Delta x/2}^{\Delta x/2} F\big(U(x,t)\big)\,dx\,dt \tag{2.56}$$

By using the midpoint rule, the time integration can be approximated at $t = \frac{1}{2}\Delta t$ as

$$F_{i+\frac{1}{2}}^{waf} = \frac{1}{\Delta x}\int_{-\Delta x/2}^{\Delta x/2} F\left(U_{i+\frac{1}{2}}\left(x, \frac{1}{2}\Delta t\right)\right)\,dx \tag{2.57}$$

The integral in equation (2.57) can be calculated with the summation

$$F_{i+\frac{1}{2}}^{waf} = \sum_{k=1}^{N+1} \omega_k F_{i+\frac{1}{2}}^{(k)} \tag{2.58}$$

where N is the number of waves in the solution of Riemann Problem and $F_{i+\frac{1}{2}}^{(k)}$ is the flux value in the interval k. ω_k are the weights (see Figure 2.5), which are defined as

$$\omega_k = \frac{1}{2}(c_k - c_{k-1}) \tag{2.59}$$

for $k = 1$ to $N + 1$. c_k is the Courant number for wave k which is defined as

$$c_k = \frac{\Delta t S_k}{\Delta x} \tag{2.60}$$

where, $c_0 = -1$ and $c_{N+1} = 1$. Putting all back into the equation (2.58) the weighted averaged of the flux is obtain as

$$F_{i+\frac{1}{2}}^{waf} = \frac{1}{2}(F_i + F_{i+1}) - \frac{1}{2}\sum_{k=1}^{N} c_k \Delta F_{i+\frac{1}{2}}^{(k)} \tag{2.61}$$

where

$$\Delta F_{i+\frac{1}{2}}^{(k)} = F_{i+\frac{1}{2}}^{(k+1)} - F_{i+\frac{1}{2}}^{(k)} \tag{2.62}$$

is the flux jump over wave k.

2.3.4.1. Total Variation Diminishing (TVD) and Monotonicity

First order upwind schemes are stable and non-oscillatory schemes, but they introduce artificial and fallacious diffusivity into the solutions. On the other hand, higher order schemes are more accurate, but they can be oscillatory. However, higher order schemes based on the Total Variation Diminishing (TVD) exist, that although they bring higher order accuracy, they are also oscillation free.

A scheme is said to be monotonicity preserving, if it holds two conditions, a) if it does not create new minimums/maximums in the solution and b) if it does not amplify the already existing minimums/maximums; In other word, if the scheme does not create overshoots or undershoots. Monotonicity is related to "Total Variation (TV)" of a discrete solution. Consider the arbitrary solution domain with the solution data φ as in Figure 2.6.

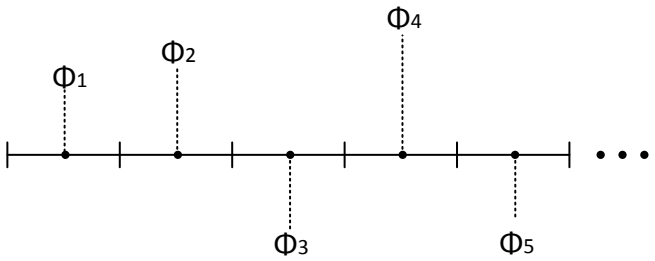

Figure 2.6. An arbitrary solution domain presentation.

Total variation of the variable φ can be written as a summation below,

$$TV = \sum_{1}^{N} |\varphi_{i+1} - \varphi_i| = |\varphi_2 - \varphi_1| + |\varphi_3 - \varphi_2| + |\varphi_4 - \varphi_3| + \cdots \qquad (2.63)$$

If the total variation (2.63) does not grow in time, then the monotonicity is preserved. This property is guaranteed in TVD schemes.

TVD schemes uses limiters function ψ. This function is defined according to the definition r, which is the ratio of the upwind-side gradient to the downwind-side gradient of the variable, as written in equation (2.64).

$$r = \frac{\Delta\varphi_{upwind}}{\Delta\varphi_{downwind}} \qquad (2.64)$$

According to Sweby, 1984, a scheme is TVD if the function ψ lies in the region in $\psi - r$ diagram shown in Figure 2.7.

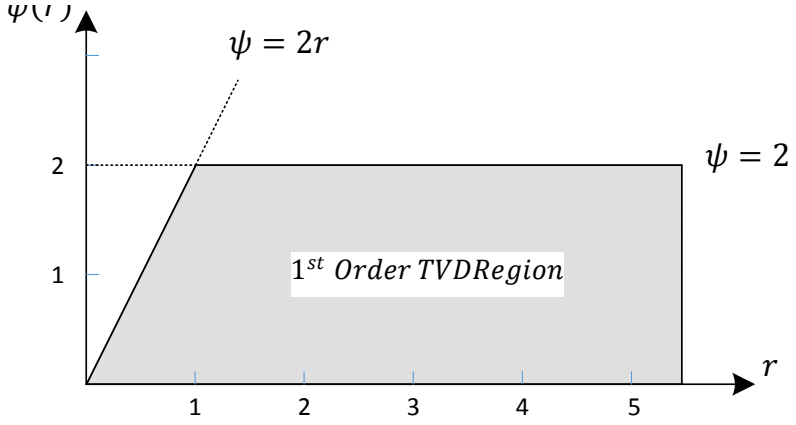

Figure 2.7. First order TVD region

And, Sweby, 1984 showed that a TVD scheme is second order if it lies in region shown in Figure 2.8.

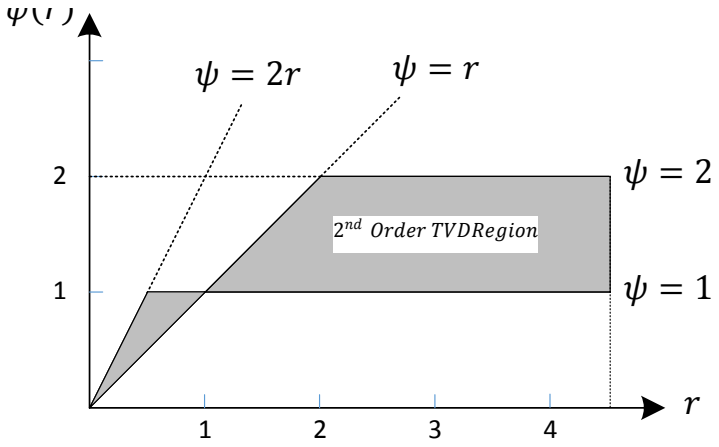

Figure 2.8. Second order TVD region

Among the several possibilities, some choices for TVD limiter function are SUPERBEE, van Leer, van Albada and Min-Mod, which are defined as below:

$$\psi_{SUPERBEE}(r) = \max[0, \min(1,2r), \min(2, r)] \tag{2.65}$$

$$\psi_{Van\ Leer}(r) = \frac{r + |r|}{1 + r} \tag{2.66}$$

$$\psi_{Van\ Albada}(r) = \frac{r + r^2}{1 + r^2} \tag{2.67}$$

$$\psi_{Min-Mod}(r) = \min(1, r) \tag{2.68}$$

All the second order limiter functions pass through the point (1,1) in $\psi - r$ diagram and they all are zero if the r value is negative. Comparison of some famous limiter functions are illustrated in Figure 2.9.

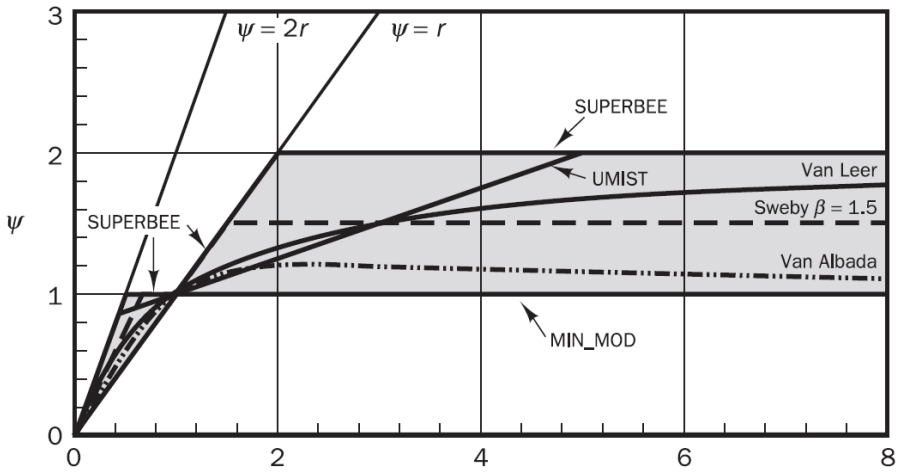

Figure 2.9. Illustration of some famous second-order limiter functions (Versteeg & Malalasekera, 2007).

2.3.4.2. TVD Version of WAF and TVD Limiters

Equation (2.61) is oscillatory near the high gradients (Toro, 1989) and should be modified with the Total Variation Diminishing constraint. TVD version of the equation (2.61) can be written as

$$F_{i+\frac{1}{2}}^{waf} = \frac{1}{2}(F_i + F_{i+1}) - \frac{1}{2}\sum_{k=1}^{N} sign(c_k) A_k \Delta F_{i+\frac{1}{2}}^{(k)} \tag{2.69}$$

where A_k is the WAF limiter function. A_k is defined as

$$A_k = 1 - (1 - |c|)\psi(r) \tag{2.70}$$

where c is the Courant number, ψ in the limiter function and r is defined as

$$r^{(k)} = \begin{cases} \dfrac{q_i^{(k)} - q_{i-1}^{(k)}}{q_{i+1}^{(k)} - q_i^{(k)}} & if\ c_k > 0 \\ \dfrac{q_{i+2}^{(k)} - q_{i+1}^{(k)}}{q_{i+1}^{(k)} - q_i^{(k)}} & if\ c_k < 0 \end{cases} \tag{2.71}$$

For two-dimensional shallow water equations, in $x - direction$, q can be selected as $q = h$ for non-linear waves and $q = v$ for the shear wave (Toro, 2001).

2.3.5. Well-Balanced Hydrostatic Reconstruction

A numerical scheme solving the shallow water equations is said to be well-balanced if the source term corresponding to the bed slope in the momentum equation is treated in such a way that it preserves exactly the water at rest or stationary solution, i.e.,

$$\begin{aligned} u &= 0 \\ h + z &= constant. \end{aligned} \tag{2.72}$$

In stationary situation, the shallow water equations reduce to

$$\left(\frac{1}{2} g h^2\right)_x = -ghz_x \tag{2.73}$$

To obtain a well-balanced scheme, the hydrostatic flux term in left hand side of the equation (2.73) should be numerically well-balanced with the bed slope source term in the right hand side. Among the several well-balanced schemes, (Audusse, et al., 2004) propose “hydrostatic reconstruction scheme” and obtain first order and second order well-balanced schemes. Later, higher order well-balanced scheme called WENO is introduced by (Noelle, et al., 2006).

2.3.5.1. Discretization of the Source Term

Semidiscrete finite volume form of the discretized equations can be written as

$$\Delta x_i \frac{\partial}{\partial t} U_i(t) + \left(F_{i+\frac{1}{2}} - F_{i-\frac{1}{2}}\right) = S_i \tag{2.74}$$

where U_i is the vector of cell-averaged variables $(h_i, q_i)^T$and $F_{i\pm\frac{1}{2}}$ are the flux functions calculated from solving the Riemann problem according to the Riemann states at left and right of the cell interfaces as

$$\begin{aligned} F_{i+\frac{1}{2}} &= F\left(U_{i+\frac{1}{2}^{(l)}}, U_{i+\frac{1}{2}^{(r)}}\right) \\ F_{i-\frac{1}{2}} &= F\left(U_{i-\frac{1}{2}^{(l)}}, U_{i-\frac{1}{2}^{(r)}}\right) \end{aligned} \tag{2.75}$$

where $U_{i+\frac{1}{2}^{(l)}}$ and $U_{i+\frac{1}{2}^{(r)}}$ stand for the U at the left and right of the cell interface $i+\frac{1}{2}$, respectively. For nearly stationary state, i.e. $u \ll \sqrt{gh}$, equation (2.73) is the necessary condition to hold the balance between hydrostatic pressure term and the bed slope source term. According to this equality, Audusse, et al., 2004 use the discrete gradient of the hydrostatic momentum flux $\left(\frac{1}{2}gh^2\right)_x$ instead of the bed slope source term. By integrating equation (2.73) over cell i from $x_{i-1/2}$ to $x_{i+1/2}$, the source term, S_i in equation (2.74) can be obtained as

$$-\int_{x\, i-1/2^{(r)}}^{x\, i+1/2^{(l)}} ghz_x = \int_{x\, i-1/2^{(r)}}^{x\, i+1/2^{(l)}} \frac{\partial}{\partial x}\left(\frac{1}{2}gh^2\right) = \frac{g}{2}\left(h^2_{i+1/2^{(l)}} - h^2_{i-1/2^{(r)}}\right)$$

$$S_i = \frac{g}{2}\begin{pmatrix} 0 \\ h^2_{i+1/2^{(l)}} - h^2_{i+1/2^{(r)}} \end{pmatrix} \tag{2.76}$$

Indeed, with this kind of discretization, cell-averaged source term is distributed to the cell interfaces. The details are shown in equations (2.83) ~ (2.86) for the first order scheme and (2.98) ~ (2.102) for the second order scheme.

Audusse, et al., 2004 suggest the following reconstructed value for h and z at cell interfaces

$$z^*_{i+\frac{1}{2}} = max\left(z_{i,r}, z_{i+1,l}\right) \tag{2.77}$$

$$h^*_{i+\frac{1}{2}^-} = max\left(0, z_{i,r} + h_{i,r} - z^*_{i+\frac{1}{2}}\right) \tag{2.78}$$

$$h^*_{i+\frac{1}{2}^+} = max\left(0, z_{i+1,l} + h_{i+1,l} - z^*_{i+\frac{1}{2}}\right) \tag{2.79}$$

where $z_{i,r}$ and $z_{i+1,l}$ are the bed elevation at the right of the cell i and the left of the cell $i+1$, respectively. $h_{i,r}$ and $h_{i+1,l}$ are defined at the same manner. Audusse, et al., 2004 prove that this reconstruction of the variables provides non-negativity of the water height, even while cell starts to dry out.

2.3.5.2. First Order Well-Balanced Scheme Based on Hydrostatic Reconstruction

For the first order well-balanced scheme the reconstructed values become

$$z^*_{i+\frac{1}{2}} = max(z_i, z_{i+1}) \tag{2.80}$$

$$h^*_{i+1/2^{(l)}} = max\left(0, z_i + h_i - z^*_{i+\frac{1}{2}}\right) \tag{2.81}$$

$$h^*_{i+1/2^{(r)}} = max\left(0, z_{i+1} + h_{i+1} - z^*_{i+\frac{1}{2}}\right) \tag{2.82}$$

The location of the reconstructed variables is depicted in Figure 2.10.

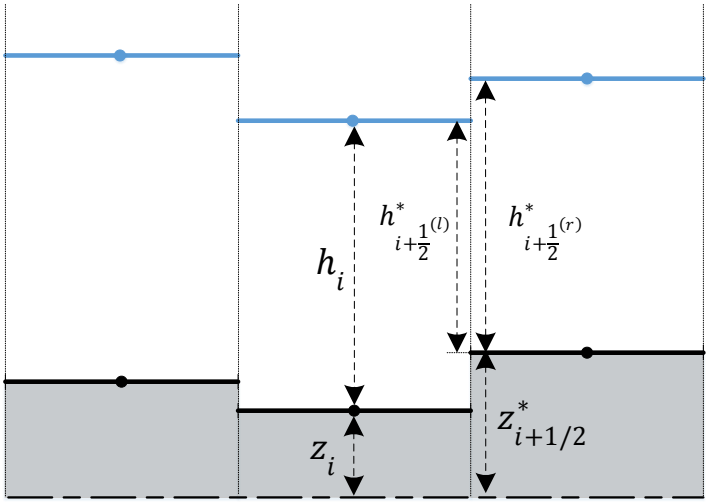

Figure 2.10. Illustration of the reconstructed variables for the first-order well-balanced scheme.

The source term (2.76) can be rewritten as

$$S_i = S_{i+1/2^{(l)}} + S_{i-1/2^{(r)}} = \frac{g}{2}\begin{pmatrix} 0 \\ h^{*\,2}_{i+1/2^{(l)}} - h_i^2 \end{pmatrix} + \frac{g}{2}\begin{pmatrix} 0 \\ h_i^2 - h^{*\,2}_{i-1/2^{(r)}} \end{pmatrix} \tag{2.83}$$

Now, the equation (2.74) can be modified by distributing the source term (2.83) to left and right fluxes and can be rewritten as

$$\Delta x_i \frac{\partial}{\partial t} U_i(t) + F^{left}_{i+\frac{1}{2}}(U_i, U_{i+1}, z_i, z_{i+1}) - F^{right}_{i-\frac{1}{2}}(U_{i-1}, U_i, z_{i-1}, z_i) = 0 \tag{2.84}$$

with modified fluxes

$$\begin{aligned} F^{left}_{i+\frac{1}{2}}(U_i, U_{i+1}, z_i, z_{i+1}) &= F_{i+\frac{1}{2}}\left(U_{i+1/2^{(l)}}, U_{i+1/2^{(r)}}\right) - S_{i+\frac{1}{2}^{(l)}} \\ &= F_{i+\frac{1}{2}}\left(U_{i+1/2^{(l)}}, U_{i+1/2^{(r)}}\right) + \frac{g}{2}\begin{pmatrix} 0 \\ h_i^2 - h^{*\,2}_{i+1/2^{(l)}} \end{pmatrix} \end{aligned} \tag{2.85}$$

$$F^{right}_{i-\frac{1}{2}}(U_{i-1}, U_i, z_{i-1}, z_i) = F_{i-\frac{1}{2}}\left(U_{\,i-1/2^{(l)}}, U_{\,i-1/2^{(r)}}\right) + S_{\,i-\frac{1}{2}^{(r)}}$$
$$= F_{i-\frac{1}{2}}\left(U_{\,i-1/2^{(l)}}, U_{\,i-1/2^{(r)}}\right) + \frac{g}{2}\begin{pmatrix} 0 \\ h_i^2 - h^{*\,2}_{\,i-1/2^{(r)}} \end{pmatrix} \tag{2.86}$$

where $F^{left}_{(.)}$ and $F^{right}_{(.)}$ are denoted to the F at the left and right of the cell interface (.) respectively. With the CFL condition of $CFL \leq 1$ and uniform mesh size, the fully discrete form of the equations can be written as

$$U_i^{n+1} = U_i^n - \frac{\Delta t}{\Delta x}\left[F^{left}_{i+\frac{1}{2}}(U_i, U_{i+1}, z_i, z_{i+1}) - F^{right}_{i-\frac{1}{2}}(U_{i-1}, U_i, z_{i-1}, z_i)\right] \tag{2.87}$$

where the fluxes are calculated from (2.85) and (2.86).

2.3.5.3. Second Order Well-Balanced Scheme Based on Hydrostatic Reconstruction

One way to reach the second order accuracy is to reconstruct the variables at the cell interfaces with a piecewise linear approximation and use those value as Riemann states to calculate interface fluxes. For uniformly discretized domain with constant mesh size, the interface values for water depth h and unit discharge q can be obtained by linear approximation as

$$h_{\,i+\frac{1}{2}^{(l)}} = \max\left(0, \eta_i + \frac{1}{2}\delta\eta_i\Delta x - z^*_{\,i+\frac{1}{2}}\right) \tag{2.88}$$

$$h_{\,i+\frac{1}{2}^{(r)}} = \max\left(0, \eta_{i+1} - \frac{1}{2}\delta\eta_{i+1}\Delta x - z^*_{\,i+\frac{1}{2}}\right) \tag{2.89}$$

$$q_{\,i+\frac{1}{2}^{(l)}} = q_i + \frac{1}{2}\delta q_i\Delta x \tag{2.90}$$

$$q_{i+\frac{1}{2}^{(r)}} = q_{i+1} - \frac{1}{2}\delta q_{i+1}\Delta x \tag{2.91}$$

where η shows the water surface elevation. Accordingly, the velocities at the left and right of the cell interfaces are calculated as

$$u_{i+\frac{1}{2}^{(l)}} = \begin{cases} 0 & if\ h_{i+\frac{1}{2}^{(l)}} < \varepsilon \\ q_{i+\frac{1}{2}^{-}}/h_{i+\frac{1}{2}^{-}} & else \end{cases} \tag{2.92}$$

$$u_{i+\frac{1}{2}^{(r)}} = \begin{cases} 0 & if\ h_{i+\frac{1}{2}^{(r)}} < \varepsilon \\ q_{i+\frac{1}{2}^{+}}/h_{i+\frac{1}{2}^{+}} & else \end{cases} \tag{2.93}$$

where ε is the tolerance for the dry bed. In this study ε is chosen as 10^{-10}.

$\delta\eta_i$ and δq_i are the gradients of w and q in each cell. To avoid spurious oscillations, nonlinear slope limiters can be used to define $\delta\eta_i$ and δq_i as

$$\begin{aligned} \delta\eta_i &= L\left(\frac{\eta_i - \eta_{i-1}}{x_i - x_{i-1}}, \frac{\eta_{i+1} - \eta_i}{x_{i+1} - x_i}\right) \\ \delta q_i &= L\left(\frac{q_i - q_{i-1}}{x_i - x_{i-1}}, \frac{q_{i+1} - q_i}{x_{i+1} - x_i}\right) \end{aligned} \tag{2.94}$$

where L is the slope limiter function. One choice for L can be *minmod* function, which leads to second order accurate scheme (Randall J. Leveque, 2004).

$$L(a,b) = max[0, \min(a,b)] \tag{2.95}$$

Kurganov & Petrova, 2007 use generalized form of the *minmod* limiter which can be written as

$$\begin{aligned} \delta\eta_i &= L\left(\theta\frac{\eta_i - \eta_{i-1}}{x_i - x_{i-1}}, \frac{\eta_{i+1} - \eta_{i-1}}{x_{i+1} - x_{i-1}}, \theta\frac{\eta_{i+1} - \eta_i}{x_{i+1} - x_i}\right) \\ \delta q_i &= L\left(\theta\frac{q_i - q_{i-1}}{x_i - x_{i-1}}, \frac{q_{i+1} - q_{i-1}}{x_{i+1} - x_{i-1}}, \theta\frac{q_{i+1} - q_i}{x_{i+1} - x_i}\right) \end{aligned} \tag{2.96}$$

where the function L is defined as

$$L(a_1, a_2, a_3) = \begin{cases} \min(a_i) & if\ a_i > 0\ for\ i = 1,2,3 \\ \max(a_i) & if\ a_i < 0\ for\ i = 1,2,3 \\ 0 & otherwise. \end{cases} \quad (2.97)$$

and θ is the numerical viscosity amount which is in the interval of $\theta \in [1,2]$.

In second order scheme, $z_{i,r}$ and $z_{i,l}$ should also be defined and to preserve consistency, cell-centered source term S_{ci} should also be added to the discretized equation (Audusse, et al., 2004).

Second order well balanced scheme can be summarized as

$$\Delta x_i \frac{\partial}{\partial t} U_i(t) + \left(F_{i+\frac{1}{2}} - F_{i-\frac{1}{2}}\right) = S_i + S_{ci} \quad (2.98)$$

$$\Delta x_i \frac{\partial}{\partial t} U_i(t) + F^{left}_{i+\frac{1}{2}}\left(U_{i,r}, U_{i+1,l}, z_{i,r}, z_{i+1,l}\right) - F^{right}_{i-\frac{1}{2}}\left(U_{i-1,r}, U_{i,l}, z_{i-1,r}, z_{i,l}\right) = S_{ci} \quad (2.99)$$

where

$$\begin{aligned} F^{left}_{i+\frac{1}{2}}\left(U_{i,r}, U_{i+1,l}, z_{i,r}, z_{i+1,l}\right) &= F_{i+\frac{1}{2}}\left(U_{i+1/2^{(l)}}, U_{i+1/2^{(r)}}\right) - S_{i+\frac{1}{2}^{(l)}} \\ &= F_{i+\frac{1}{2}}\left(U_{i+1/2^{(l)}}, U_{i+1/2^{(r)}}\right) + \frac{g}{2}\begin{pmatrix} 0 \\ h^2_{i,r} - h^{*\,2}_{i+1/2^{(l)}} \end{pmatrix} \end{aligned} \quad (2.100)$$

$$\begin{aligned} F^{right}_{i-\frac{1}{2}}\left(U_{i-1,r}, U_{i,l}, z_{i-1,r}, z_{i,l}\right) &= F_{i-\frac{1}{2}}\left(U_{i-1/2^{(l)}}, U_{i-1/2^{(r)}}\right) + S_{i-\frac{1}{2}^{(r)}} \\ &= F_{i-\frac{1}{2}}\left(U_{i-1/2^{(-)}}, U_{i-1/2^{(+)}}\right) + \frac{g}{2}\begin{pmatrix} 0 \\ h^2_{i,l} - h^{*\,2}_{i-1/2^{(r)}} \end{pmatrix} \end{aligned} \quad (2.101)$$

Cell-centered source term is defined as

$$S_{ci} = \begin{bmatrix} 0 \\ g h_i\left(z_{i,l} - z_{i,r}\right) \end{bmatrix} \quad (2.102)$$

The location of the reconstructed variables in the second-order scheme is depicted in Figure 2.11.

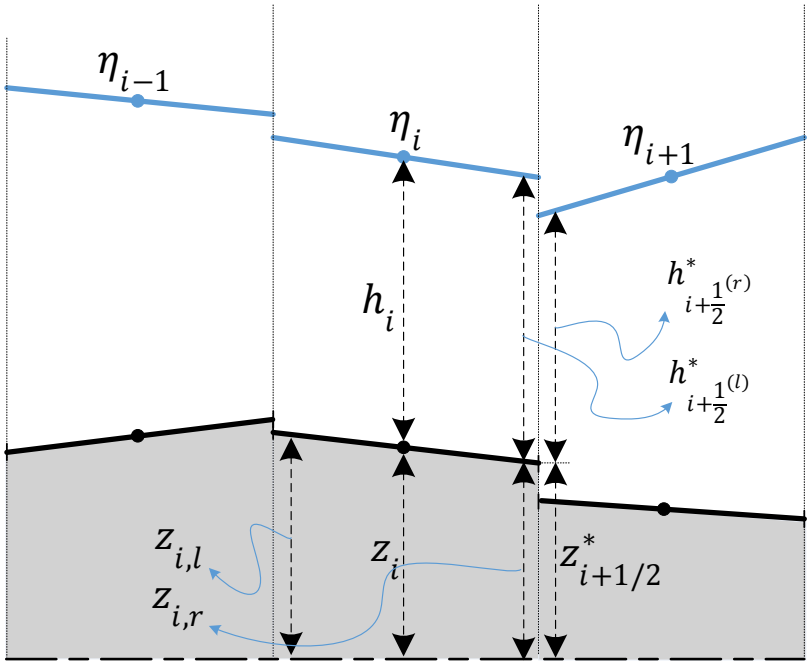

Figure 2.11. Illustration of the reconstructed variables for the second-order well-balanced scheme.

Fully discrete form of the equations can be written as

$$U_i^{n+1} = U_i^n - \frac{\Delta t}{\Delta x}\left[F^{left}_{i+\frac{1}{2}}\left(U_{i,r}, U_{i+1,l}, z_{i,r}, z_{i+1,l}\right) - F^{right}_{i-\frac{1}{2}}\left(U_{i-1,r}, U_{i,l}, z_{i-1,r}, z_{i,l}\right)\right] + \frac{\Delta t}{\Delta x} S_{ci} \tag{2.103}$$

2.3.6. Reconstruction of the Wet/Dry Fronts

Second order reconstruction of the water surface elevation using piecewise linear function may lead to negative depth near dry area. Therefore, special treatments are needed to prevent creation of negative depths, since they will destroy the computation. Illustration of such situation is depicted in Figure 2.12.

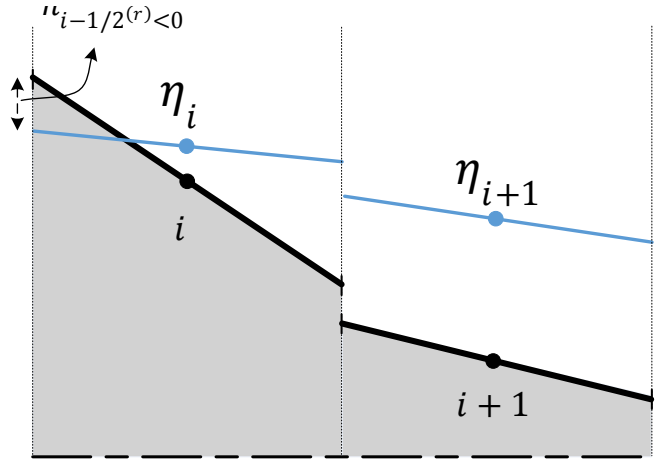

Figure 2.12. Creation of negative depth during piecewise reconstruction step.

To prevent such situation, the water surface slope should be corrected in the cases that $\eta^{+}_{i-\frac{1}{2}} < z_{i-\frac{1}{2}}$ or $\eta^{-}_{i+\frac{1}{2}} < z_{i+\frac{1}{2}}$. In this study, the corrections are done according to Kurganov & Petrova, 2007, as follows:

Case 1: if the negative depth appears at the left edge of the cell, i.e., $\eta^{+}_{i-\frac{1}{2}} < z_{i-\frac{1}{2}}$, then the water surface slope will be corrected as

$$\delta\eta_i = \frac{\eta_i - z_{i-\frac{1}{2}}}{\Delta x/2} \tag{2.104}$$

and therefore

$$\begin{cases} \eta^{+}_{i-\frac{1}{2}} = z_{i-\frac{1}{2}} \\ \eta^{-}_{i+\frac{1}{2}} = 2\eta_i - z_{i-\frac{1}{2}} \end{cases} \tag{2.105}$$

Then, the depth at the left and right of the cell will be

$$\begin{cases} h^{+}_{i-\frac{1}{2}} = 0 \\ h^{-}_{i+\frac{1}{2}} = 2h_i \end{cases} \tag{2.106}$$

Case 2: if the negative depth appears at the right edge of the cell, i.e., $\eta^{-}_{i+\frac{1}{2}} < z_{i+\frac{1}{2}}$, then the water surface slope will be corrected as

$$\delta\eta_i = \frac{z_{i+\frac{1}{2}} - \eta_i}{\Delta x/2} \tag{2.107}$$

and therefore

$$\begin{cases} \eta^{+}_{i-\frac{1}{2}} = 2\eta_i - z_{i+\frac{1}{2}} \\ \eta^{-}_{i+\frac{1}{2}} = z_{i+\frac{1}{2}} \end{cases} \tag{2.108}$$

Then, the depth at the left and right of the cell will be

$$\begin{cases} h^{+}_{i-\frac{1}{2}} = 2h_i \\ h^{-}_{i+\frac{1}{2}} = 0 \end{cases} \tag{2.109}$$

The correction procedure is depicted in Figure 2.13.

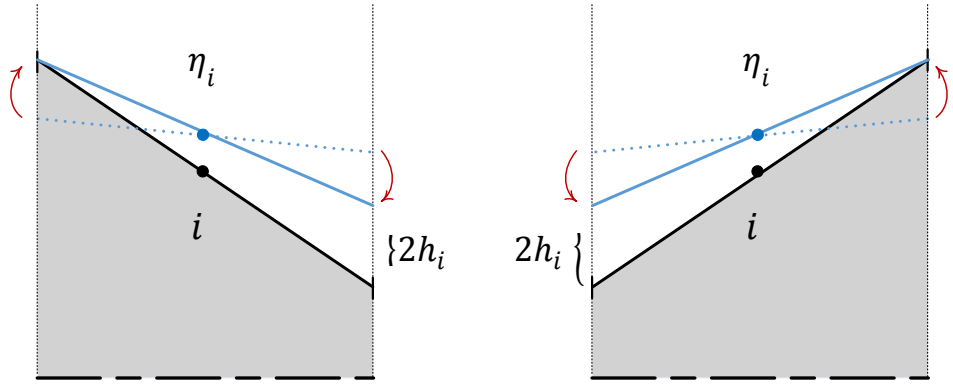

Figure 2.13. correction procedure of the negative depth at the left edge of the cell (left) and right edge of the cell (right). Dotted line and solid lines represent the water surface before and after correction, respectively.

2.3.7. Adopted Numerical Solutions and Developed Codes in FORTRAN

Three codes are developed in FORTRAN to solve the shallow water equations. One of the codes is written to solve the discretized equation (2.45). In equation (2.45), the source term is neglected; therefore, the source term is added to the right-hand side of it as

$$U_i^{n+1} = U_i^n - \frac{\Delta t}{\Delta x}\left[F_{i+\frac{1}{2}} - F_{i-\frac{1}{2}}\right] + \Delta t\, S_i^n \tag{2.110}$$

where $U = [h\,, q]^T$, and the source term is defined as

$$S_i^n = \begin{bmatrix} 0 \\ -gh_i\left(S_{0\,i} + S_{f\,i}\right) \end{bmatrix} \tag{2.111}$$

$S_{0\,i}$ is the bed slope of the cell i, and $S_{f\,i}$ is the friction source term and is defined as

$$S_{f\,i} = \frac{n^2 u|u|}{R_h^{4/3}} \tag{2.112}$$

where R_h= hydraulic radius. Hereafter, this code will be referred as WAF code for simplicity. The WAF code does not have well-balanced property. In the WAF code, fluxes are calculated using equation (2.69), where $F_L = F_i$ and $F_R = F_{i+1}$.

Another code is developed to solve the 1st order well-balanced scheme, and hereafter will be called WAF1WB. WAF1WB solves equation (2.87) with included friction source term as

$$\begin{aligned} U_i^{n+1} = U_i^n - \frac{\Delta t}{\Delta x}\left[F_{i+\frac{1}{2}}^{left}(U_i, U_{i+1}, z_i, z_{i+1}) - F_{i-\frac{1}{2}}^{right}(U_{i-1}, U_i, z_{i-1}, z_i)\right] \\ + \Delta t \begin{bmatrix} 0 \\ -gh_i S_{f\,i} \end{bmatrix} \end{aligned} \tag{2.113}$$

where $S_{f\,i}$ is defined by equation (2.112).

Beside WAF and WAF1WB, another code, which will be referred hereafter as WAF2WB, is written to solve second order well-balanced scheme, the discretized form of which is like equation (2.103) with added friction source term as

$$U_i^{n+1} = U_i^n - \frac{\Delta t}{\Delta x}\left[F_{i+\frac{1}{2}}^{left}\left(U_{i,r}, U_{i+1,l}, z_{i,r}, z_{i+1,l}\right) - F_{i-\frac{1}{2}}^{right}\left(U_{i-1,r}, U_{i,l}, z_{i-1,r}, z_{i,l}\right)\right] + \Delta t\begin{bmatrix}0\\ -gh_i\left(S_{0\,i} + S_{f\,i}\right)\end{bmatrix} \quad (2.114)$$

Again $S_{0\,i}$ is the bed slope of the cell i and $S_{f\,i}$ is calculated using equation (2.112). Modifications of the wet/dry fronts are done according to equations (2.104) ~ .

Nine test cases will be used to validate the developed codes. Definition of the test cases is given in chapter 3 and the corresponding numerical solutions using WAF, WAF1WB, and WAF2WB are given in chapter 4.

CHAPTER 3

DEFINITION OF NUMERICAL TEST CASES

3.1. Test Case 1: Subcritical Flow in a Rectangular Channel with Various Bed Slope

Test case 1 is selected to evaluate the developed codes in solving steady-state subcritical flow with smoothly varying bed slope. This test case is a steady-state flow problem and is introduced by I. MacDonald, et al., 2002. According to Ian MacDonald, 1996, corresponding bed slope to a given smooth water surface profile $h(x)$ can be obtained by

$$S_0(x) = f_1 h'(x) + f_2 \tag{3.1}$$

where

$$\begin{aligned} f_1 &= 1 - \frac{Q^2 T}{g A^3} = 1 - Fr^2 \\ f_2 &= \frac{Q^2 n^2 P^{4/3}}{A^{10/3}} - \frac{Q^2}{g A^3}\frac{\partial A}{\partial x} \end{aligned} \tag{3.2}$$

and T = Top Width, n = Manning's Roughness Coefficient, and P = Wetted Perimeter.

Test case 1 has a rectangular cross section 10 m wide and the channel is 1000 m long. Flow is subcritical in the whole channel with a discharge equal to 20 m^3/s. Manning's roughness coefficient is 0.03. Water depth profile is given by

$$h(x) = \left(\frac{4}{g}\right)^{1/3}\left\{1 + \frac{1}{2}\exp\left[-16\left(\frac{x}{1000} - \frac{1}{2}\right)^2\right]\right\} \tag{3.3}$$

Corresponding bed slope to the water depth profile (3.3) is obtained using (3.1) and (3.2) as

$$S_0(x) = \left(1 - \frac{4}{g[h(x)]^3}\right) h'(x) + 0.36 \frac{(2h(x) + 10)^{4/3}}{\left(10h(x)\right)^{10/3}} \tag{3.4}$$

The exact water surface and water depth profiles are depicted in Figure 3.1 and Figure 3.2, respectively.

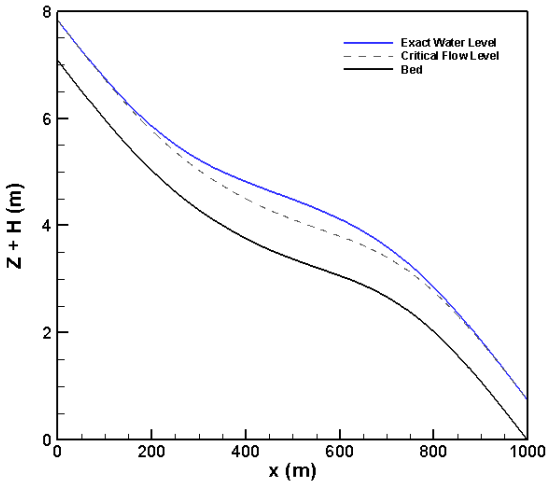

Figure 3.1. Exact water surface and critical flow elevations for Test Case 1: Subcritical Flow in a Rectangular Channel with Various Bed Slope.

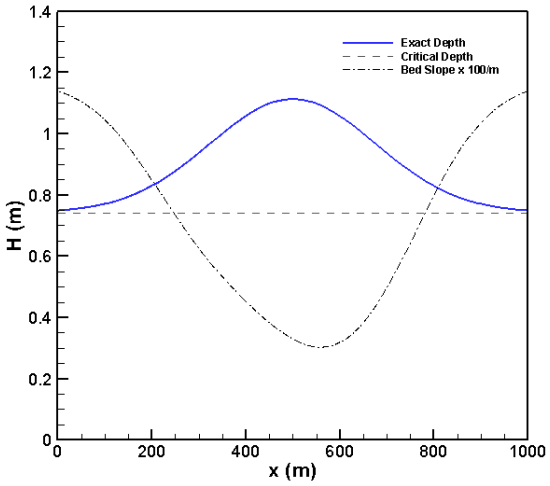

Figure 3.2. Exact water depth and critical flow depth for Test Case 1: Subcritical Flow in a Rectangular Channel with Various Bed Slope.

3.2. Test Case 2: Various Bed Slope with Subcritical Inflow and Hydraulic Jump

Test cases 2 is also introduced by Ian MacDonald, 1996 and is considered by many authors; for example Delis & Skeels, 1998. This test case is selected to see how the developed codes deal with the transition from subcritical flow to supercritical flow, and contrariwise, the transition from supercritical flow to subcritical flow, i.e., hydraulic jump, in a steady-state flow problem.

Test case 2 starts with subcritical inflow and enters to supercritical region. A hydraulic jump occurs at the middle section of the channel and flow regime changes to subcritical again. Water surface profile is given by

$$h(x) = \begin{cases} \left(\frac{4}{g}\right)^{1/3}\left(\frac{4}{3} - \frac{x}{100}\right) - \frac{9x}{1000}\left(\frac{x}{100} - \frac{2}{3}\right) & x \le \frac{200}{3} \\ \left(\frac{4}{g}\right)^{\frac{1}{3}}\left(0.674202\left(\frac{x}{100} - \frac{2}{3}\right)^4 + 0.674202\left(\frac{x}{100} - \frac{2}{3}\right)^3\right. & x > \frac{200}{3} \\ \left. -21.7112\left(\frac{x}{100} - \frac{2}{3}\right)^2 + 14.492\left(\frac{x}{100} - \frac{2}{3}\right) + 1.4305\right. & \end{cases} \quad (3.5)$$

Channel has a rectangular cross section with a constant width equal to 10 m. Length of the channel is 100 m, and Manning's roughness coefficient is 0.03. Bed slope corresponded to the water depth profile defined by (3.5) is again obtained using equation (3.1) and (3.2) as

$$S_0(x) = \left(1 - \frac{4}{g[h(x)]^3}\right)h'(x) + \frac{9}{2500[h(x)]^2}\left(\frac{1}{5} + \frac{1}{h(x)}\right)^{4/3} \quad (3.6)$$

Inflow discharge of the channel is 20 m³/s, and the Manning's roughness coefficient is equal 0.03. The exact water surface elevation and exact water depth are plotted in Figure 3.3 and Figure 3.4, respectively.

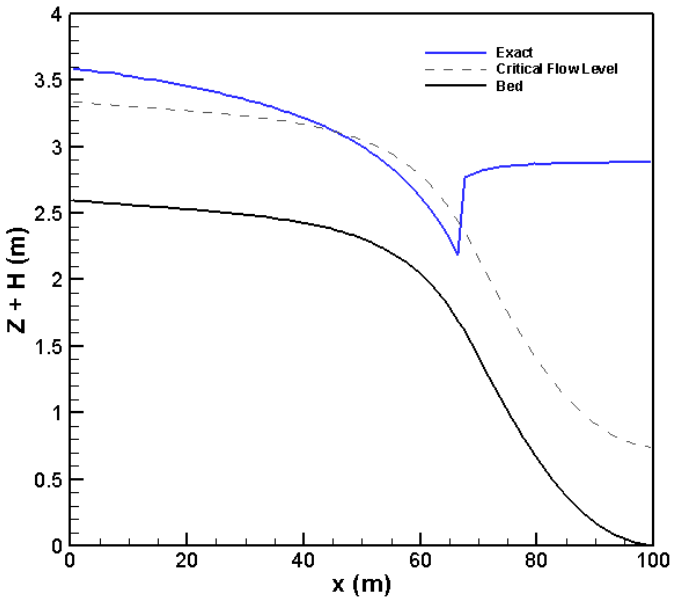

Figure 3.3. Exact water surface and critical flow elevations for Test Case 2: Various Bed Slope with Subcritical Inflow and Hydraulic Jump.

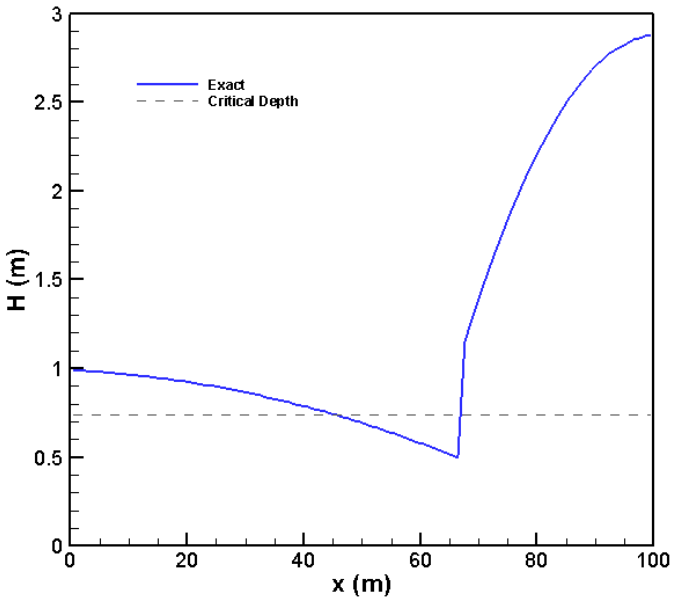

Figure 3.4. Exact water depth and critical flow depth for Test Case 2: Various Bed Slope with Subcritical Inflow and Hydraulic Jump.

3.3. Test Case 3: Various Bed Slope with Supercritical Inflow and Hydraulic Jump

This test case is also introduced by Ian MacDonald, 1996 and considered by Delis & Skeels, 1998. The channel is 100 m long and 10 m wide, and the Manning's roughness coefficient of the channel is 0.03 as same as the previous test case. In this case, the bed slope of the channel is given by

$$S_0(x) = \left(1 - \frac{4}{g[h(x)]^3}\right) h'(x) + \frac{9}{2500[h(x)]^2}\left(\frac{1}{5} + \frac{1}{h(x)}\right)^{4/3} \tag{3.7}$$

where water depth $h(x)$ is defined by

$$h(x) = \begin{cases} \left(\frac{4}{g}\right)^{\frac{1}{3}} \left(-10.7872\left(\frac{x}{100} - \frac{1}{3}\right)^4 + 18.8777\left(\frac{x}{100} - \frac{1}{3}\right)^3 \right. & x \le \frac{200}{3} \\ \left. +17.9329\left(\frac{x}{100} - \frac{1}{3}\right)^2 + 3.1725\left(\frac{x}{100} - \frac{1}{3}\right) + 0.850042\right) & \\ \left(\frac{4}{g}\right)^{\frac{1}{3}} \left(\frac{5}{6} + \frac{(100 - x)}{200}\right) + \frac{4}{10}\left(\frac{x}{100} - \frac{1}{3}\right)\left(\frac{x}{100} - 1\right) & x > \frac{200}{3} \end{cases} \tag{3.8}$$

This case is also selected to evaluate the behavior of the numerical solutions near the discontinuity in the water surface, i.e., hydraulic jump. The differences between this test case and the previous one are in the sequence of changes in flow regime and boundary conditions. Here, flow is supercritical at the inflow with a discharge of 20 m^3/s. Flow regime changes to subcritical at the central section of the channel by a hydraulic jump and then turns back into supercritical at the outflow section again. The exact water surface elevation and water depth are shown in Figure 3.5 and Figure 3.6, respectively.

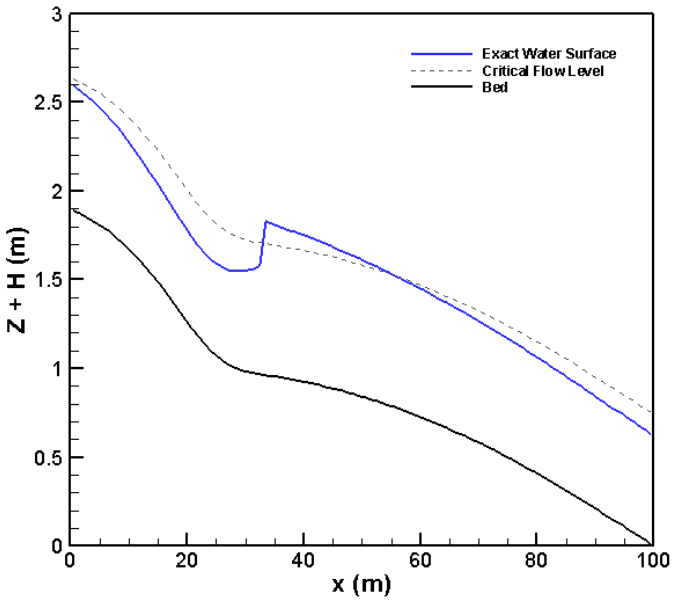

Figure 3.5. Exact water surface and critical flow elevations for Test Case 3: Various Bed Slope with Supercritical Inflow and Hydraulic Jump.

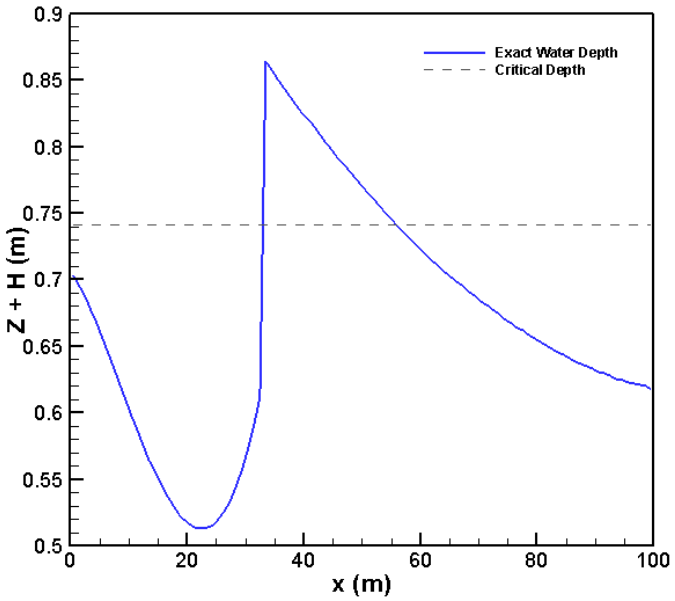

Figure 3.6. Exact water depth and critical flow depth for Test Case 3: Various Bed Slope with Supercritical Inflow and Hydraulic Jump.

3.4. Test Case 4: Steady Flow over a Bump; Transcritical Flow with Hydraulic Jump

Test cases 3.4, 3.5, and 3.6 are a set of steady state flow over a bump with different boundary conditions and flow situations. These test cases are well-known test cases and are considered by several authors, for example by María Elena Vázquez-Cendón, 1999. These test cases are considered to study the behavior of the numerical solutions used in this thesis in dealing with obstacle in the channel bed, in the presence of different flow situations in the channel.

The computational domain is a frictionless channel with a rectangular cross section. The length and breadth of the channel are 25 m and 1 m, respectively. A bump with a maximum height of 0.2 m is located at the bottom of the channel from $x = 8\,m$ to $x = 12\,m$. Channel bed elevation is defined by

$$z(x) = \begin{cases} 0.2 - 0.05(x-10)^2, & for\ 8 < x < 12 \\ 0\,, & otherwise \end{cases} \tag{3.9}$$

Depending on the initial and boundary conditions, the flow in the channel may be a) transcritical with a hydraulic jump, b) subcritical all over the domain (see section 3.5), and c) transcritical without hydraulic jump (see section 3.6). In the case of transcritical flow with a hydraulic jump, flow is subcritical at inflow, it passes through the critical depth at the top of the bump and the flow regime changes to supercritical, and finally, at the end region of the bump, a hydraulic jump occurs and flow regime changes back to subcritical again.

Discharge of the channel is $0.18\,m^3/s$ and the depth of the flow at the downstream end of the channel is $0.33\,m$.

The exact solution to this problem is obtained by using the hydraulic principles. At the top of the bump, flow passes through the critical depth. Specific energy of the flow is minimum in that point and is equal to

$$E_{min} = \frac{3}{2}\sqrt[3]{\frac{q^2}{g}} = 0.22338\ m \tag{3.10}$$

Thus, the specific energy before the bump is

$$E_{upstream} = E_{min} + \Delta z_{zenith} = 0.42338\ m \tag{3.11}$$

Therefore, the exact depth of the water before the hydraulic jump can be obtained by solving the equation

$$y + \frac{q^2}{2gy^2} = 0.42338 - \Delta z_i \tag{3.12}$$

where Δz_i is the height of the cell i with respect to the channel bed before the bump. Before the zenith of the bump, flow is subcritical, and after that, flow is supercritical. Therefore, before the zenith, the roots corresponding to the subcritical flow and after the zenith, the roots corresponding to the supercritical flow should be selected.

The flow depth at the downstream end of the channel is 0.33 m, and specific energy of the flow at the downstream of the channel is

$$E_{downstream} = y + \frac{q^2}{2g \times y^2} = 0.34516\ m \tag{3.13}$$

Since there is no head loss in the channel after the hydraulic jump, depth of the flow after the jump can be obtained by solving the equation

$$y + \frac{q^2}{2gy^2} = 0.34516 - \Delta z_i \tag{3.14}$$

Flow regime after the bump is subcritical; therefore, the roots corresponding to the subcritical flow should be selected.

Location of the hydraulic jump can be determined by using the specific force concept of the flow. The hydraulic jump occurs at a point that the specific forces of the flow

before and after the jump are equal. Specific force for a rectangular channel can be written as

$$\frac{F}{b} = \frac{1}{2}y^2 + \frac{q^2}{gy} \tag{3.15}$$

The specific force before and after the jump should be equal as

$$\frac{1}{2}y_1^2 + \frac{q^2}{gy_1} = \frac{1}{2}y_2^2 + \frac{q^2}{gy_2} \tag{3.16}$$

By solving the equations (3.12), (3.14), and (3.16) simultaneously, the location of the jump is obtained at the point with $x = 11.6677\ m$, and the height of the hump is $\Delta z = 0.0613\ m$ at the jump location.

Exact solution of this test case is plotted in Figure 3.7.

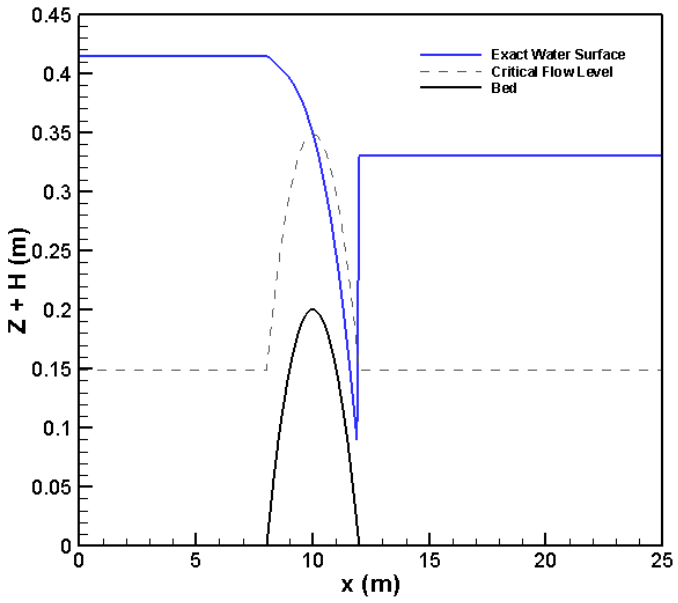

Figure 3.7. Exact water surface and critical flow elevations for Test Case 4: Steady Flow over a Bump (Transcritical Flow with a Hydraulic Jump).

3.5. Test Case 5: Steady Flow over a Bump; Subcritical Flow All over the Domain

In this case, flow is subcritical in the whole domain. The bed elevation is defined by equation (3.9), as same as the previous test case. The discharge of the channel is 4.42 m^3/s and the downstream water depth is 2 m.

Specific energy at the downstream boundary of the channel is calculated as

$$E_{downstream} = y + \frac{q^2}{2g \times y^2} = 2.24893\ m \tag{3.17}$$

The exact solution for this case can be obtained by solving the equation

$$y + \frac{q^2}{2gy^2} = 2.24893 - \Delta z_i \tag{3.18}$$

and selecting the roots corresponding to the subcritical flow. Exact solution of this problem is plotted in Figure 3.8.

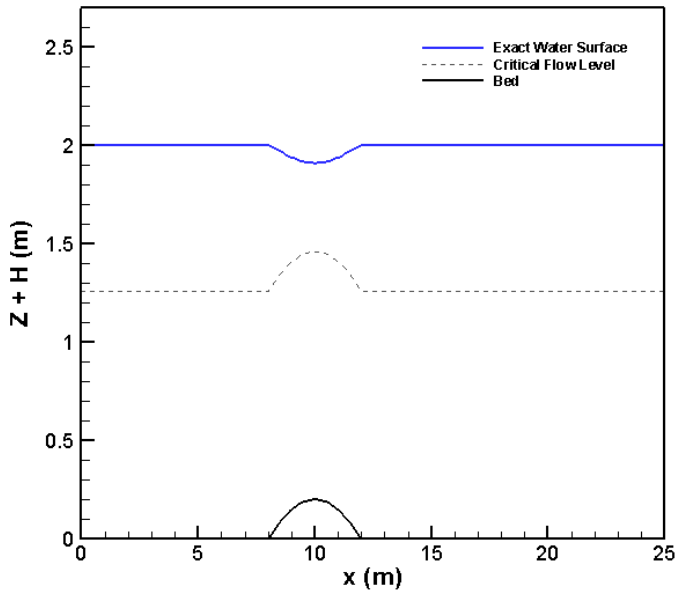

Figure 3.8. Exact water surface and critical flow elevations for Test Case 5: Steady Flow over a Bump (Subcritical Flow All over the Domain).

3.6. Test Case 6: Steady Flow over a Bump; Transcritical Flow without Hydraulic Jump

In this case, the bed elevation is also defined by equation (3.9). The discharge in the channel is equal to $1.53\ m^3/s$. Flow regime changes from subcritical to supercritical over the zenith of the bump and flow remains supercritical until the end of the channel.

The exact solution to this problem is again obtained by using the specific energy concepts. Flow passes through the critical depth at the zenith of the bump and specific energy is minimum there. The specific energy of the flow at the zenith is equal to

$$E_{min} = \frac{3}{2}\sqrt[3]{\frac{q^2}{g}} = 0.93038\ m \tag{3.19}$$

Therefore, the specific energy before and after the bump is

$$E = E_{min} + \Delta z_{zenith} = 1.13038\ m \tag{3.20}$$

and the depths can be obtained by solving the equation

$$y + \frac{q^2}{2gy^2} = 1.13038\ - \Delta z_i \tag{3.21}$$

Flow before the climax of the bump is subcritical and after that is supercritical. Therefore, before the climax, the roots corresponding to the subcritical flow and after the climax, the roots corresponding to the supercritical flow should be selected.

The exact solution to this problem is plotted in Figure 3.9.

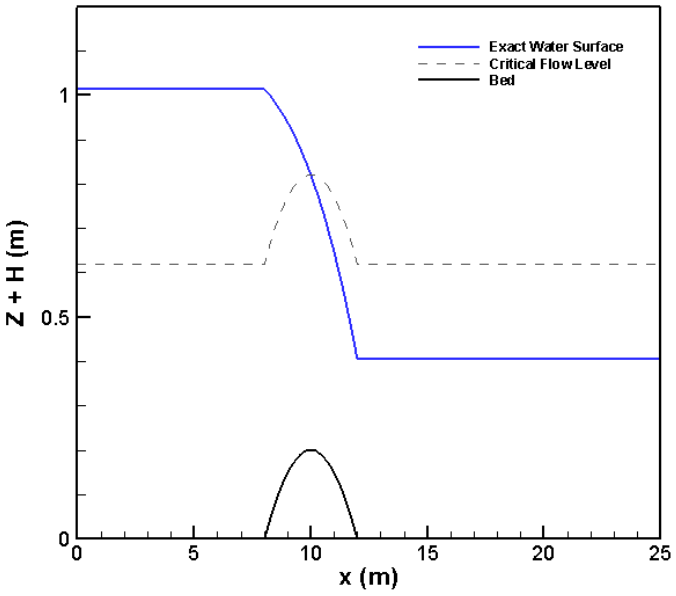

Figure 3.9. Exact water surface and critical flow elevations for Test Case 6: Steady Flow over a Bump (Transcritical Flow without Hydraulic Jump).

3.7. Test Case 7: Surge Crossing a Step

This is an unsteady test case and is used by Hu, et al., 2000. This test case is selected to see the capability of the numerical solutions in this study in solving an unsteady state flow problem with a step-like discontinuity in the channel bed. The length of the channel is 10 km. Channel is assumed to be frictionless. A step of the height $2\ m$ is located at x = 5 km. Initially, water is at rest in the whole channel with water surface elevation of $5\ m$ with respect to the channel bed before the step. A 10 m high surge enters from the left boundary and travels to the downstream. The velocity of the surge is obtained from equation (3.22) as $6.065\ m/s$.

$$v_1 = \frac{(d_1 - d_2)}{d_1}\sqrt{\frac{g d_1 (d_1 + d_2)}{2 d_2}} \tag{3.22}$$

where d_1 and d_2 are the height of the surge (i.e., $d_1 = 10\ m$) and the initial height of water before the step (i.e., $d_2 = 5\ m$), respectively. Due to the presence of the step, the incoming surge splits into the two new surges when it crosses over the step; one travels in the upstream direction, and the other travels to the downstream. The analytical solution to this problem can be obtained following Chow, 1959, by solving the equations (3.23), simultaneously (Hu, et al., 2000) (see Figure 3.10).

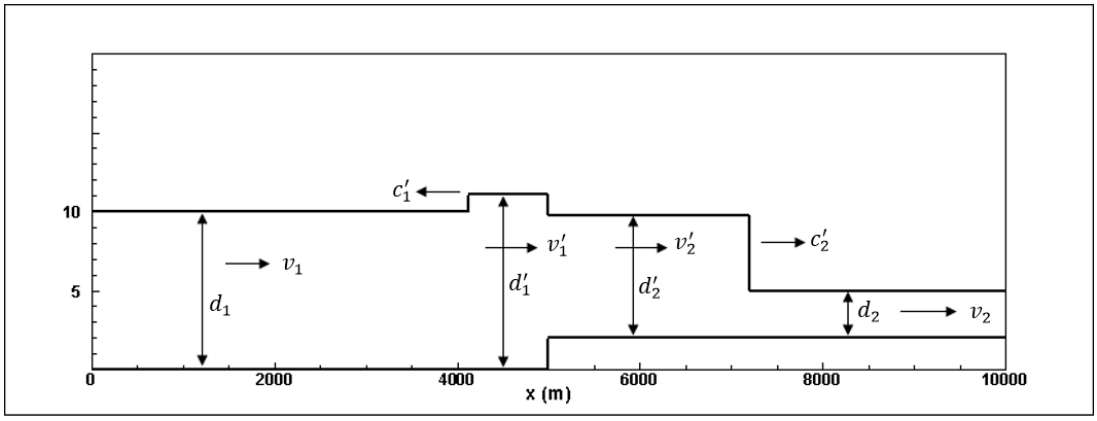

Figure 3.10. Schematic view of a surge crossing a step.

$$
\begin{aligned}
(v_2 - v_2')^2 &= (d_2 - d_2')^2 \frac{(d_2 + d_2')g}{2d_2 d_2'} \\
(v_1 - v_1')^2 &= (d_1 - d_1')^2 \frac{(d_1 + d_1')g}{2d_1 d_1'} \\
d_1' + \frac{v_1'^2}{2g} - \Delta z - \frac{v_2'^2}{2g} &= d_2' \\
v_1' d_1' &= v_2' d_2'
\end{aligned}
\tag{3.23}
$$

The analytical solutions are obtained as $d_1' = 11.094\ m$, $v_1' = 5.009\ m/s$, $d_2' = 7.756\ m$, and $v_2' = 7.163\ m/s$. The exact water surface profile and velocity field after t = 600.5 s are plotted in Figure 3.11 and Figure 3.12.

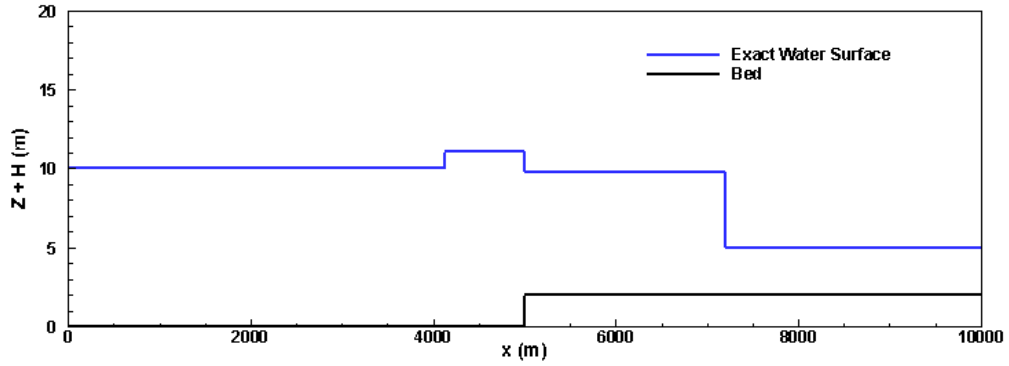

Figure 3.11. Exact water surface and critical flow elevations at t = 600.5 s for Test Case 7: Surge Crossing a Step.

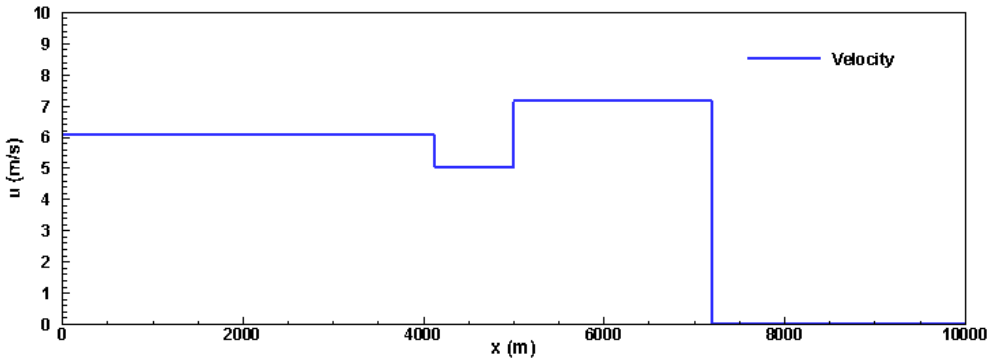

Figure 3.12. Exact velocity at t = 600.5 s for Test Case 7: Surge Crossing a Step.

3.8. Test Case 8: Oscillation on a Parabolic Bed

This is another unsteady test case problem with an oscillatory water surface profile in a parabolic basin. This problem is chosen to demonstrate the ability of the numerical solutions in dealing with wet/dry areas. The parabolic bed is defined as

$$z = \frac{D_0}{L^2}(x - 2L)^2 \tag{3.24}$$

where D_0 = maximum water depth, and $2L$ = water surface length when the it is horizontal. The initial velocity is $u = 0$ and initial water surface is

$$\eta = D_0 + \frac{2AD_0}{L^2}\left(x - 2L - \frac{A}{2}\right) \tag{3.25}$$

where A = amplitude of the oscillation. The analytical solution at time *t* is obtained following Thacker, 1981 (Mungkasi & Roberts, 2010), as

$$\eta = D_0 + \frac{2AD_0}{L^2}\cos(\omega t)\left(x - 2L - \frac{A}{2}\cos(\omega t)\right) \tag{3.26}$$

where ω = frequency and T = period of oscillation and are defined as

$$\begin{aligned} \omega &= \frac{\sqrt{2gD_0}}{L} \\ T &= \frac{2\pi}{\omega} \end{aligned} \tag{3.27}$$

The parameters used in this test case are D_0 = 10 m, L = 2500 m, $A = L/2$, and computational domain is considered as $[0,4L]$.

Analytical water surface elevation at time t = T (1121.425 s) is plotted in Figure 3.13.

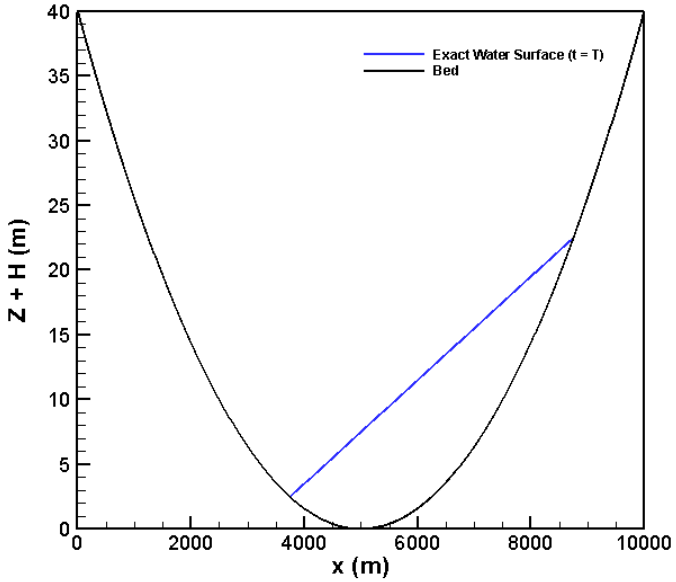

Figure 3.13. Exact water surface for Test Case 8: Oscillation on a Parabolic Bed at t = T (1121.425s).

3.9. Test Case 9: Comparison with Experimental Data; Dam-Break Flood Waves in a Dry Channel with a Hump

The purpose of this test case is to verify the developed codes with experimental data. This is a suitable test problem since it contains both dry regions and discontinuity on the channel bed. In this case, experimental data on the evolution of dam-break flow in a dry channel with a triangular hump are compared with the numerical solutions. The experiments have been done by Ozmen-Cagatay, et al., 2014 in a smooth rectangular channel with 0.30×0.34 m^2 dimensions and the channel length of 8.90 m. Channel geometry and location of the reservoir and the hump are shown in Figure 3.14. Experimental data in dimensionless form are plotted in at different dimensionless times T = 15.16, 17.54, 20.67, 23.05, 29.69, 35.83, 41.84, 49.99, and 62.77, where the origin of the x-axis is located at the location of the plate keeping the water in the reservoir. Dimensionless time is calculated by

$$T = t\sqrt{\frac{g}{h_0}} \tag{3.28}$$

where, t is the actual time.

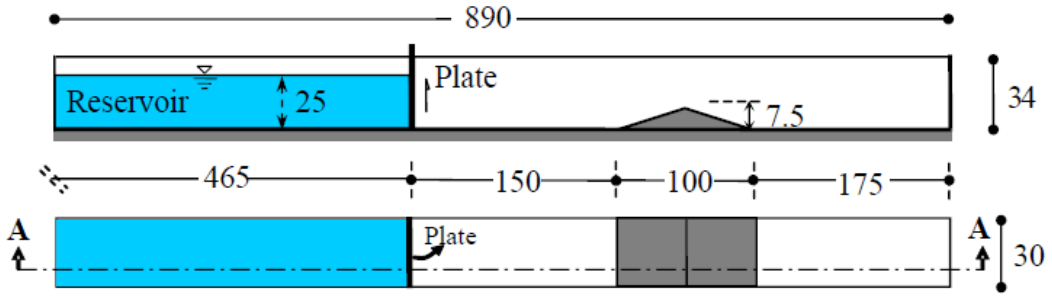

Figure 3.14. Channel geometry; cross-section view (up), and plan view (dawn) (Ozmen-Cagatay, et al., 2014).

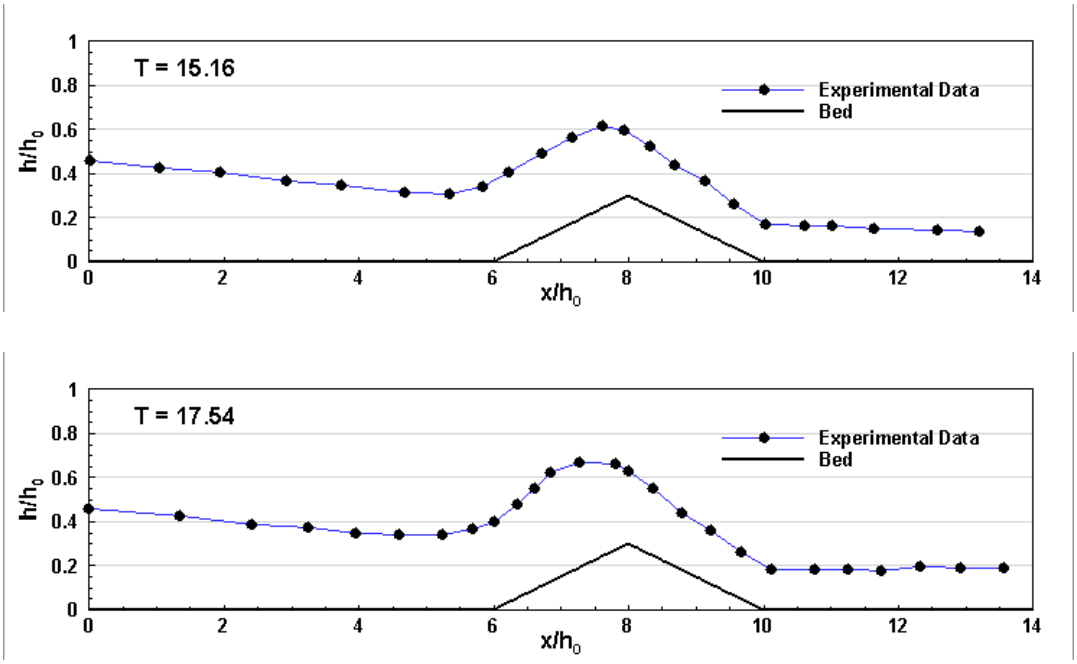

Figure 3.15. Measured water surface profile at different dimensionless times.

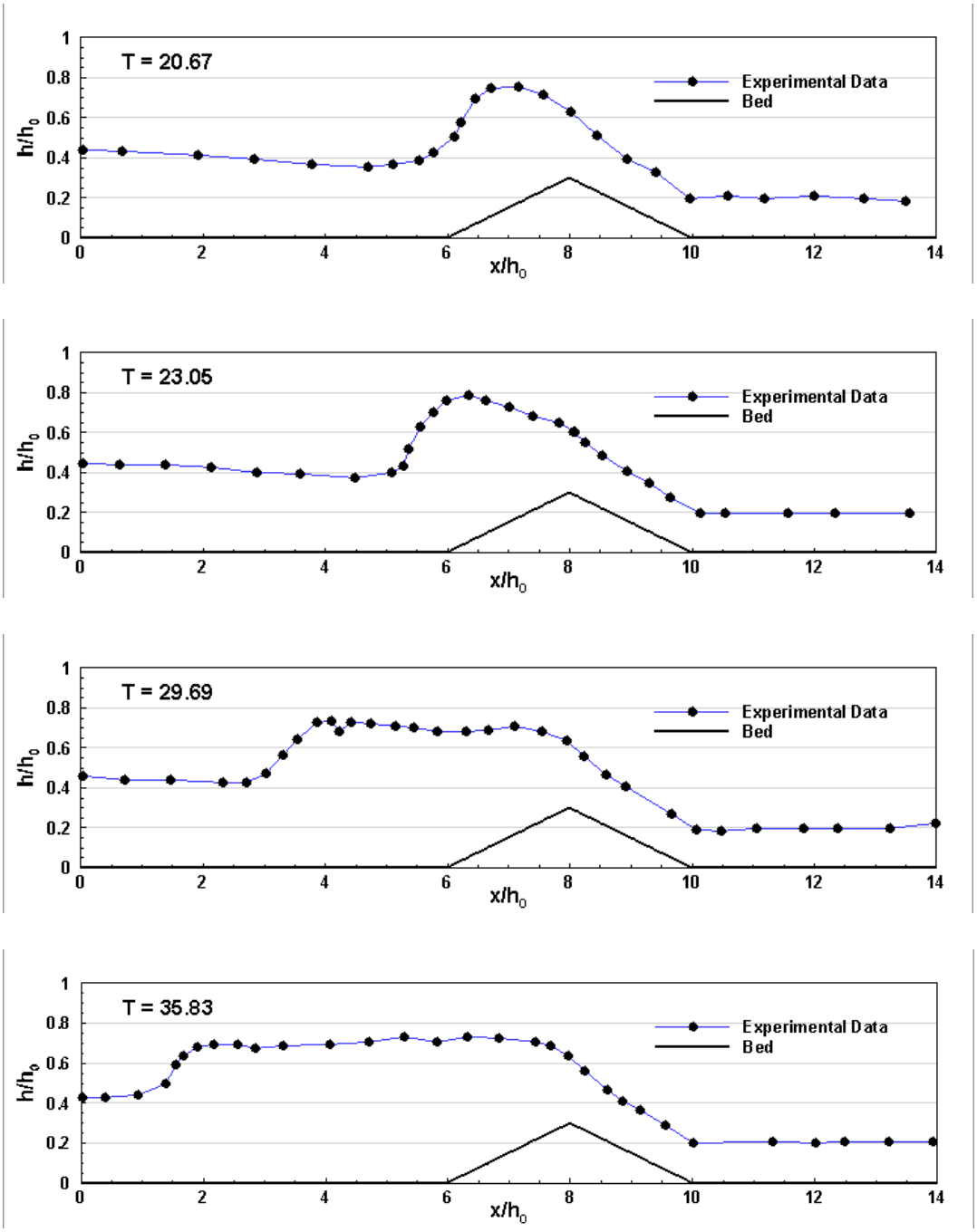

Figure 3.15 (Continued) Measured water surface profile at different dimensionless times.

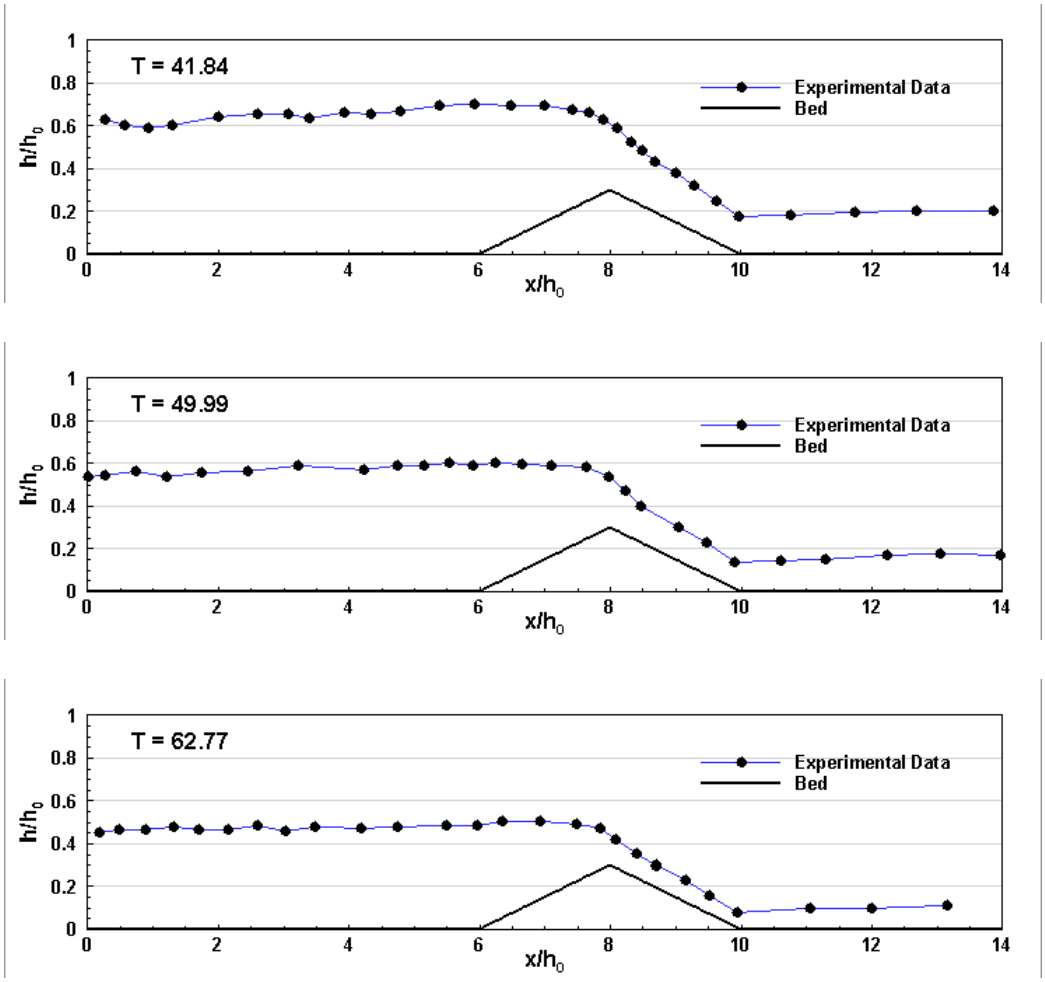

Figure 3.15 (Continued) Measured water surface profile at different dimensionless times.

3.10. Dam Break Flow over Champion-Stage like Step

At the end, a new test problem is introduced to test the robustness of the numerical solution in dealing with a more challenging problem. The proposed problem forces the numerical solution to confront with many difficulties, such as the presence of dry area, sudden discontinuity in the channel bed with positive and negative slopes, and moving of the wet/dry fronts.

The domain is a prismatic channel with unit width and the length of the channel is 100 m. The Manning's roughness coefficient is taken as 0.03. Discontinuity in the channel

bed is considered as champion-stage like step, which is located in the channel from $x = 40$ m to $x = 90$ m. The height of the first step is $1\,m$, the second step is $1\,m$ higher than the first step, and the third one is $1\,m$ higher than the second step. The fourth and fifth steps are $1\,m$ and $2\,m$ lower than the highest step, respectively. The channel geometry is defined as follows:

$$z = \begin{cases} 1 & if\ 40 \le x < 50 \\ 2 & if\ 50 \le x < 60 \\ 3 & if\ 60 \le x < 70 \\ 2 & if\ 70 \le x < 80 \\ 1 & if\ 80 \le x < 90 \\ 0 & otherwise \end{cases} \tag{3.29}$$

Dam-break flow and overtopping of the flow over the steps will be simulated in the channel. The reservoir is considered at the left of the channel from $x = 0$ to $x = 10$ m. The height of the water is $10\,m$ in the reservoir. The left and right ends of the channel are considered to be walls.

At time $t = 0$ the imaginary wall keeping the water in the reservoir will be suddenly removed and dam-break flow will occur. The geometry of the channel and the initial condition are illustrated in Figure 3.16.

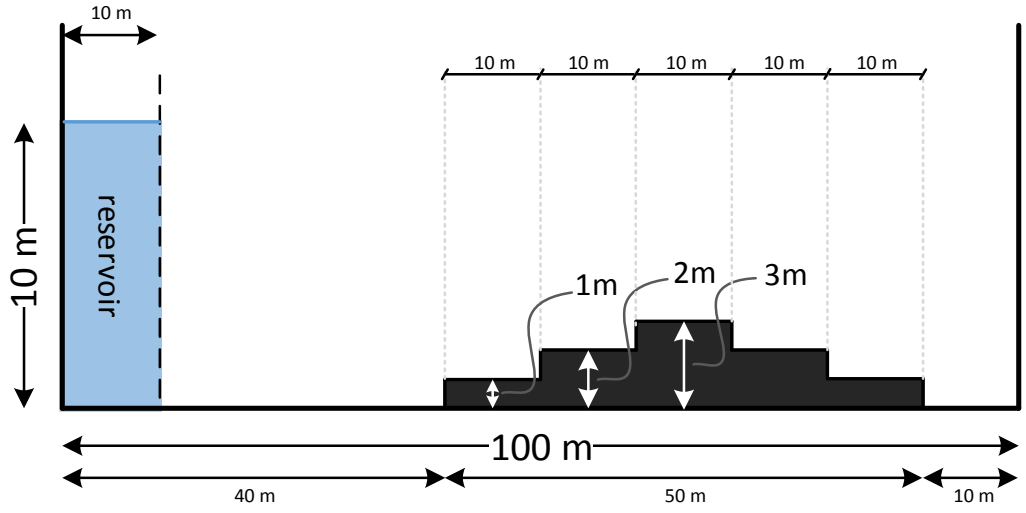

Figure 3.16. Geometry and initial condition of the test case 10.

CHAPTER 4

NUMERICAL SOLUTIONS OF THE TEST CASES

In this chapter numerical solutions of the test cases are compared with the exact and analytical solutions of them to assess the capability of the developed codes and numerical solutions in solving the test cases.

Test case 1, test case 2, test case3, test case 4, test case 5, test case 6, and test case 7 are solved with pure WAF (WAF code), 1st order well-balanced (WAF1WB code) and 2nd order well-balanced (WAF1WB code) methods. Test case 8, test case 9, and test case 10 are only solved with well-balanced methods (i.e., WAF1WB and WAF2WB codes).

There are some additional modifications in solving the test cases with the 2nd order well-balanced scheme. First, in reconstructing the variables at cell interfaces by using the piecewise linear function (i.e., slope limiters), to avoid probable oscillations and to allow for the use of higher CFL number, a relaxation factor is applied to the slope limiters. The relaxation factor, α, is defined as

$$\begin{aligned} \delta\eta &= \alpha\ \delta\eta^{new} + (1-\alpha)\delta\eta^{old} \\ \delta q &= \alpha\ \delta q^{new} + (1-\alpha)\delta q^{old} \end{aligned} \tag{4.1}$$

where, $\delta\eta^{old}$ and δq^{old} are the value of them from the previous time step. δw and δq are defined by equations (2.96) and (2.97). The relaxation factor is in the range of $0 \leq \alpha \leq 1$. This modification is only applied to the steady-state problems and for unsteady problems α is taken equal to 1.

Another modification is applied in the presence of partially flooded cells, inside which there is no sufficient water to fill the cell with a flat water surface. Those cells may need very small time step to prevent the creation of negative depths. Therefore, instead

of restricting the general CFL condition, the draining time step, in the cells that are in the risk of draining out, is defined following Bollermann, et al., 2011. The idea behind this definition is that there will be no flux going out of a cell if it is empty (Bollermann, et al., 2013). Draining time step can be obtained as follows

$$h_i^{n+1} = h_i^n - \frac{\Delta t}{\Delta x}\left(F^h_{i+\frac{1}{2}} - F^h_{i-\frac{1}{2}}\right) \geq 0 \tag{4.2}$$

and

$$\Delta t_i^{drain} = \frac{\Delta x h_i^n}{\left(F^h_{i+\frac{1}{2}} - F^h_{i-\frac{1}{2}}\right)} \tag{4.3}$$

where F^h is the flux function in the continuity equation. Now, Equation (4.2) is modified as

$$h_i^{n+1} = h_i^n - \frac{\Delta t_{i+1/2} F^h_{i+1/2} - \Delta t_{i-1/2} F^h_{i-1/2}}{\Delta x} \tag{4.4}$$

where the time steps at cell interfaces are selected as

$$\begin{aligned} \Delta t_{i+\frac{1}{2}} &= \min\left(\Delta t, \Delta t_k^{drain}\right), \qquad k = i + \frac{1}{2} - \frac{\text{sign}\left(F^h_{i+1/2}\right)}{2} \\ \Delta t_{i-\frac{1}{2}} &= \min\left(\Delta t, \Delta t_k^{drain}\right), \qquad k = i - \frac{1}{2} + \frac{\text{sign}\left(F^h_{i-1/2}\right)}{2} \end{aligned} \tag{4.5}$$

In addition, to have an idea about the number of iteration required for the convergence of the numerical solutions in steady-state test cases, the average residuals for the depth and the unit discharge are calculated using

$$\begin{aligned} R_h &= \frac{1}{M}\sum_{1}^{M}\left|h_i^{n+1} - h_i^n\right| \\ R_q &= \frac{1}{M}\sum_{1}^{M}\left|q_i^{n+1} - q_i^n\right| \end{aligned} \tag{4.6}$$

where M is the number of computational cells.

4.1. Numerical Solution of Test Case 1: Subcritical Flow in a Rectangular Channel with Various Bed Slope

This test case is solved using the WAF, WAF1WB, WAF2WB codes. In all methods, the initial water depth is equal 1 m and the discharge in the channel is initially equal to zero. The problem is solved in 1000 computational cells with the grid size of 1 m. Two ghost cells at the left and two ghost cells at the right of the domain are added to imply the boundary conditions. Manning's roughness coefficient is set to 0.03. CFL number is set to 0.9 for all methods. WAF2WB code, the relaxation factor α is set to 0.1. Boundary conditions at the inflow are implied as

$$\begin{aligned} Q(-1) &= 2 \\ Q(0) &= 2 \\ H(-1) &= H(1) \\ H(0) &= H(1) \end{aligned} \tag{4.7}$$

and at the outflow are implied as

$$\begin{aligned} Q(M+1) &= Q(M) \\ Q(M+2) &= Q(M) \\ H(M+1) &= 0.748409 \\ H(M+2) &= 0.748409 \end{aligned} \tag{4.8}$$

where M shows the number of computational cells, -1 and 0 denote to the ghost cells at the left of the channel, and $M+1$ and $M+2$ denote to the ghost cells at the right of the domain. Q and H represent the unit discharge and the depth, respectively.

Numerical and analytical water surface elevation, water depth, and the unit discharge of the channel are shown in Figure 4.1, Figure 4.2, and Figure 4.3, respectively.

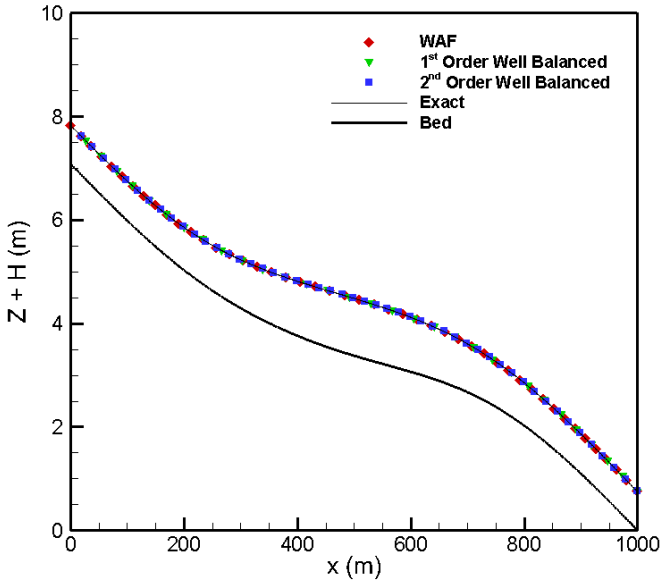

Figure 4.1. Comparison between numerical and analytical water surface elevations for test case 1: Rectangular Channel with Various Bed Slope and Subcritical Flow

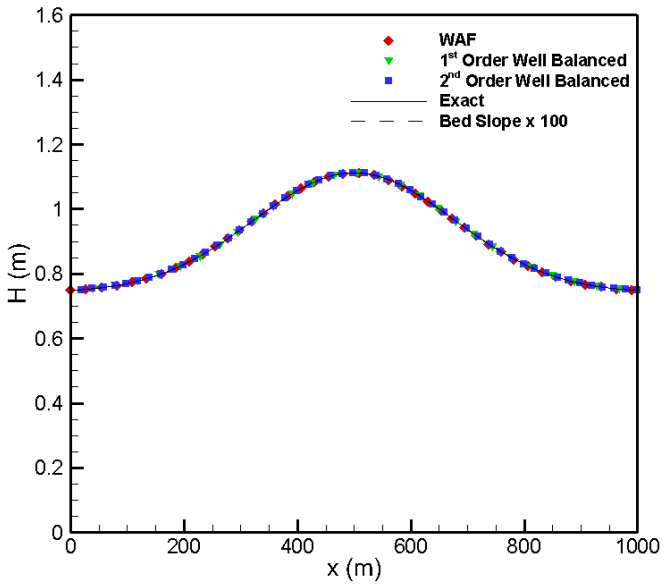

Figure 4.2. Comparison between numerical and analytical water depths for test case 1: Rectangular Channel with Various Bed Slope and Subcritical Flow

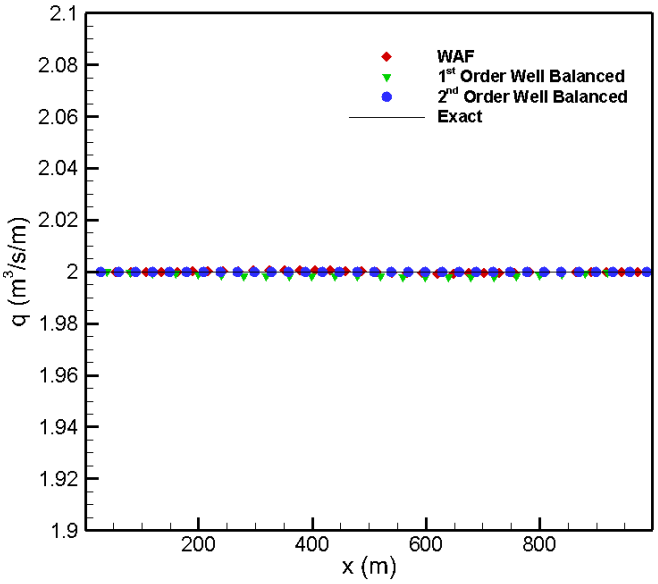

Figure 4.3. Comparison between numerical and analytical unit discharges for test case 1: Rectangular Channel with Various Bed Slope and Subcritical Flow

The numerical residuals of the numerical depth and unit discharge are depicted in Figure 4.4.

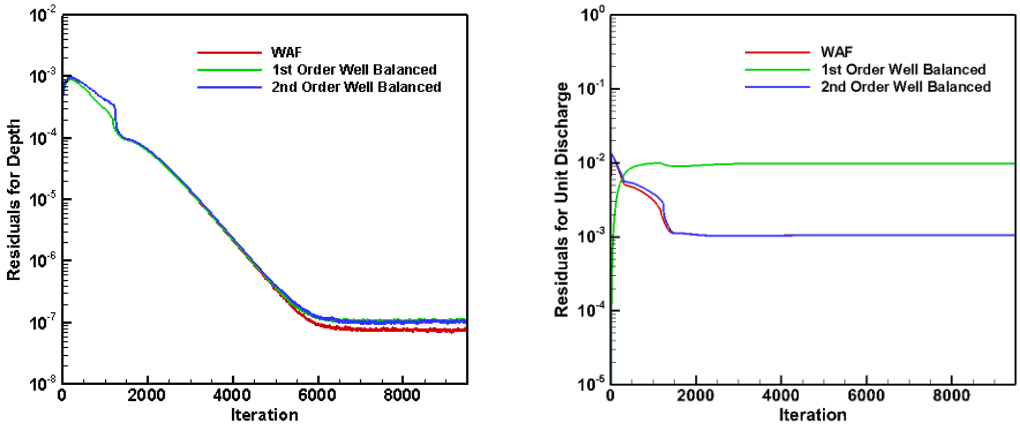

Figure 4.4. Residuals for Test Case 1: Rectangular Channel with Various Bed Slope and Subcritical Flow

For this test case, numerical solutions using all three schemes are compared with the analytical solution and the results are presented. From the residuals presented in Figure 4.4, it can be seen that the problem is converged after almost 6000 iterations. All the three schemes have excellent agreement with the analytical solutions by the use of 1000 number of grids, which confirms that all three schemes used in this thesis solve the subcritical flow problems in channels with smooth variation in the bed slope with sufficient accuracy. However, it can be seen from Figure 4.3 that the 1st order well-balanced scheme calculates the unit discharge not as accurate as the WAF and 2nd order well-balanced scheme.

4.2. Numerical Solution of Test Case 2: Various Bed Slope with Subcritical Inflow and Hydraulic Jump

Here, numerical solutions of the test case 2 using pure WAF, 1st order well-balanced, and 2nd order well-balanced methods are compared with the analytical solution. To be coincident with results of Delis & Skeels, 1998, the computational domain is divided into 100 cells with the constant grid size of 1 m. Initially, water depth is equal 1 m and discharge is equal zero in the whole domain. Manning's roughness coefficient is 0.03 for this case. CFL number of 0.9 is selected for all methods. For 2nd order well-balanced method the relaxation factor α is set to 0.1.

Inflow boundary conditions are applied as inflow unit discharge of $2\ m^3/s/m$ and depth of the ghost cells equal to the one in cell 1 as in equations (4.9).

$$\begin{aligned} Q(-1) &= 2 \\ Q(0) &= 2 \\ H(-1) &= H(1) \\ H(0) &= H(1) \end{aligned} \tag{4.9}$$

At the downstream of the channel outflow boundary conditions are applied and the depth of the ghost cells are taken as $2.877056\ m$ as

$$
\begin{aligned}
Q(M+1) &= Q(M) \\
Q(M+2) &= Q(M) \\
H(M+1) &= 2.877056 \\
H(M+2) &= 2.877056
\end{aligned}
\tag{4.10}
$$

Numerical results and analytical solution of water surface elevation, water depth, and unit discharge of the channel are plotted in Figure 4.5, Figure 4.6, and Figure 4.7, respectively. The solutions of the water depth are also compared with the results presented in Delis & Skeels, 1998 for the shock region in Figure 4.8.

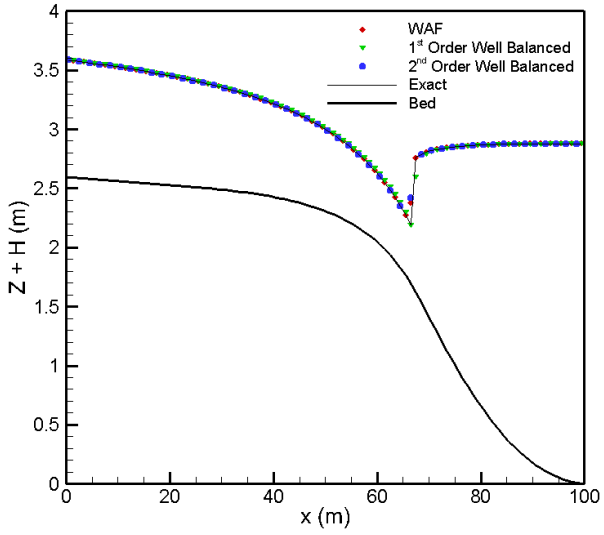

Figure 4.5. Comparison between numerical and analytical water surface elevations for test case 2: Various Bed Slope with Subcritical Inflow and Hydraulic Jump

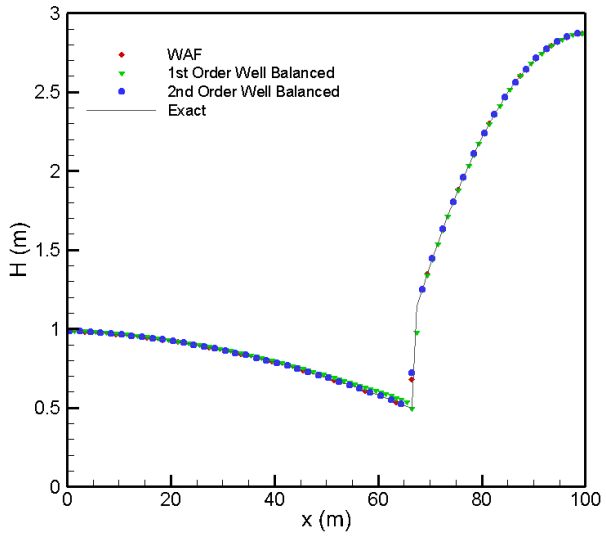

Figure 4.6. Comparison between numerical and analytical water depths for test case 2: Various Bed Slope with Subcritical Inflow and Hydraulic Jump

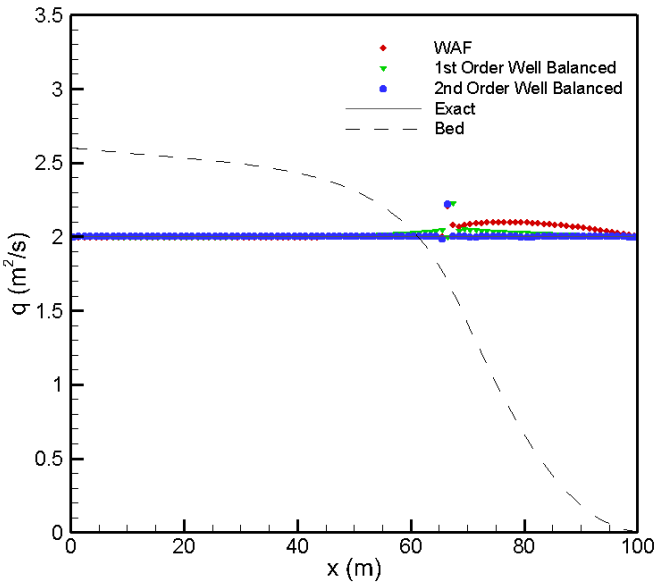

Figure 4.7. Comparison between numerical and analytical unit discharges for test case 2: Various Bed Slope with Subcritical Inflow and Hydraulic Jump

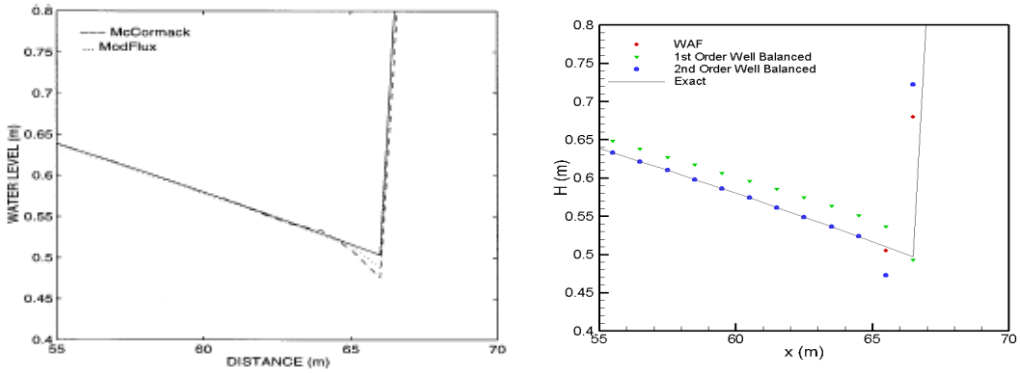

Figure 4.8. comparison of the magnified shock region with the results in Delis & Skeels, 1998

The calculated residuals of the depth and the unit discharge are plotted in Figure 4.9.

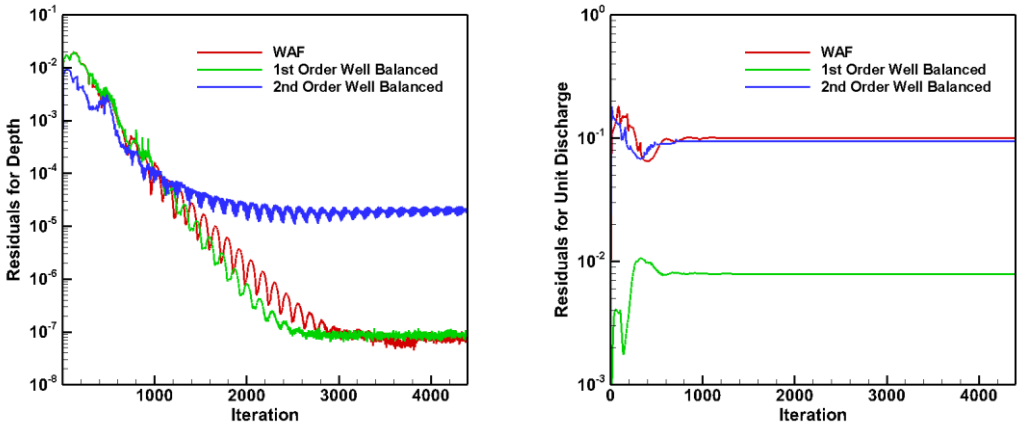

Figure 4.9. Residuals for Test Case 2: Various Bed Slope with Subcritical Inflow and Hydraulic Jump

As expected, the second order well-balanced scheme gives the best results for numerical solution to the depth and unit discharge compared with the first order well-balanced and pure WAF schemes, due to the better approximation of the Riemann states (by using linear piecewise function in the flux calculations), and linear definition of the bed. Numerical solutions of the depth by the pure WAF and the second order well-balanced schemes have excellent agreements with the exact depth profile (see

Figure 4.6). First order well-balanced scheme has also very good results for the depth, but not as much good as the pure WAF and the second-order scheme. However, the comparison of the numerical solutions for the unit discharge (see Figure 4.7) shows that first order well-balanced scheme gives better results compared with the WAF method due to the well-balancing property of the scheme.

4.3. Numerical Solution of Test Case 3: Various Bed Slope with Supercritical Inflow and Hydraulic Jump

The numerical comparison with the exact solution of the water surface elevation, water depth, and unit discharge of the channel has been done by solving the problem with the WAF, WAF1WB, and WAF2WB codes. Time steps are calculated with the CFL condition of 0.9 in the WAF and WAF1WB codes and 0.6 in the WAF2WB code. Relaxation factor is set to 0.4 for 2nd order well-balanced scheme. Initial conditions with velocities equal to zero and water depth equal to 1 m are used in all methods. The computational domain is divided for 100 cells for all cases as in (Delis & Skeels, 1998). Boundary conditions are implied as

$$\begin{aligned} Q(-1) &= 2 \\ Q(0) &= 2 \\ H(-1) &= 0.70303 \\ H(0) &= 0.70303 \end{aligned} \tag{4.11}$$

at the inflow (left) , and

$$\begin{aligned} Q(M+1) &= Q(M) \\ Q(M+2) &= Q(M) \\ H(M+1) &= H(M) \\ H(M+2) &= H(M) \end{aligned} \tag{4.12}$$

at the outflow (right).

Numerical results for water surface elevation, water depth, and unit discharge of the channel are shown in Figure 4.10, Figure 4.11, and Figure 4.12, respectively.

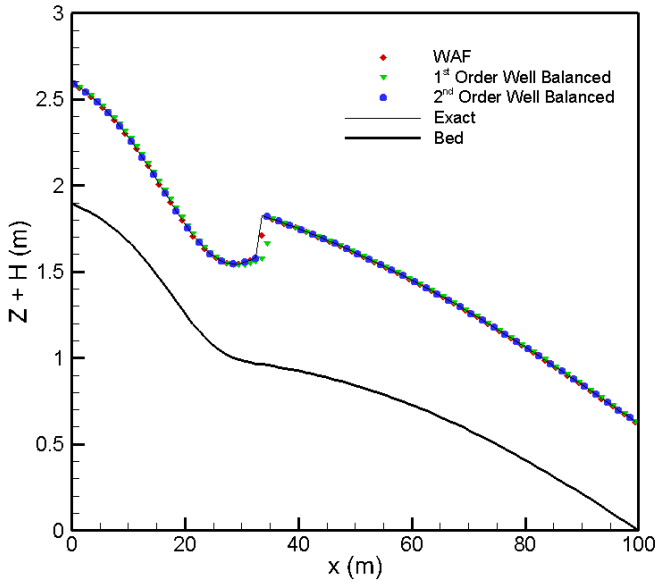

Figure 4.10. Comparison between numerical and analytical water surface elevations for test case 3: Various Bed Slope with Supercritical Inflow and Hydraulic Jump

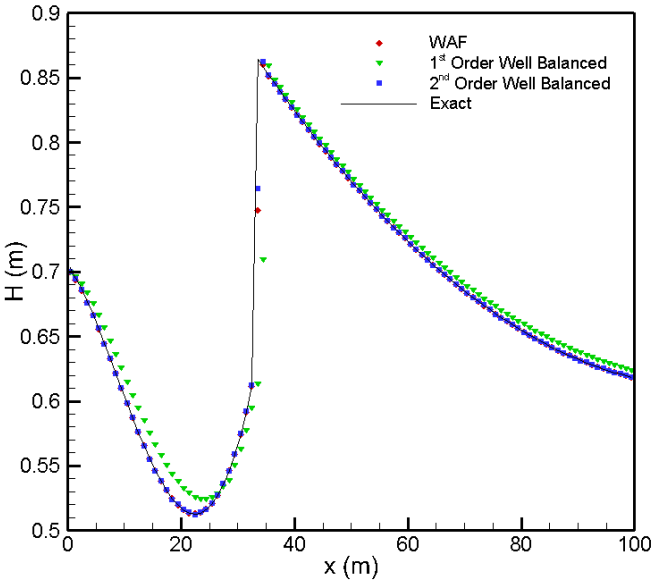

Figure 4.11. Comparison between numerical and analytical water depths for test case 3: Various Bed Slope with Supercritical Inflow and Hydraulic Jump

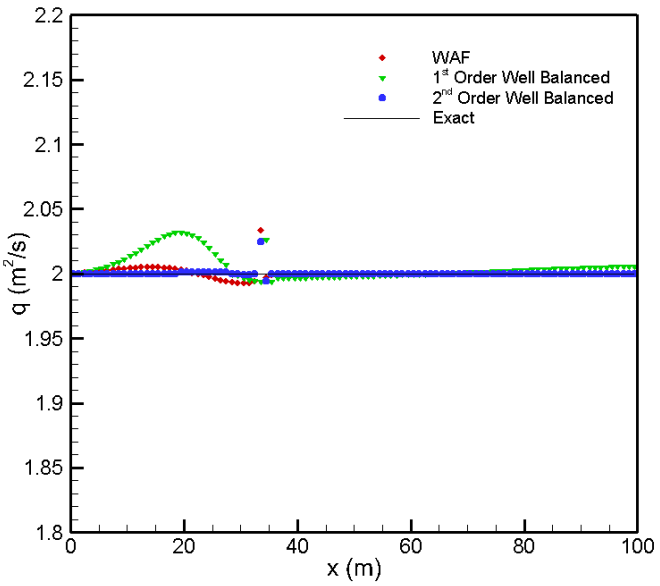

Figure 4.12. Comparison between numerical and analytical unit discharges for test case 3: Various Bed Slope with Supercritical Inflow and Hydraulic Jump

Numerical residuals for this case are plotted in Figure 4.13.

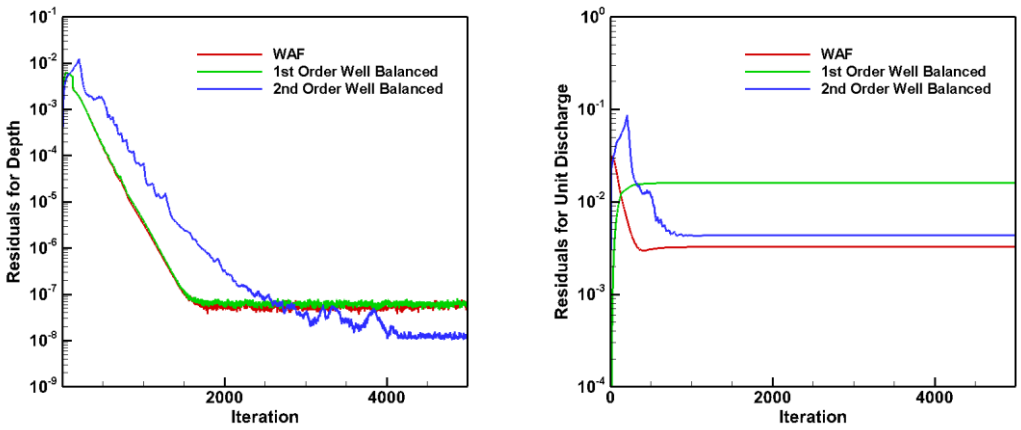

Figure 4.13. Residuals for Test Case 3: Various Bed Slope with Supercritical Inflow and Hydraulic Jump

1st order well-balanced scheme did not predict the location of the jump exactly in this test case. It is also less accurate in computing the depth and the unit discharge of the channel compared with the pure WAF and 2nd order well-balanced method. Pure WAF method and 2nd order well-balanced scheme compute the flow depth in the channel accurately. Figure 4.12 shows the general agreement between the numerical and analytical solutions. However, it can be seen that the numerical solution of the unit discharge is more challenging where the channel bed slope is much steeper.

4.4. Numerical Solution of Test Case 4: Steady Flow over a Bump; Transcritical Flow with Hydraulic Jump

As mentioned in the previous chapter, based on the initial and boundary condition, three flow conditions may occur in the channel (see sections 3.4, 3.5, and 3.6). In the numerical solutions presented here, transcritical flow with hydraulic jump occurs when the initial flow velocity and initial flow depth are equal zero and $0.5\,m$, respectively, and boundary conditions are inflow discharge of $0.18\,m^3/s$ and flow depth of $0.33\,m$ at the end of the channel. The channel assumed to be frictionless and is divided to 200 number of control volumes. Boundary conditions at the inflow are applied as

$$\begin{aligned} Q(-1) &= 0.18 \\ Q(0) &= 0.18 \\ H(-1) &= H(1) \\ H(0) &= H(1) \end{aligned} \tag{4.13}$$

and the outflow boundary conditions are applied as

$$\begin{aligned} Q(M+1) &= Q(M) \\ Q(M+2) &= Q(M) \\ H(M+1) &= 0.33 \\ H(M+2) &= 0.33 \end{aligned} \tag{4.14}$$

Numerical results obtained by pure WAF, 1st order well-balanced, and 2nd order well-balanced approaches are plotted in Figure 4.14 and Figure 4.15. Results are obtained

with CFL number equal to 0.9 for all cases and relaxation factor of 0.1 for the 2nd order well-balanced scheme.

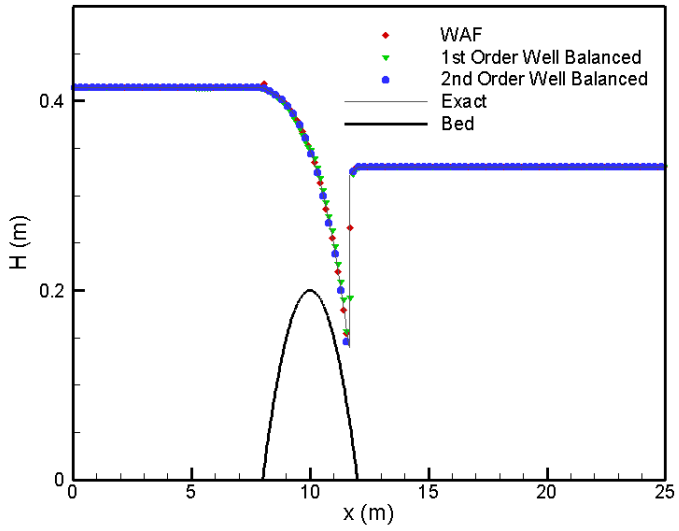

Figure 4.14. Comparison between numerical and analytical water surface elevations for test case 4: Steady Flow over a Bump; Transcritical Flow with Hydraulic Jump

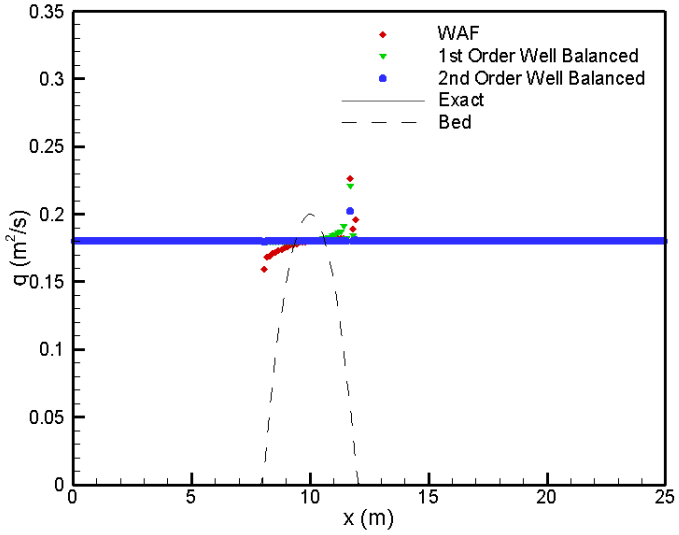

Figure 4.15. Comparison between numerical and analytical unit discharges for test case 4: Steady Flow over a Bump; Transcritical Flow with Hydraulic Jump

Average residuals for depth and unit discharge are plotted in Figure 4.16.

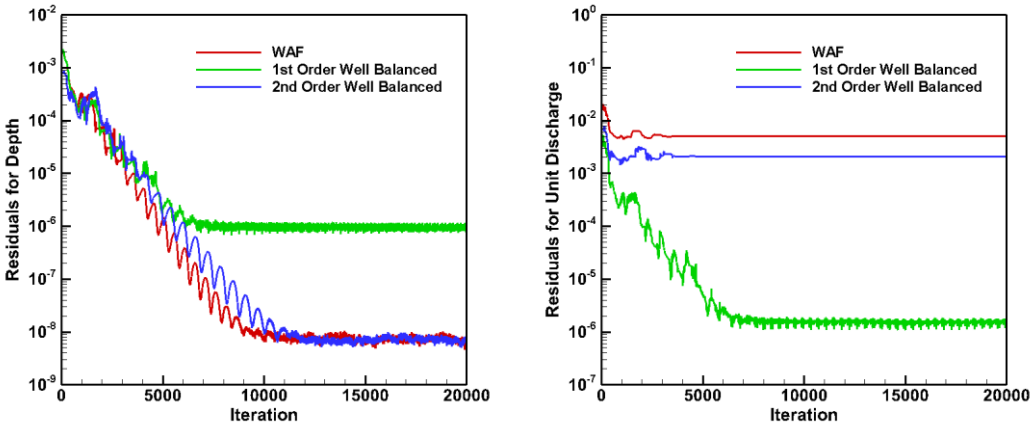

Figure 4.16. Residuals for Test Case 4: Steady Flow over a Bump; Transcritical Flow with Hydraulic Jump

Figure 4.14 shows that all methods used to solve this problem predict the water surface elevation accurately. Figure 4.15 shows excellent agreement between the result of the 2nd order well-balanced scheme and analytical value for unit discharge. However, there is a jump on calculated unit discharge near the hydraulic jump. The computing of the unit discharge by Pure WAF and first order well-balanced scheme is more challenging over the bump as it is obvious in Figure 4.15.

4.5. Numerical Solution of Test Case 5: Flow over a Bump; Subcritical Flow All over the Domain

Subcritical flow in the channel with the hump defined by happens when the incoming flow discharge is set to $4.42\ m^3/s$ and the flow depth at the end of the channel imposed as $2\ m$. These boundary conditions are applied as (4.15) and (4.16). Initially, the water depth and the flow velocity are equal $2\ m$ and zero, respectively. Problem is solved in a domain with 200 number of cells with the cell size of $\Delta x = 0.125\ m$. Manning's roughness coefficient is equal to zero. Time steps are calculated by setting

CFL number equal to 0.9 in all schemes. In the 2nd order well-balanced scheme, the relaxation factor α is taken as 0.05.

$$\begin{aligned} Q(-1) &= 4.42 \\ Q(0) &= 4.42 \\ H(-1) &= H(1) \\ H(0) &= H(1) \end{aligned} \tag{4.15}$$

and

$$\begin{aligned} Q(M+1) &= Q(M) \\ Q(M+2) &= Q(M) \\ H(M+1) &= 2 \\ H(M+2) &= 2 \end{aligned} \tag{4.16}$$

Numerical results of the water surface elevation and unit discharge of the channel are shown in Figure 4.17 and Figure 4.18. The calculated residuals for depth and unit discharge are plotted in Figure 4.19.

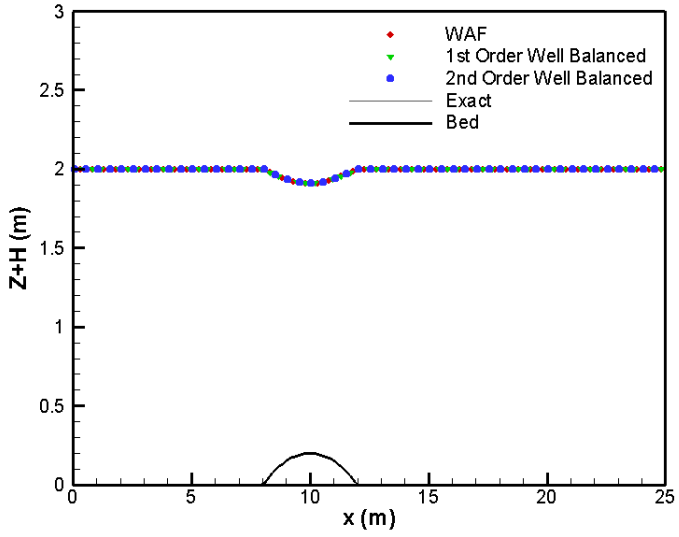

Figure 4.17. Comparison between numerical and analytical water surface elevations for test case 5: Flow over a Bump; Subcritical Flow All over the Domain

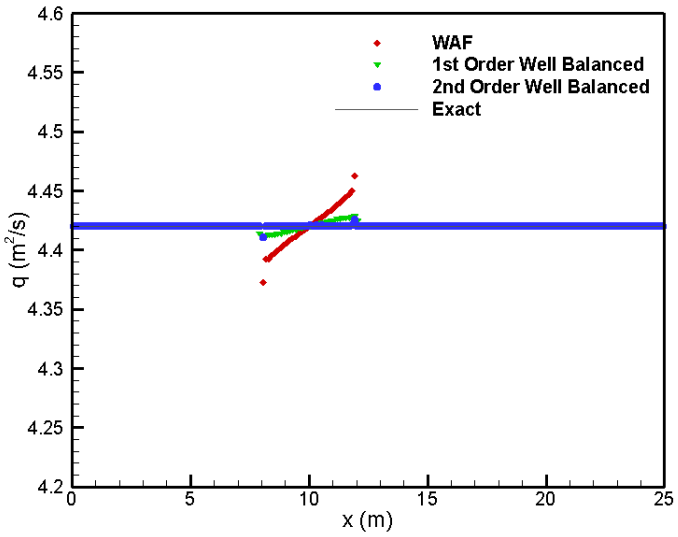

Figure 4.18. Comparison between numerical and analytical unit discharges for test case 5: Flow over a Bump; Subcritical Flow All over the Domain

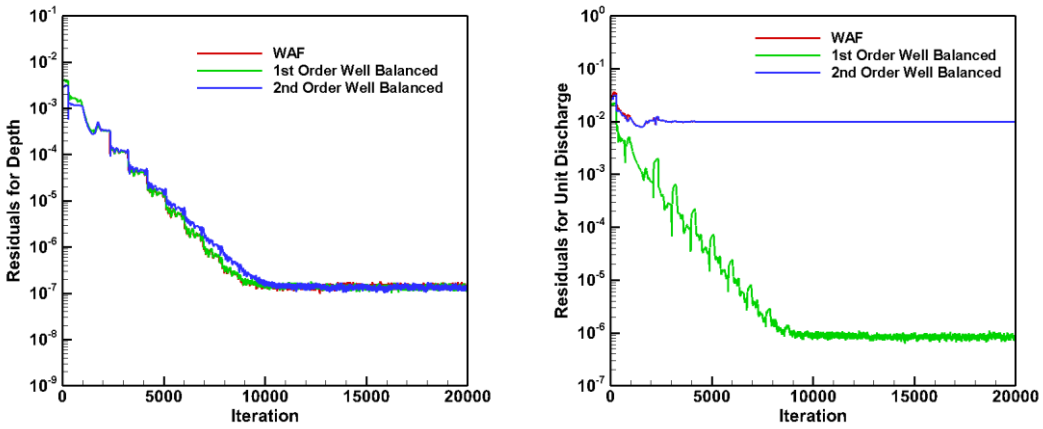

Figure 4.19. Residuals for Test Case 5: Flow over a Bump; Subcritical Flow All over the Domain

Same as the previous test case, the water surface elevations are perfectly calculated by all three schemes, and the challenging part is in predicting the unit discharge over the bump (see Figure 4.17). 2nd order well-balanced scheme calculates the unit discharge

precisely, nevertheless, there is an underestimating near the beginning of the bump and an overestimating at the end of the bump (see Figure 4.18). Compared with well-balanced schemes, pure WAF method gives the less accurate solution over the bump, where the unit discharge varies between $4.373 \sim 4.463\ m^3/s/m$, while the variation in unit discharge over the bump is in the range of $4.412 \sim 4.429\ m^3/s/m$ for the 1st order well-balanced scheme. As it is obvious in Figure 4.19, all numerical solutions converged after around 10000 iterations.

4.6. Numerical Solution of Test Case 6: Steady Flow over a Bump; Transcritical Flow without Hydraulic Jump

Here, initial and boundary conditions that cause the flow to be transcritical without hydraulic jump are initial water elevation of $0.25\ m$, initial velocity of zero, and the inflow discharge of $1.53\ m^3/s$. Again, channel assumed to be frictionless with Manning's roughness coefficient of zero. The boundary conditions for the unit discharge and depth are imposed as

$$\begin{aligned} Q(-1) &= 1.53 \\ Q(0) &= 1.53 \\ H(-1) &= H(1) \\ H(0) &= H(1) \end{aligned} \tag{4.17}$$

at the start of the channel, and

$$\begin{aligned} Q(M+1) &= Q(M) \\ Q(M+2) &= Q(M) \\ H(M+1) &= H(M) \\ H(M+2) &= H(M) \end{aligned} \tag{4.18}$$

at the end of the channel. For all cases, the CFL number is set to 0.9. Relaxation factor is set to 0.1 for the 2nd order well-balanced scheme. The domain is again divided to 200 cells with the mesh size of $\Delta x = 0.125\ m$. The numerical results are plotted in Figure 4.20 and Figure 4.21.

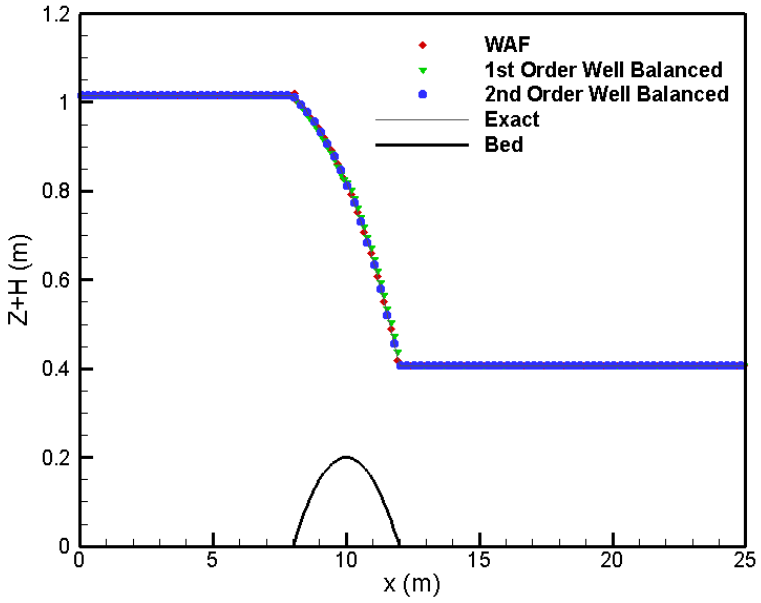

Figure 4.20. Comparison between numerical and analytical water surface elevations for test case 6: Steady Flow over a Bump; Transcritical Flow without Hydraulic Jump

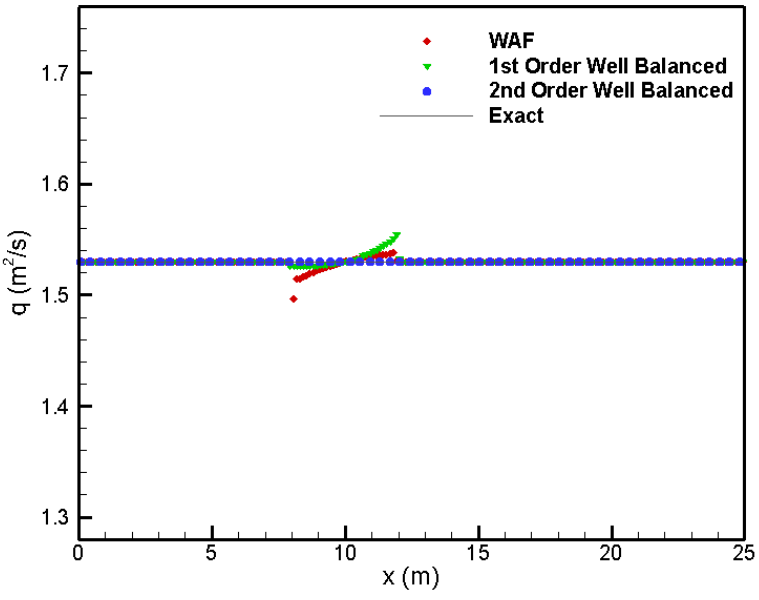

Figure 4.21. Comparison between numerical and analytical unit discharges for test case 6: Steady Flow over a Bump; Transcritical Flow without Hydraulic Jump

Numerical residuals of calculated depth and unit discharge are plotted in Figure 4.22.

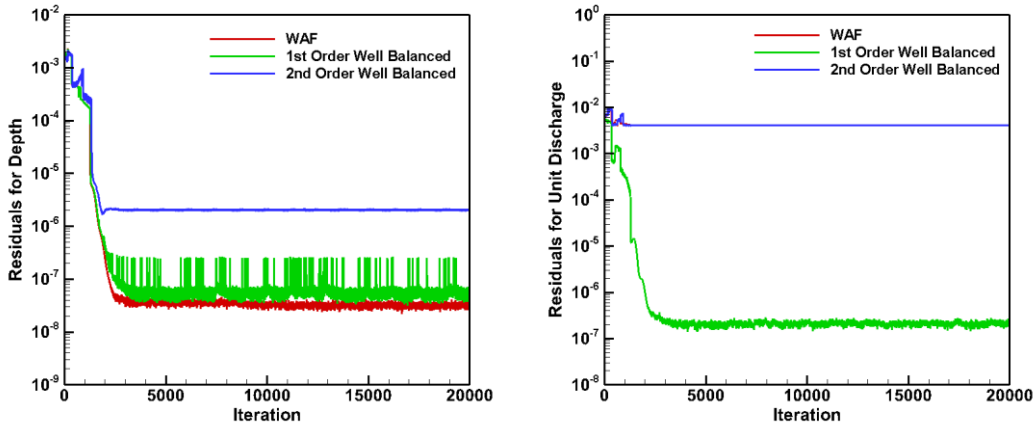

Figure 4.22. Residuals of depth for Test Case 6: Steady Flow over a Bump; Transcritical Flow without Hydraulic Jump

From residuals in Figure 4.22, it is obvious that the numerical solutions have converged after around 3000 iterations. Same as the last two steady flows over the bump, for all cases, there are excellent agreement between the numerical water surface elevations and exact solution (see Figure 4.21). Numerical unit discharge calculated by the 2nd order well-balanced scheme is very accurate (see Figure 4.21). Unit discharge calculated from the pure WAF and the 1st order well-balanced scheme vary between the ranges $1.497 \sim 1.539\, m^3/s/m$ and $1.526 \sim 1.533\, m^3/s/m$ over the bump, respectively.

4.7. Numerical Solution of Test Case 7: Surge Crossing a Step

This case is solved by pure WAF, 1st order well-balanced, and 2nd order well-balanced codes and the results for water surface elevations and the velocities are compared with the analytical results. The CFL number is set to 0.9, 0.9, and 0.4 for pure WAF, 1st order well-balanced and 2nd order well-balanced schemes, respectively. Relaxation factor is not applied here (i.e., α is teken 1). Initial conditions are imposed as water surface elevation of 5 m and zero velocity in the whole domain. Incoming surge is

imposed as a boundary condition at the left. Boundary conditions are implied as (4.19) and (4.20) for left and right of the channel respectively. Incoming unit discharge of the surge is obtained by multiplying the velocity obtained from (3.22) by the depth of the surge at the entrance.

$$\begin{aligned} Q(-1) &= 60.65269986 \\ Q(0) &= 60.65269986 \\ H(-1) &= 10 \\ H(0) &= 10 \end{aligned} \tag{4.19}$$

$$\begin{aligned} Q(M+1) &= -\mathrm{Q}(M) \\ Q(M+2) &= -\mathrm{Q}(M) \\ H(M+1) &= H(M) \\ H(M+2) &= H(M) \end{aligned} \tag{4.20}$$

The computational domain is divided for 400 cells in all solutions with the grid size of $dx = 25\ m$.

Comparisons of the numerical results with exact solutions are shown in Figure 4.23 and Figure 4.24.

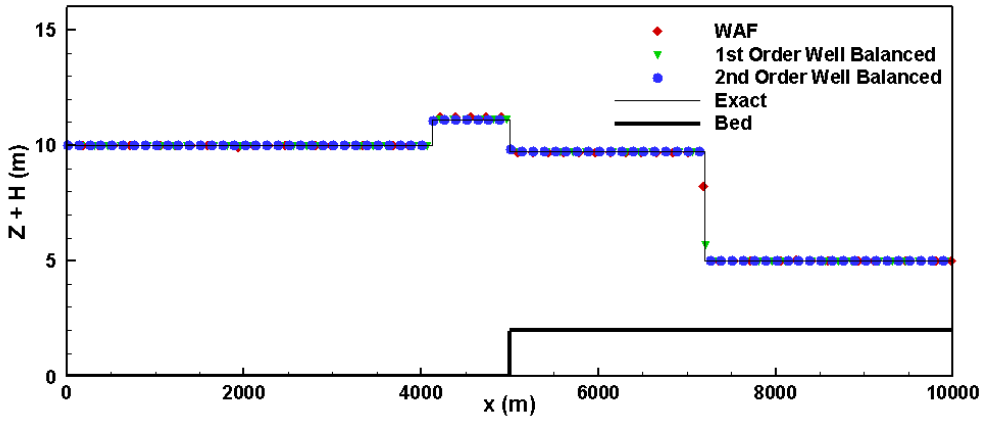

Figure 4.23. Comparison between numerical and analytical water surface elevations at t = 600.5 s for test case 7: Surge Crossing a Step

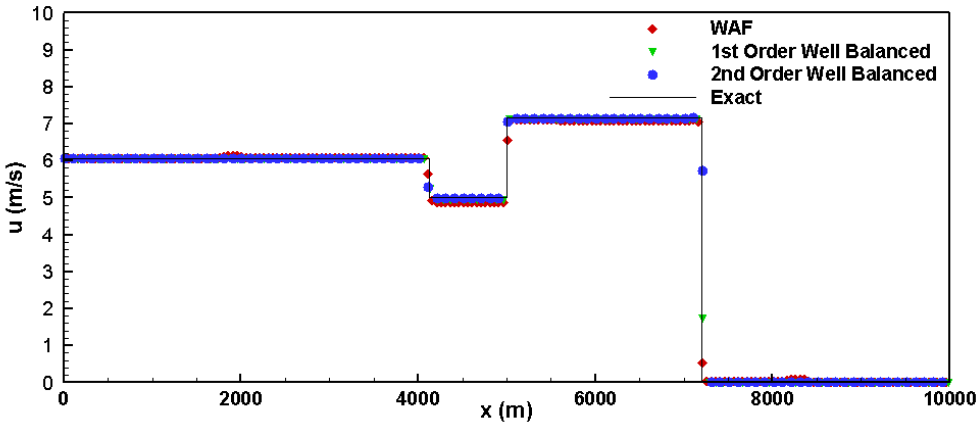

Figure 4.24. Comparison between numerical and analytical velocities at t = 600.5 s for test case 7: Surge Crossing a Step

Solving this test case with pure WAF results in some unrealistic waves that are initiated over the cell at the beginning of the vertical step and they travel to the left and right of the domain. Those waves are visible in Figure 4.24 near $x \approx 2000\ m$ and $x \approx 8200\ m$. That is because the pure WAF scheme is not well-balancing the bed slope source term with the numerical fluxes. On the other hand, both 1st order and 2nd order well-balanced schemes solve the problem perfectly and predict the velocity and height of the surges accurately.

4.8. Numerical Solution of Test Case 8: Oscillation on a Parabolic Bed

1st order and 2nd order well-balanced schemes are used to solve this problem. 10000 number of grids with $dx = 1\ m$ are used in both schemes. Initially, the lake is stationary with zero velocity everywhere and the initial water surface profile is defined by (3.25)**.** Wall boundary conditions are imposed on both end of the computational domain using ghost cells as

$$Q(-1) = -Q(1) \tag{4.21}$$

$$
\begin{aligned}
Q(0) &= -Q(1) \\
H(-1) &= H(1) \\
H(0) &= H(1) \\
Q(M+1) &= -Q(\mathrm{M}) \\
Q(M+2) &= -Q(\mathrm{M}) \\
H(M+1) &= H(\mathrm{M}) \\
H(M+2) &= H(\mathrm{M})
\end{aligned}
\tag{4.22}
$$

Time steps are calculated using the CFL number 0.9 for both 1st order and 2nd order schemes.

The numerical results are compared with the analytical solution in Figure 4.25 and Figure 4.26. The results of the numerical solutions after one oscillation show general agreement between the numerical and analytical solutions. Although there still remains unrealistic unit discharge in both schemes, the range of error in computed unit discharge is narrower in the 2nd order scheme rather than the one in the 1st order scheme. Also, 2nd order well-balanced scheme acts better in the prediction of the water surface elevations compared with the 1st order well-balanced scheme.

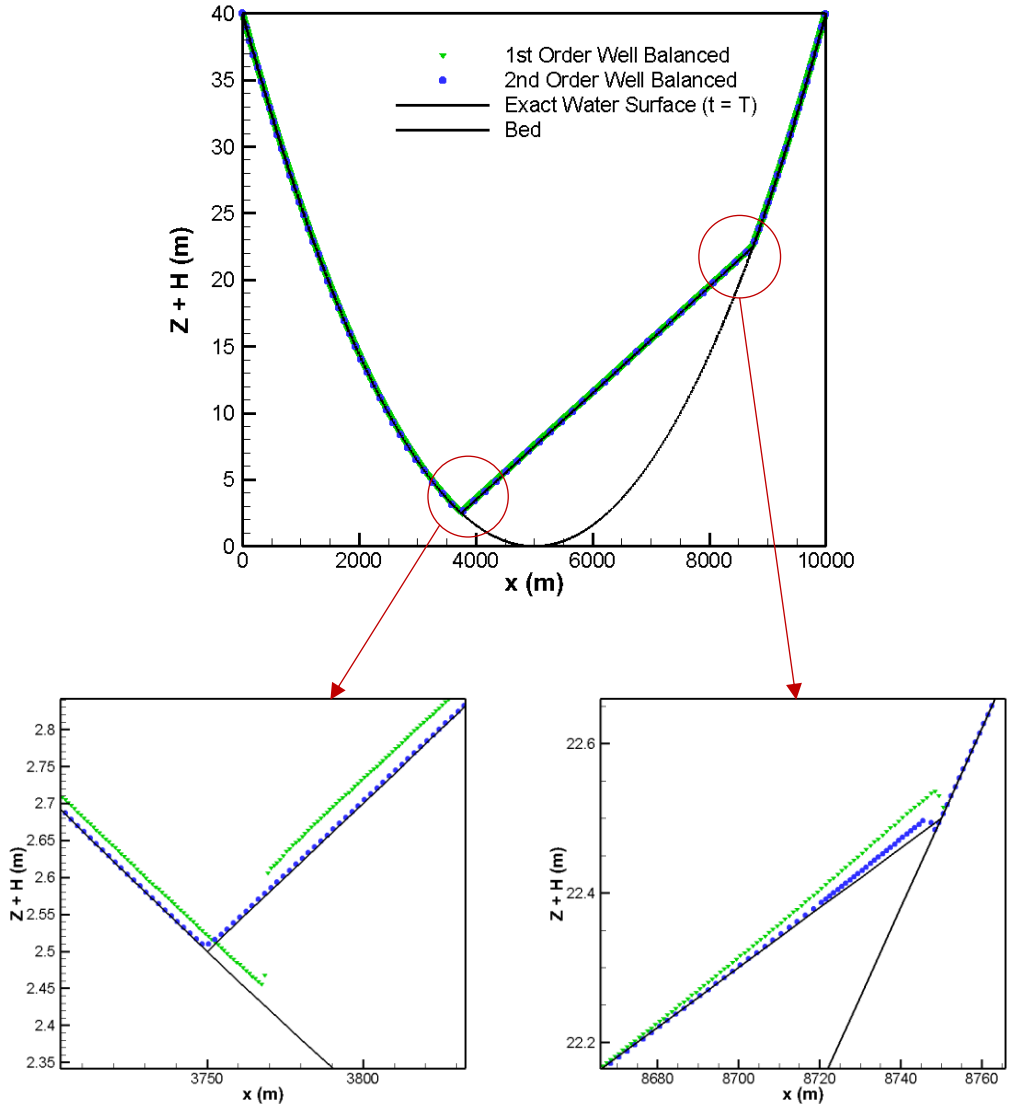

Figure 4.25. Comparison between numerical and analytical water surface elevations for test case 8: Oscillation on a Parabolic Bed; Up) full plot and dawn) magnified regions.

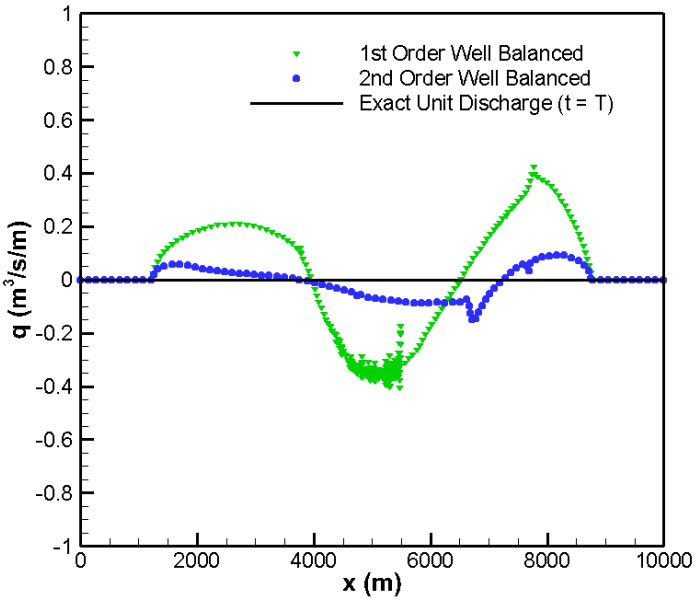

Figure 4.26. Comparison between numerical and analytical unit discharges for test case 8: Oscillation on a Parabolic Bed

4.9. Numerical Solution of Test Case 9: Comparison with Experimental Data; Dam-Break Flood Waves in a Dry Channel with a Hump

In this case, the computational domain is divided into 1780 computational cells. The size of each grid is equal to 0.005 m. Manning's roughness coefficient is taken equal to 0.01. Wall boundary condition at the left and outflow boundary condition at the right are imposed as

$$\begin{aligned} Q(-1) &= -Q(1) \\ Q(0) &= -Q(1) \\ H(-1) &= H(1) \\ H(0) &= H(1) \end{aligned} \tag{4.23}$$

$$\begin{aligned} Q(M+1) &= Q(\mathrm{M}) \\ Q(M+2) &= Q(\mathrm{M}) \\ H(M+1) &= H(\mathrm{M}) \\ H(M+2) &= H(\mathrm{M}) \end{aligned} \tag{4.24}$$

The numerical results using CFL number of 0.9 for 1st order scheme and 0.45 for 2nd order well-balanced schemes are plotted in Figure 4.27.

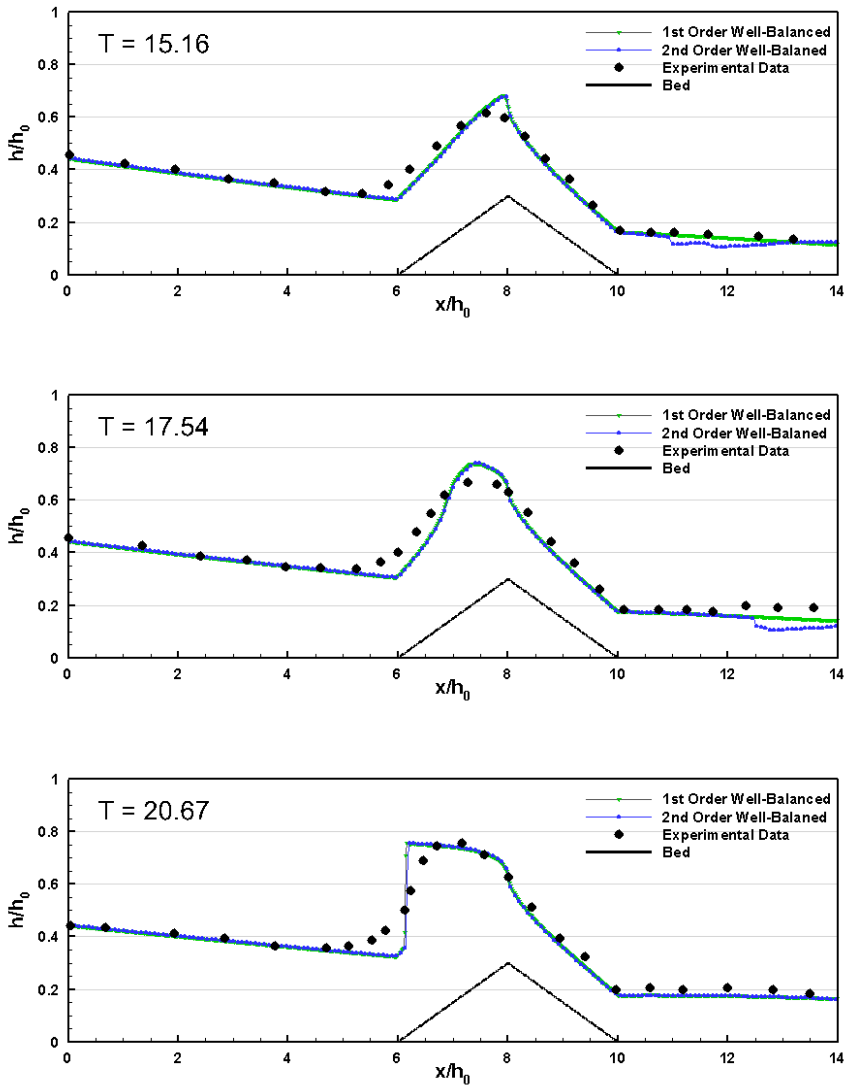

Figure 4.27. Comparison between numerical and experimental water surface elevation in different dimensionless times for test case 9: Dam-Break Flood Waves in a Dry Channel with a Hump

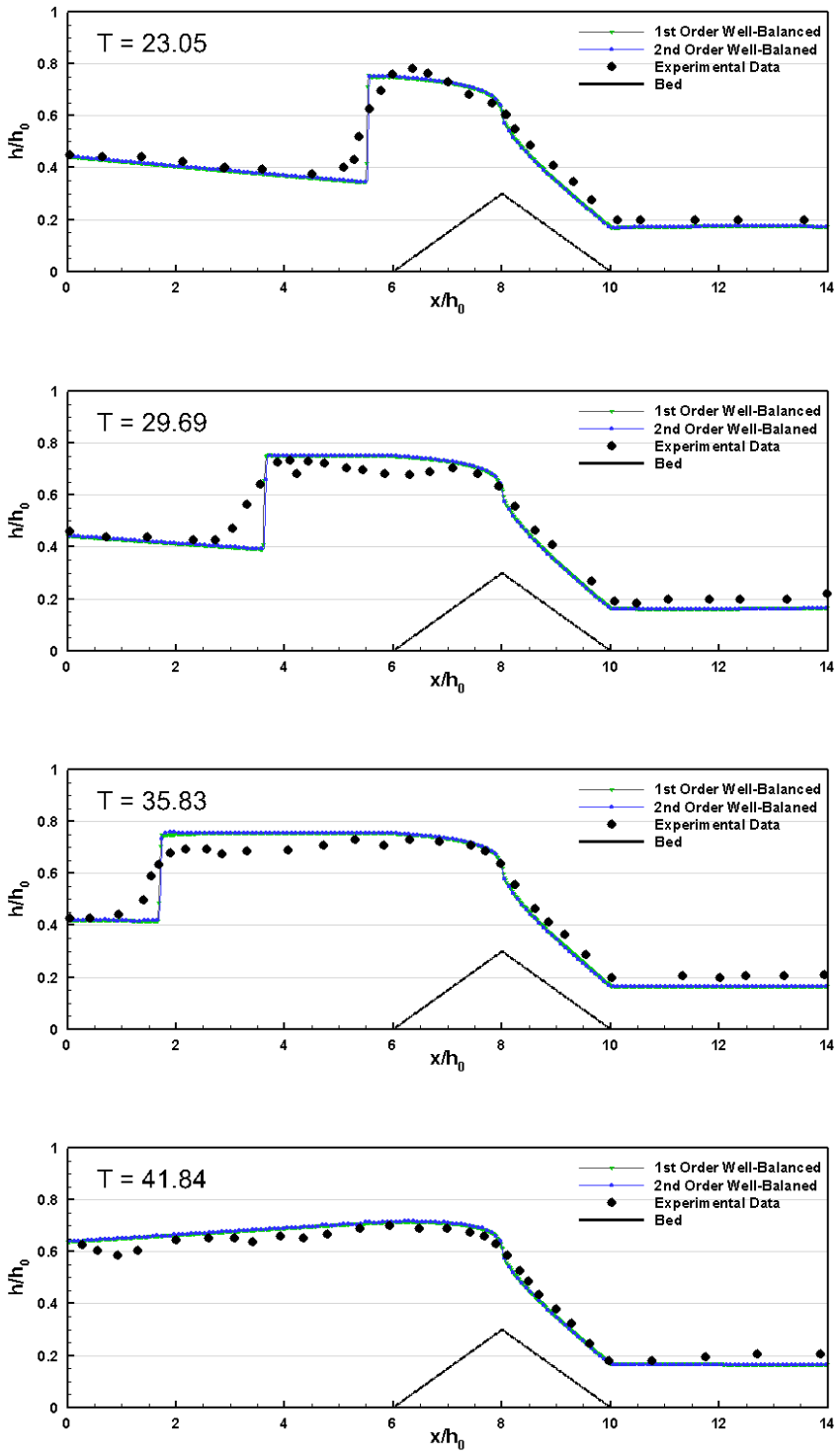

Figure 4.27 (Continued) Comparison between numerical and experimental water surface elevation in different dimensionless times for test case 9: Dam-Break Flood Waves in a Dry Channel with a Hump

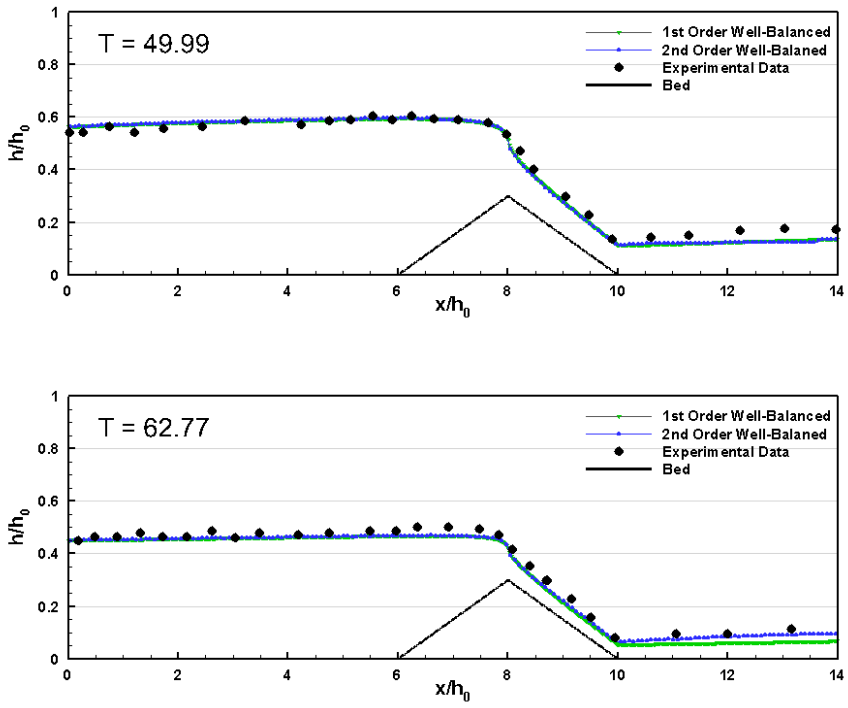

Figure 4.27 (Continued) Comparison between numerical and experimental water surface elevation in different dimensionless times for test case 9: Dam-Break Flood Waves in a Dry Channel with a Hump

The verification of the developed well-balanced codes shows very good agreement between the experimental measurements and numerical solutions. After the dame break flood wave passes over the obstacle a bore wave is generated at dimensionless time $T = 15.16$ and moves in the negative direction. Shallow water equations simulate the bore vertically as a shock wave and predict the location of the negative bore satisfactorily. One noticeable difference between the experimentally measured water surface profile and the one obtained by solving the shallow water equations numerically is that the shallow water equations compute the negative bore much steeper than the one obtained by experimental data. This situation is apparent at dimensionless times 20.67, 23.05, 29.69, and 35.83.

This test case is also solved with coarser meshes to see the effects of the mesh sizes in the numerical solutions. In addition to the grid size of $\Delta x = 0.005\, m$ with 1780

number of grids, 2 coarser grids with 178 and 89 number of grids are also selected, which produce 10 and 20 times coarser meshes with the sizes of $\Delta x = 0.05\,m$ and $\Delta x = 0.1\,m$, respectively. The results are presented in Figure 4.28 for both WAF1WB and WAF2WB codes at the dimensionless time $T = 35.33$ only. The results show that the general forms of the water surface profiles for this problem are also obtained with coarser grids. However, as the meshes get coarser, the negative wave gets milder angles.

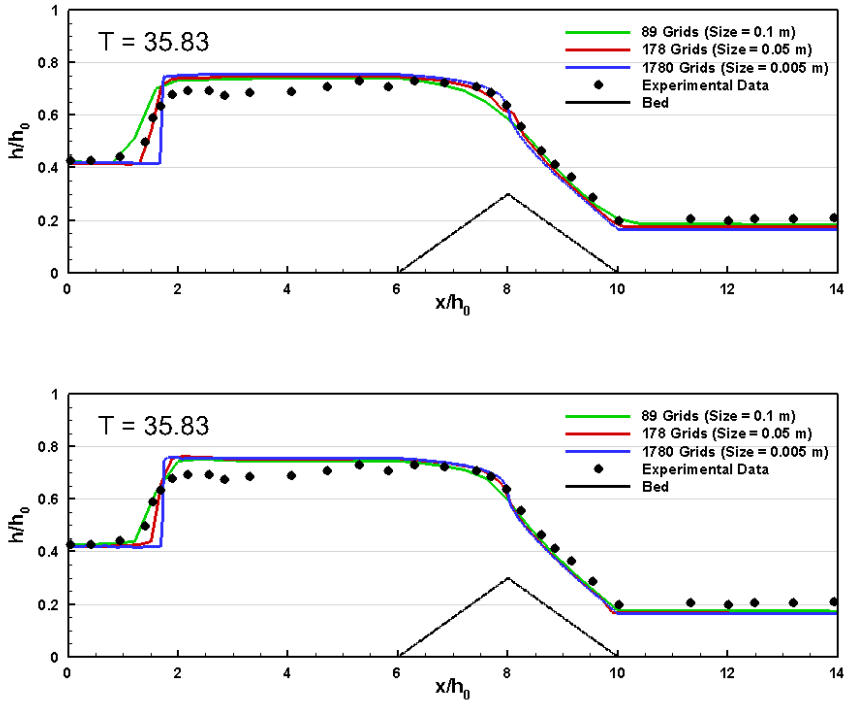

Figure 4.28. Comparison between the numerical water surface elevations obtained by WAF1WB (up) and WAF2WB (down) codes using different mesh sizes for test case 9.

4.10. Numerical Solution of Test Case 10: Dam Break Flow over Champion-Stage like Step

This problem is solved by the WAF1WB and WAF2WB codes. The domain is divided into 200 computational cells. Wall boundary conditions are considered at left and right of the domain as

$$\begin{aligned} Q(-1) &= -Q(1) \\ Q(0) &= -Q(1) \\ H(-1) &= H(1) \\ H(0) &= H(1) \end{aligned} \tag{4.25}$$

$$\begin{aligned} Q(M+1) &= -Q(\mathrm{M}) \\ Q(M+2) &= -Q(\mathrm{M}) \\ H(M+1) &= H(\mathrm{M}) \\ H(M+2) &= H(\mathrm{M}) \end{aligned} \tag{4.26}$$

The code has run until $t = 1000\ s$ with the CFL number of 0.9 for both codes. Dam break flow starts by removing the imaginary wall at time = 0 s and it reaches the first step at $t \approx 2.2\ s$, approximately. Then, the flow crosses over the steps one by one. By hitting the flow with the positive steps, waves are created that travels in the negative direction. The incoming flow is divided into two portions; one portion crosses over the steps and goes to the right of the stage, and the other portion remains in the left side of the stage. The goal was to recover the hydrostatic water surface without any noise and discontinuity on it, specially over the sharp corners, after the waves disappeared and water reached the nearly stationary state. This goal is achieved using both WAF1WB and WAF2WB codes. The results of the simulation are presented in a set of screenshots at different time steps in Figure 4.29.

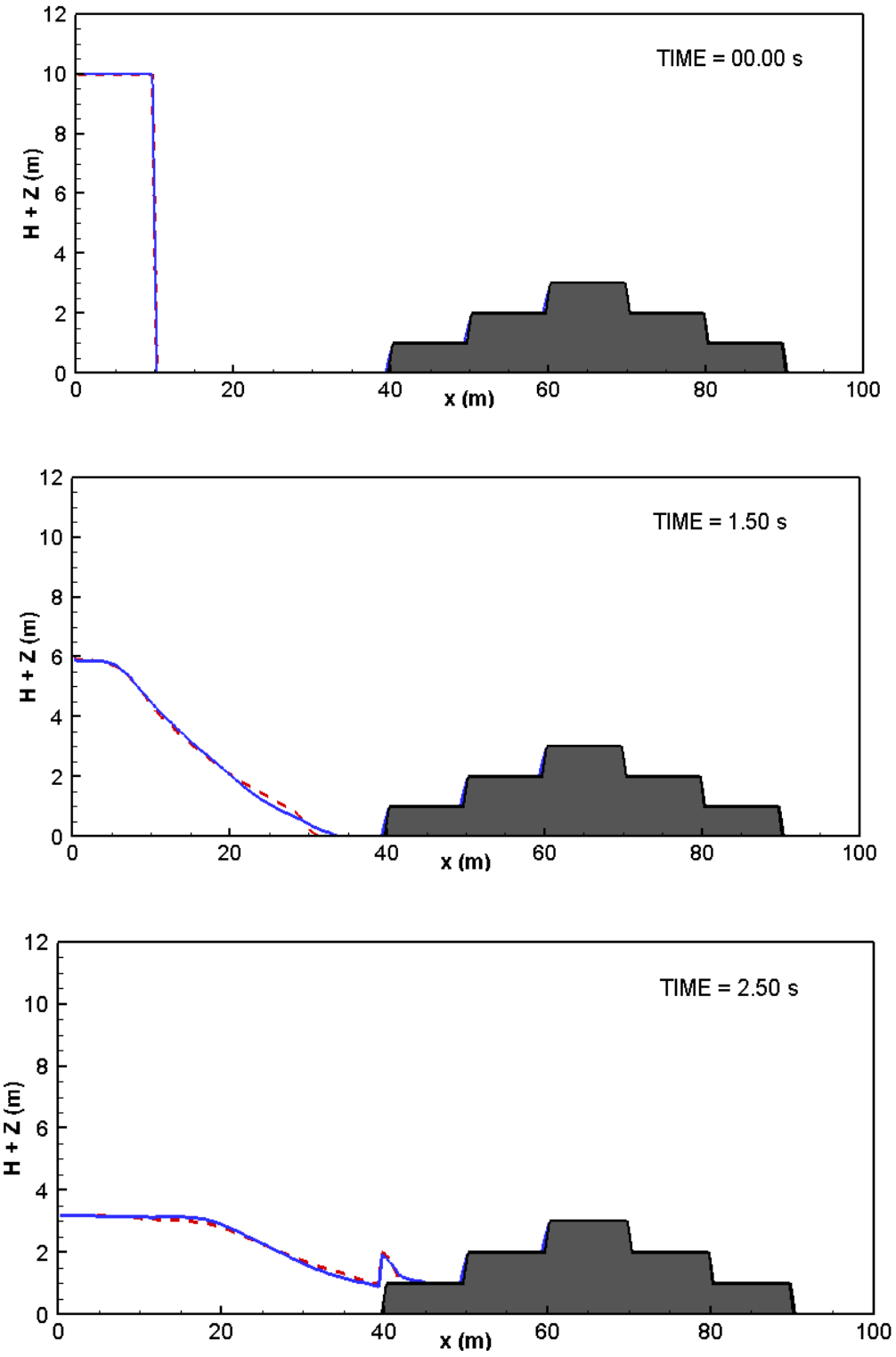

Figure 4.29. Solution of test case 10 at different time steps using WAF1WB (dashed line) and WAF2WB (solid line) codes.

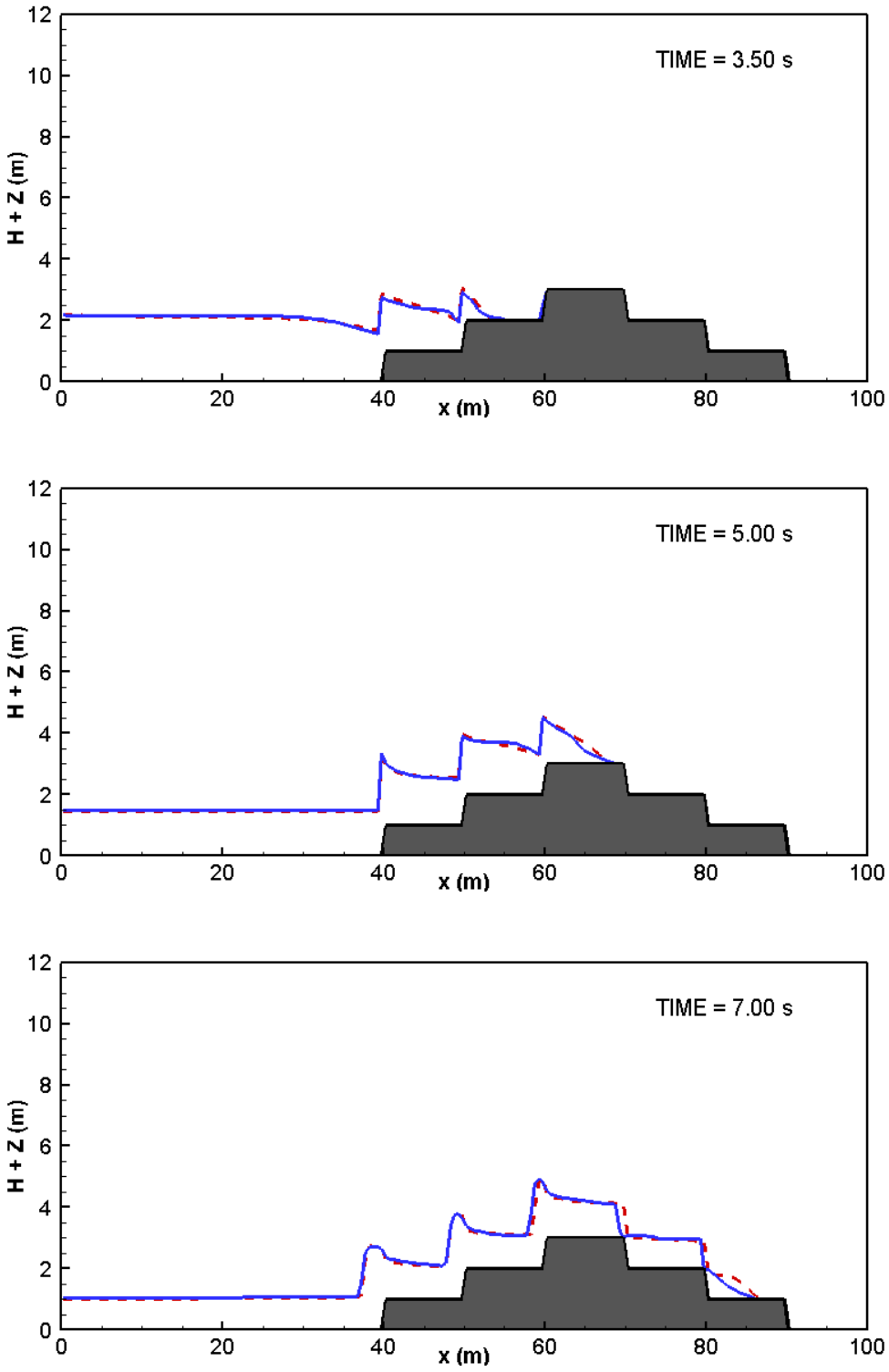

Figure 4.29 (continued) Solution of test case 10 at different time steps using WAF1WB (dashed line) and WAF2WB (solid line) codes.

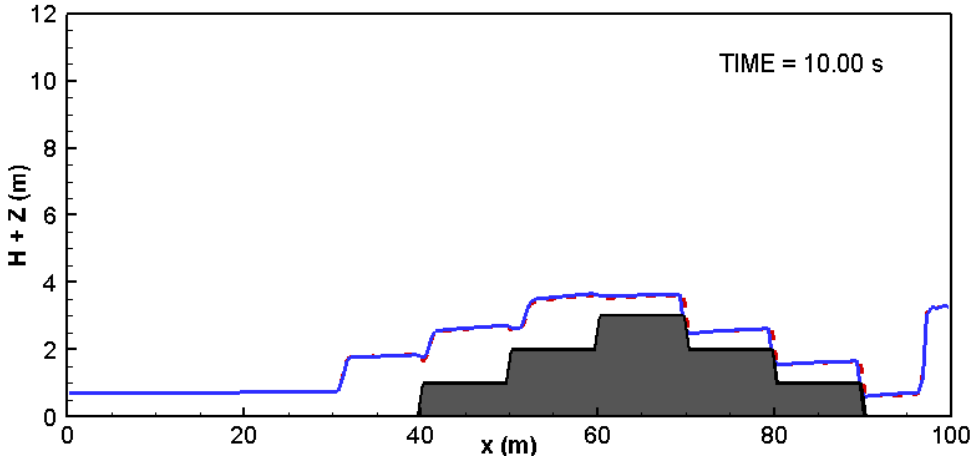

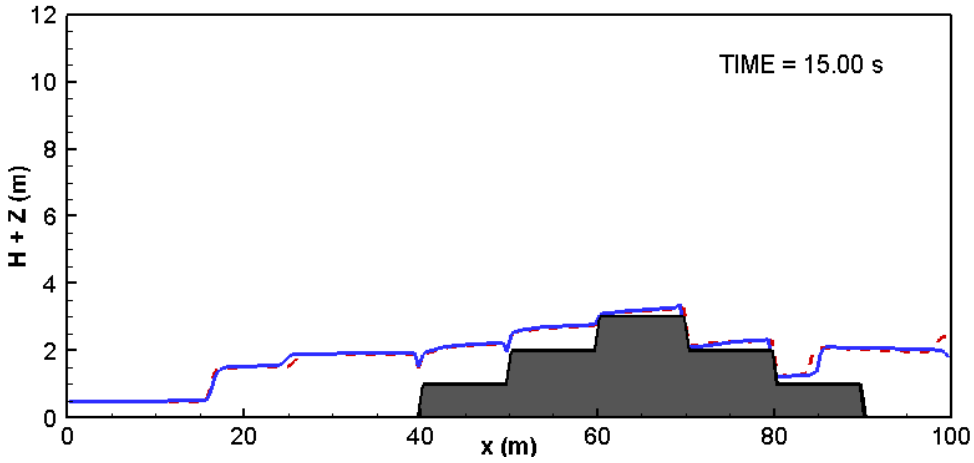

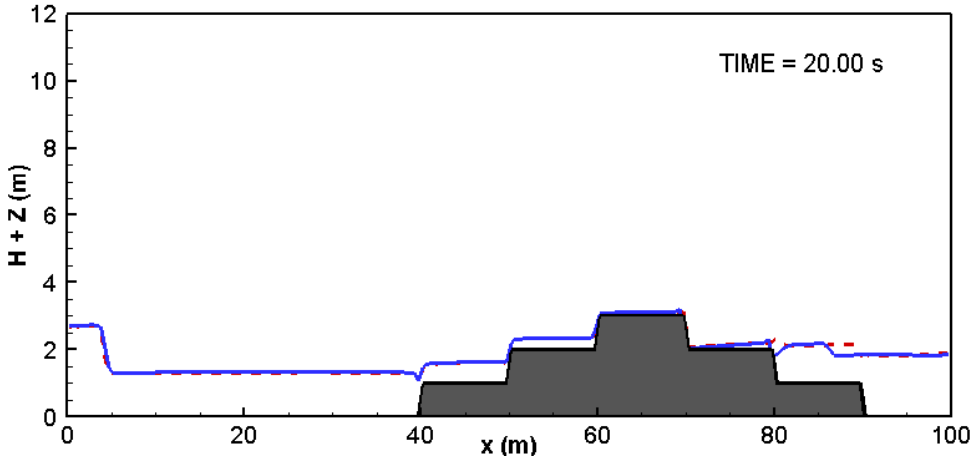

Figure 4.29 (continued) Solution of test case 10 at different time steps using WAF1WB (dashed line) and WAF2WB (solid line) codes.

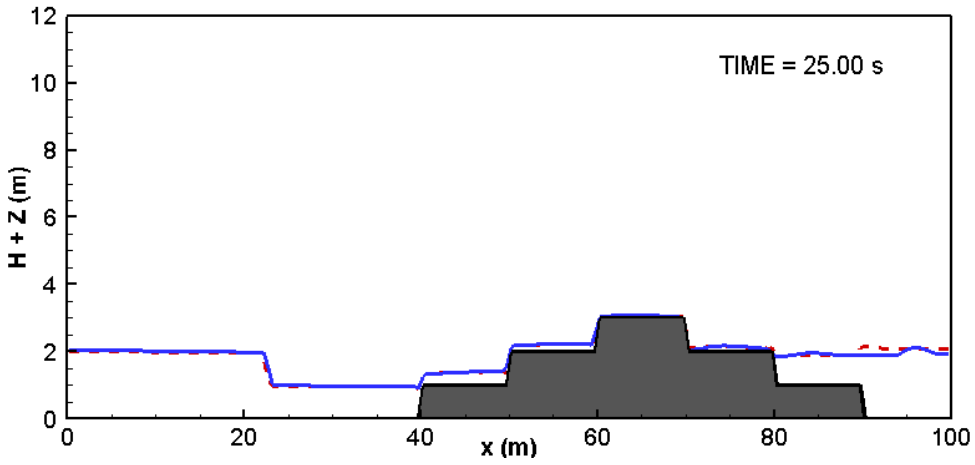

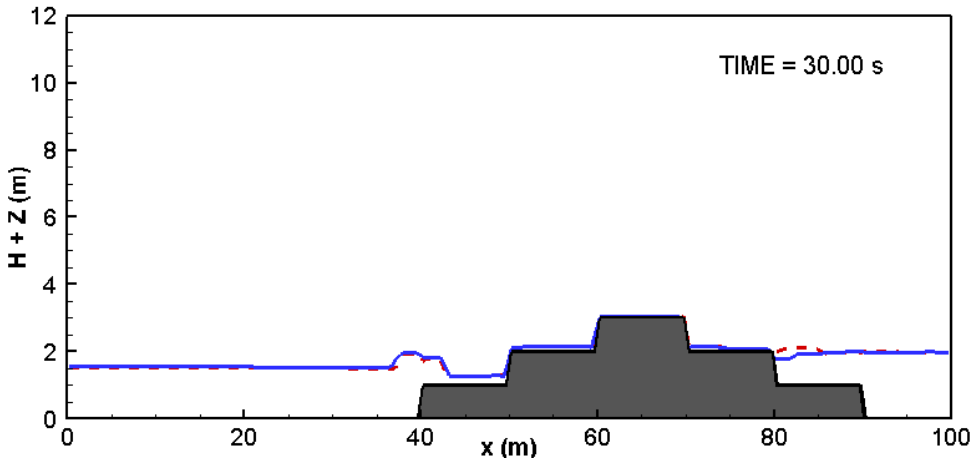

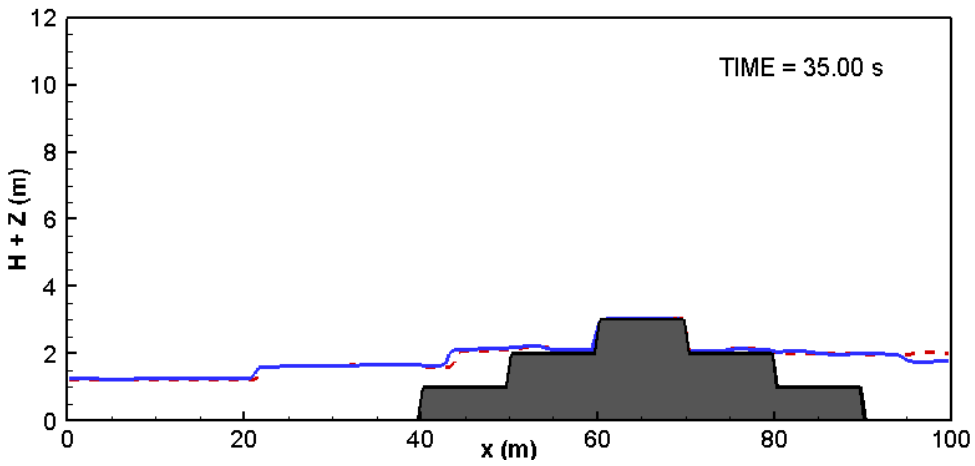

Figure 4.29 (continued) Solution of test case 10 at different time steps using WAF1WB (dashed line) and WAF2WB (solid line) codes.

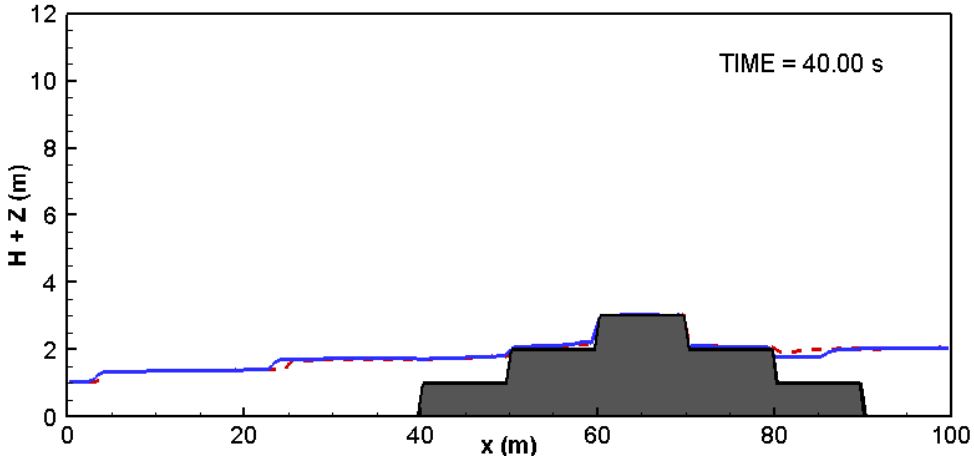

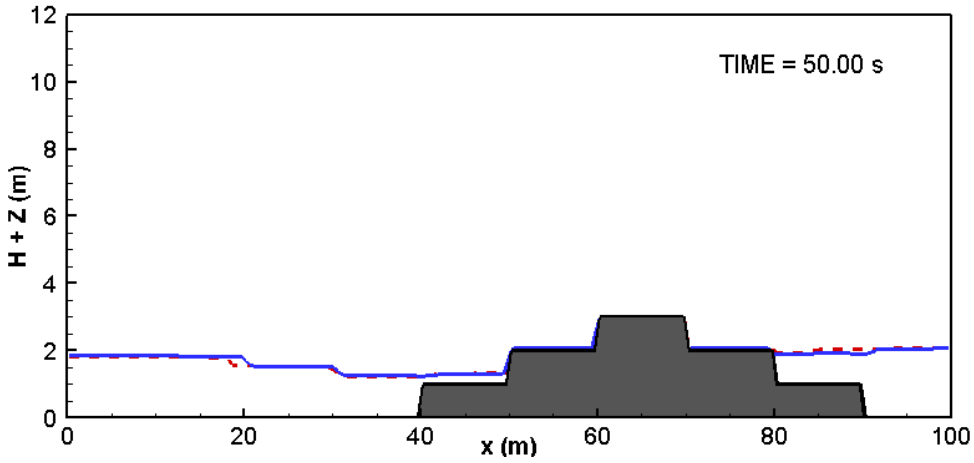

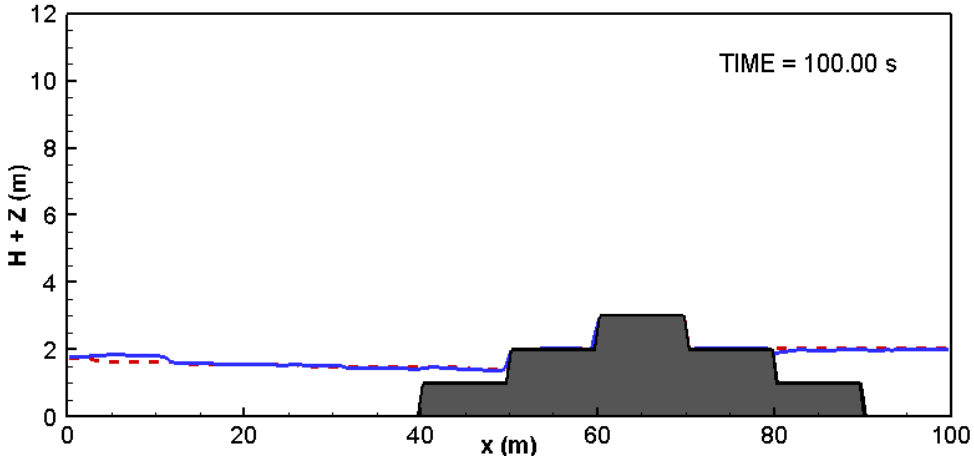

Figure 4.29 (continued) Solution of test case 10 at different time steps using WAF1WB (dashed line) and WAF2WB (solid line) codes.

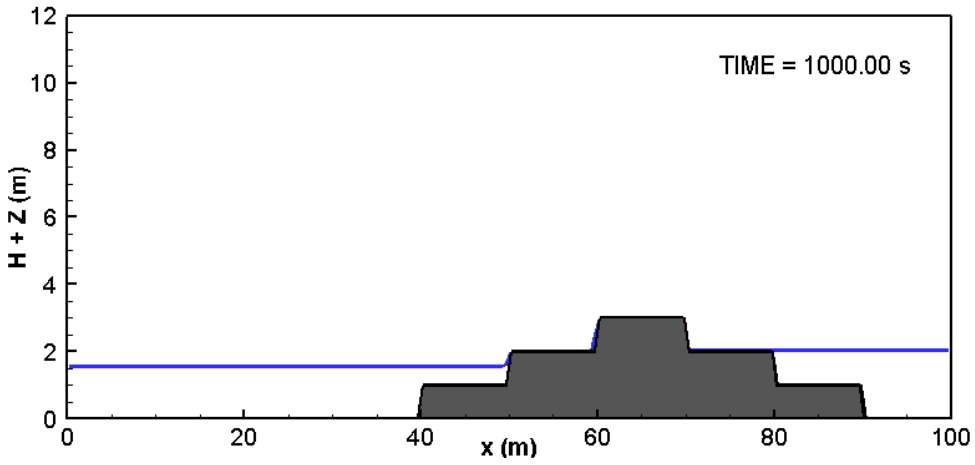

Figure 4.29 (continued) Solution of test case 10 at different time steps using WAF1WB (dashed line) and WAF2WB (solid line) codes.

One important feature of numerical solutions of shallow water equations is how much accurate they are in preserving the amount of fluid in the domain or in another word, the accuracy in ensuring the continuity condition. To evaluate the performance of the scheme in preserving the continuity and effects of the mesh sizes on it, the amount of water at each time step is calculated. Different mesh sizes with 200, 400, 800, 1600, and 3200 number of grids are selected to see the effects of the mesh size. The results for the first order and second order well-balanced schemes are presented in Figure 4.30.

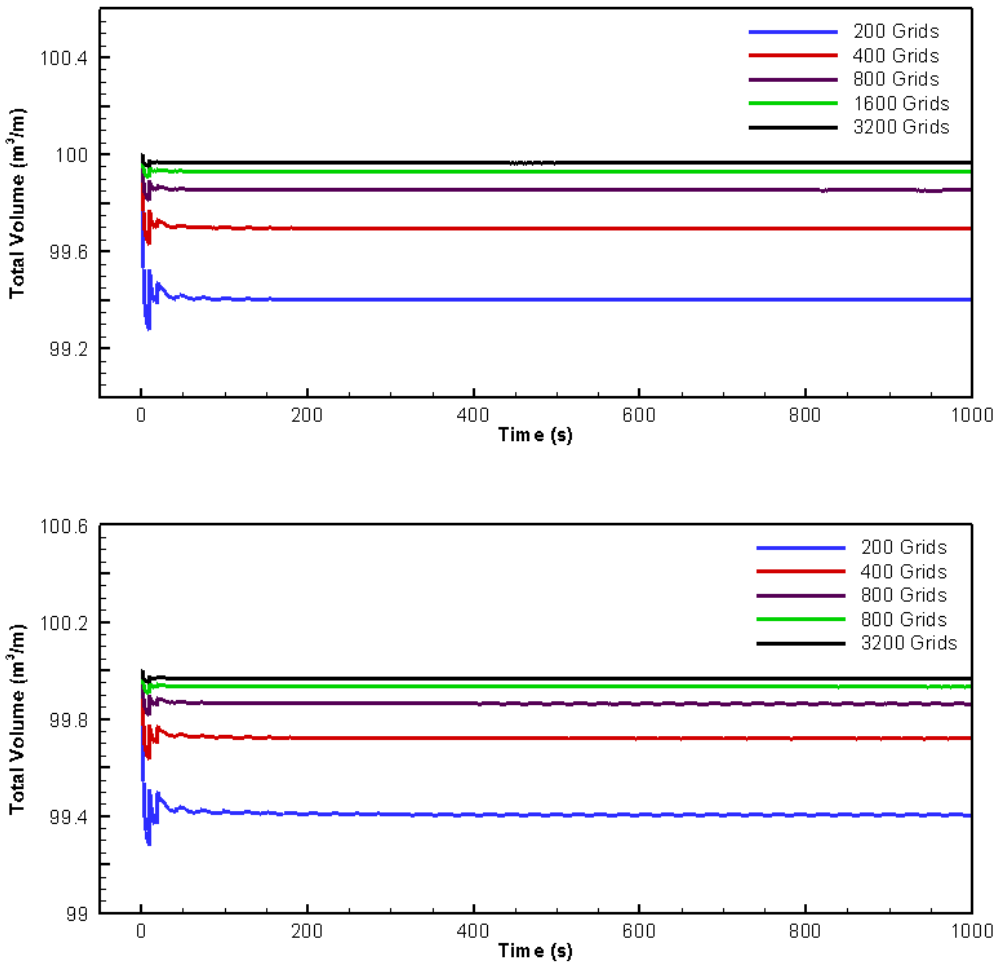

Figure 4.30. The calculated amount of water in the domain at each time step using WAF1WB (up) and WAF2WB (down) codes, and different mesh sizes.

Initially, there is $100\ m^3/m$ water in the domain. After the dam break flow occurs however, it reduces unreallasticly. Although, the finer grids yelds in less error.

CHAPTER 5

CONCLUSION AND RECOMMENDATION

Numerical solutions of shallow water equations which are widely used in tsunamis, tides, wind waves, river floods, dam-break flows and open channel flows have been studied in this thesis. Numerical solution of the shallow water equations can be challenging when the equations are solved in domains containing discontinuities in the channel beds which cause abrupt change in the source term of the governing equations. Another difficulty in the solution of the shallow water equations appears in the presence of dry regions in the domain.

Three schemes have been used as numerical solutions of shallow water equations in this study, namely 1) pure WAF method without well-balancing property, where the finite volume method has been used to discretize the governing equations, HLL method has been used as an approximate Riemann solver, and the fluxes have been computed by the TVD version of Weighted Average Flux (WAF) method, 2) first order well-balanced method, which is the same as the pure WAF scheme, but the source term has been treated by the use of first order "Hydrostatic Reconstruction" method, and 3) second order well-balanced scheme, which is the same as the first order well-balanced scheme, but the piecewise linear function has been used to define the water surface slope in each cell to provide better approximation for Riemann states used in the Riemann solver and the bottom has been defined linearly.

Three codes have been developed in FORTRAN based on the above mentioned schemes. The programs have been called WAF, WAF1WB, and WAF2WB for the pure WAF scheme, first order well-balanced scheme, and second order well-balanced scheme, respectively. These codes have been validated by using nine well-known steady and unsteady test cases in the literature and the results of each are compared

with each other and with the available analytical solutions or experimental data. Although distinctions between the accuracy of the numerical results have been observed, more or less, in the studied test cases, the general agreement between the numerical results and analytical solutions or experimental data has been obtained for all test cases. Generally, predicting the water surface profile was not challenging part for all three schemes. However, there were distinguishable differences in the numerical unit discharges that are calculated by solving the momentum equation. As expected, the WAF2WB was more accurate in solving the shallow water equations compared with the other two methods since in the second order scheme, the bed is defined with better accuracy and fluxes are calculated in each cell interface by more accurately defined Riemann states that are obtained by the use of piecewise linear function. Nevertheless, using the piecewise linear function has introduced oscillations in some steady state cases. Those oscillations have been prevented by the use of relaxation factor that has been applied to the piecewise linear function (see equations 4.1).

A new test case (Test Case-10) has been introduced in chapter three, numerical solutions of which are given in chapter four. The idea behind defining this test case was to examine the developed codes in solving a problem that contains numerically challenging situations in solving of the shallow water equations namely, sharp changes in bed elevation and existing of the dry area in the domain. To do this, a champion-stage like discontinuity was located in the middle of the channel and a dam-break flow and overtopping of it over the stages was studied. The goal was to see the flow behavior when it collided to the steps, overtopped from it, and after a certain time that all the waves disappeared, to observe a flat and smooth water surface, especially over the sharp edges. This goal was achieved by both well-balanced codes, WAF1WB and WAF2WB. Flow divided into two portions, one portion overtopped the stage and one portion remained at the left of the stage. Flat and smooth water surface profile was observed at the left and right of the stage in the results of both WAF1WB and WAF2WB.

All three codes in this study have been developed to solve one-dimensional problems. Extension of the developed codes to solve two-dimensional shallow water equations can be interesting topic for the future studies. One of the difficulties in the numerical solutions of the test cases was the oscillations caused by linear piecewise reconstruction technique in the 2nd order well-balanced scheme, that have been averted by applying relaxation factor to the limiter function. However, in some test cases, there was a need for very small relaxation factor. The reason for these unwanted oscillations also can be studied elaborately in the future studies.

REFERENCES

Audusse, E., Bouchut, F., Bouchut, M., Klein, R., Perthame, B. (2004). A Fast and Stable Well-Balanced Scheme with Hydrostatic Reconstruction for Shallow Water Flows. *SIAM Journal on Scientific Computing*, *25*(6), 2050–2065. https://doi.org/10.1137/S1064827503431090

Bermúdez, A., Dervieux, A., Desideri, J. A., Vázquez, M. E. (1998). Upwind schemes for the two-dimensional shallow water equations with variable depth using unstructured meshes. *Computer Methods in Applied Mechanics and Engineering*, *155*(1–2), 49–72. https://doi.org/10.1016/S0045-7825(97)85625-3

Bermudez, A., & Vazquez, M. E. (1994). Upwind methods for hyperbolic conservation laws with source terms. *Computers & Fluids*, *23*(8), 1049–1071. https://doi.org/10.1016/0045-7930(94)90004-3

Bollermann, A., Chen, G., Kurganov, A., Noelle, S. (2013). A well-balanced reconstruction of Wet/Dry fronts for the shallow water equations. *Journal of Scientific Computing*, *56*(2), 267–290. https://doi.org/10.1007/s10915-012-9677-5

Bollermann, A., Noelle, S., Lukáčová-Medvid'ová, M. (2011). Finite Volume Evolution Galerkin Methods for the Shallow Water Equations with Dry Beds. *Communications in Computational Physics*, *10*(2), 371–404. https://doi.org/10.4208/cicp.220210.020710a

Chow, V. T. (1959). *Open Channel Hydraulics, Ven Te Chow, 1959: Open Channel Hydraulics*. Kogakusha. Retrieved from https://books.google.com.tr/books?id=N_tjDwAAQBAJ

Delis, A. I., & Skeels, C. P. (1998). TVD schemes for open channel flow. *International Journal for Numerical Methods in Fluids*, *26*(7), 791–809. https://doi.org/10.1002/(SICI)1097-0363(19980415)26:7<791::AID-FLD688>3.3.CO;2-E

Harten, A., Lax, P. D., Leer, B. van. (1983). On Upstream Differencing and Godunov-Type Schemes for Hyperbolic Conservation Laws. *SIAM Review*, *25*(1), 35–61. https://doi.org/10.1137/1025002

Hu, K., Mingham, C. G., Causon, D. M. (2000). Numerical simulation of wave

overtopping of coastal structures using the non-linear shallow water equations. *Coastal Engineering*, *41*(4), 433–465. https://doi.org/10.1016/S0378-3839(00)00040-5

Kurganov, A., & Petrova, G. (2007). A second-order well-balanced positivity preserving central-upwind scheme for the Saint-Venant system. *Communications in Mathematical Sciences*, *5*(1), 133–160. https://doi.org/10.4310/CMS.2007.v5.n1.a6

MacDonald, I., Baines, M. J., Nichols, N. K., Samuels, P. G. (2002). Analytic Benchmark Solutions for Open-Channel Flows. *Journal of Hydraulic Engineering*, *123*(11), 1041–1045. https://doi.org/10.1061/(asce)0733-9429(1997)123:11(1041)

MacDonald, Ian. (1996). Analysis and computation of steady open channel flow. *University of Reading*, (September), 219. Retrieved from http://ethos.bl.uk/OrderDetails.do?uin=uk.bl.ethos.336664?

Mungkasi, S., & Roberts, S. G. (2010). On the best quantity reconstructions for a well balanced finite volume method used to solve the shallow water wave equations with a wet/dry interface. In P. Howlett, M. Nelson, & A. J. Roberts (Eds.), *Proceedings of the 9th Biennial Engineering Mathematics and Applications Conference, EMAC-2009* (Vol. 51, pp. C48--C65).

Noelle, S., Pankratz, N., Puppo, G., Natvig, J. R. (2006). Well-balanced finite volume schemes of arbitrary order of accuracy for shallow water flows. *Journal of Computational Physics*, *213*(2), 474–499. https://doi.org/10.1016/j.jcp.2005.08.019

Ozmen-Cagatay, H., Kocaman, S., Guzel, H. (2014). Investigation of dam-break flood waves in a dry channel with a hump. *Journal of Hydro-Environment Research*, *8*(3), 304–315. https://doi.org/10.1016/J.JHER.2014.01.005

Randall J. Leveque. (2004). Finite Volume Methods for Hyperbolic Problems. *Animal Genetics*.

Sweby, P. K. (1984). High Resolution Schemes Using Flux Limiters for Hyperbolic Conservation Laws. *SIAM Journal on Numerical Analysis*, *21*(5), 995–1011. https://doi.org/10.1137/0721062

Thacker, W. C. (1981). Some exact solutions to the nonlinear shallow-water wave equations. *Journal of Fluid Mechanics*, *107*(1), 499.

https://doi.org/10.1017/S0022112081001882

Toro, E. F. (1989). A Weighted Average Flux Method for Hyperbolic Conservation Laws. *Proceedings of the Royal Society A: Mathematical, Physical and Engineering Sciences*, *423*(1865), 401–418. https://doi.org/10.1098/rspa.1989.0062

Toro, E. F. (1992). Riemann problems and the WAF method for solving the two-dimensional shallow water equations. *Philosophical Transactions of the Royal Society of London. Series A: Physical and Engineering Sciences*, *338*(1649), 43–68. https://doi.org/10.1098/rsta.1992.0002

Toro, E. F. (2001). *Shock-capturing methods for free-surface shallow flows*. Chichester ; New York : John Wiley & Sons.

van Leer, B. (1985). On the Relation Between the Upwind-Differencing Schemes of Godunov, Engquist–Osher and Roe. *SIAM Journal on Scientific and Statistical Computing*, *5*(1), 1–20. https://doi.org/10.1137/0905001

Vázquez-Cendón, M. Elena. (1999). Improved treatment of source terms in upwind schemes for the shallow water equations in chennels with irregular geometry. *Journal of Computational Physics*, *148*, 497–526.

Vázquez-Cendón, María Elena. (1999). Improved Treatment of Source Terms in Upwind Schemes for the Shallow Water Equations in Channels with Irregular Geometry. *Journal of Computational Physics*, *148*(2), 497–526. https://doi.org/10.1006/JCPH.1998.6127

Versteeg, H. K., & Malalasekera, W. (2007). *An introduction to computational fluid dynamics: the finite volume method*. Pearson education.

Zhou, J. G., Causon, D. M., Ingram, D. M., Mingham, C. G. (2002). Numerical solutions of the shallow water equations with discontinuous bed topography. *International Journal for Numerical Methods in Fluids*, *38*(8), 769–788. https://doi.org/10.1002/fld.243

Zhou, J. G., Causon, D. M., Mingham, C. G., Ingram, D. M. (2001). The Surface Gradient Method for the Treatment of Source Terms in the Shallow-Water Equations. *Journal of Computational Physics*, *168*(1), 1–25. https://doi.org/10.1006/JCPH.2000.6670